Title
Investigation of Coupled Hydrologic and Geochemical Impacts of Wildfire on Southern California Watersheds

Author
Burke, Megan Patricia

Publication Date
2012

Peer reviewed|Thesis/dissertation

UNIVERSITY OF CALIFORNIA

Los Angeles

Investigation of Coupled Hydrologic and Geochemical Impacts of Wildfire on Southern California Watersheds

A dissertation submitted in partial satisfaction of the

requirements for the degree Doctor of Philosophy

in Civil Engineering

by

Megan Patricia Burke

2012

ABSTRACT OF THE DISSERTATION

Investigation of Coupled Hydrologic and Geochemical Impacts of

Wildfire on Southern California Watersheds

by

Megan Patricia Burke

Doctor of Philosophy in Civil Engineering

University of California, Los Angeles, 2012

Professor Terri S. Hogue, Chair

Southern California's fire regime is characterized by periodic large-scale wildfires that occur in late summer and early fall, leaving little time for the landscape to recover before the winter rainy season. Recent trends suggest that fire frequency and intensity is increasing due to factors such as urban encroachment into wildlands and a changing climate. While there is an awareness of the hydrologic consequences of these fires, wildfire's potential effects on water quality in Southern California are less understood, especially at the urban-fringe. This study investigates the impacts of wildfire on regional soils with respect to mercury (Hg) storage, accumulation, and transport potential; on storm runoff chemistry in an urban fringe watershed highly impacted by regional atmospheric pollutants; and on procedures required to model post-

fire hydrologic response and predict contaminant loading. The regional soil work showed reduced influence of grain size on Hg storage and accelerated accumulation of Hg in burned soil surfaces over time, as well as sediment-facilitated Hg transport in post-fire storms. Analysis of post-fire runoff from an urban fringe watershed showed up to three orders of magnitude increases from pre-fire levels in the concentrations and loads of many trace metals, including cadmium (Cd) and lead (Pb). These results also highlighted a shift in the timing of chemical delivery in post-fire storms to coincide with, rather than precede, peak discharge, amplifying the fire's impacts on mass loading. The investigation into modeling these impacts allowed for initial estimates to be made of seasonal loading, the development of a model to simulate pre-fire hydrology, and an identification of steps required to develop a model application capable of simulating post-fire sediment and metal concentrations. The resultant body of work provides an increased understanding of wildfire's effects on Southern California's soils and water and on what is required to predict these impacts.

The Dissertation of Megan Patricia Burke is approved.

Jennifer A. Jay

Steven A. Margulis

John T. Wasson

Terri S. Hogue, Committee Chair

University of California, Los Angeles
2012

Dedication

I dedicate this dissertation to my darling mountain man husband, Damon Muehl, who braved two years in the big city and three years of bachelorhood in order to see me through this process. I would also like to dedicate this work to my parents, Patricia and Thomas Burke, who have always told me that I can achieve anything that I set out to accomplish as long as I do my best. I am grateful for their tremendous love and support.

TABLE OF CONTENTS

LIST OF FIGURES

LIST OF TABLES

ACKNOWLEDGEMENTS

First of all, I would like to thank my advisor, Dr. Terri Hogue. Thank you for inspiring me to reach beyond my perceived capabilities. I could not have done this without your encouragement and guidance. You are an inspiration to me, and I am very grateful to have you as a mentor.

I would also like to thank Dr. Jennifer A. Jay and her research group for the tremendous dedication of time and energy in training me, and especially for setting a standard for teamwork and collaboration that I that I will always aspire to.

I would like to acknowledge my committee members, Dr. Jennifer A. Jay, Dr. Steven A. Margulis, Dr. John T. Wasson, and Dr. Terri S. Hogue for their patience, support, and their commitment to my success at UCLA.

Many thanks to my professors at UCLA, who have truly provided me with a superior education, including Dr. Terri Hogue, Dr. Steven Margulis, Dr. William Yeh, Dr. Ne-Zhang Sun, Dr. Donald Kendall, Dr John Wasson, Dr. Jennifer Jay, and many more. Thanks to you, I have the skills to make a meaningful contribution in my field.

This work was certainly a group effort. I am grateful for the support and encouragement provided as a whole by the Hydrology & Water Resources and Environmental Engineering graduate students at UCLA. Special thanks to: Dr. Janet Barco, Dr. Helen Jung, Dr. Chu-Ching Lin, Dr. Rita Kampalath, Marcia Ferreira, Alicia Kinoshita, Sonya Lopez, Carolina Mendez, Bridgette Navaro, Chris Wessel, Sharon Liu, Forest Pfeiffer, and Andrea Brown.

The work presented in Chapter 2 was published in Water, Air, and Soil Pollution, as: Burke, M.P., Ferreira, M., Mendez, C.B., Navarro, B.I., Lopez, S., Jay, J.A., Hogue, T.S., 2010. The Effect of Wildfire on Soil Mercury Concentrations in Southern California Watersheds. Water Air Soil Poll. 212, 369-385. I would like to thank Marcia Ferreira, Carolina Mendez, and Bridget Navarro for their help in lab, field, and with analysis; and Professors Jennifer Jay and Terri Hogue for their guidance on this project. Funding for this work was provided by: NSF Hydrologic Sciences (SGER EAR #0707162), NSF BES Career Grant (BES #0348783), the University of California Toxics and Substances Research and Teaching Program (UCTSR&TP), the University of California's Leadership Excellence through Advanced Degrees (UC LEADS), the National Institute of Health's Minority Access to Research Careers (MARC), and the NIH/NSF UCLA Center for Academic Research and Excellence (CARE) at UCLA.

The work presented in Chapter 3 is in preparation for submission to the Journal of the American Water Resources Association as: Burke, M.P., Hogue, T.S., Barco, J., Wessel1, C., Kinoshita, A., Stein, E.D. Pre- and Post-fire Pollutant Loads in an Urban Fringe Watershed in Southern California. I would like to thank Christopher Wessell, Alicia Kinoshita, and Dr. Janet Barco for their help in lab, field, and with analysis; and Professor Terri Hogue and Dr. Eric Stein for their guidance on this project. Funding for this work was provided by: This research was supported by a National Science Foundation (NSF) Hydrologic Sciences Grant (EAR #0707162) and by an NSF GK-12 Fellowship (#DGE-0742410).

Funding for Chapter 4 was provided by an NSF GK-12 Fellowship (#DGE-0742410).

VITA

Megan Burke, daughter of Patricia and Thomas Burke, was born on May 31, 1977 in Las Vegas, NV. Megan grew up in Boulder City, NV, a town between the Hoover Dam, and what was then the fastest growing city in the nation, Las Vegas. Watching Lake Meade water levels decline as Las Vegas boomed made an impression that would ultimately become the inspiration to pursue a career in hydrology, although her initial intentions were always to become an artist. Megan graduated from Las Vegas Academy of Performing and Visual Arts in 1995, then went on to have adventures. She eventually settled in the Black Hills of South Dakota with her husband to be, Damon Muehl, and began to pursue an art degree in 2001. Along the way she found a love for earth science and got her first taste of scientific research, studying lava flow surfaces with her advisor, Dr. Steve Anderson, which inspired her to continue graduate studies in science. Megan earned a B.S. from Black Hills State University in May of 2006 with majors in both Environmental Physical Science and Art, married Damon Muehl the following June, and by August they were on their way to California. Megan began her studies in Hydrology and Water Resources at UCLA in the Fall 2006 and earned her M.S. in Civil Engineering in the Spring of 2008. She recently moved back to South Dakota to live with her husband in the summer of 2011 and has been finishing her Ph.D. work remotely while working as hydrologist for RESPEC consulting and services. She currently shares a home with Mount Rushmore in Keystone, South Dakota.

Chapter 1. Introduction

This research is comprised of a series of three unique studies that investigate wildfire's impacts on soil chemical concentrations, on chemical delivery during storm events, and on the ability of a common water quality model to predict post-fire streamflow and sediment delivery. Each phase of the work informed and directed the next. By employing a combination of field, laboratory, and modeling methods, a greater understating of how wildfire impacts the chemistry of both natural and altered system and how to better predict these impacts was achieved.

1.1 Wildfire in Southern California

Wildfire is inevitable in Southern California due to its Mediterranean climate consisting of winter rains followed by long, dry summers. Fall season Santa Ana winds dry vegetation and fuel human or lightning ignited wildfires. Southern California's fire regime has historically been characterized by periodic, catastrophic wildfires and has been exacerbated more recently by changing land use patterns (urban/wild-land encroachment) and a warming climate (Whitlock 2004; Westerling 2006; CDFFP 2007; Westerling and Bryant 2008; Keeley and Zedler 2009). As California's population continues to increase, more people move towards wildland areas, which are often developed with little consideration or understanding of ecosystem impacts, increasing risk of both fire ignition and subsequent damages to life and property (Snider et al. 2007; Pincetl et al. 2008).

Over the last decade, California has experienced some of the largest fires in its history, with eleven of the state's twenty largest recorded fires (records beginning in 1932) having occurred since the year 2000. Of these eleven fires, six have occurred in Southern California,

all of which where ignited by either humans or power lines (due to the presence of humans) and are listed below (Table 1) (CDFFF 2009b).

Table 1. Details on six of the state's 20 largest wildfires (by acreage, since 1932); all occurring in Southern California over the last decade.

Rank	Fire Name (cause)	Date	County	Acres	Structures	Deaths
1	Cedar (Human)	Oct-03	San Diego	273246	2820	15
2	Zaca (Human)	Jul-07	Santa Barbara	240207	1	0
4	Witch (Powerlines)	Oct-07	San Diego	197990	1650	2
9	Day (Human)	Sep-06	Ventura	162702	11	0
10	Station (Human)	Aug-09	Los Angeles	160557	209	2
16	Simi (Human)	Oct-03	Ventura	108204	300	0

The California Department of Forestry and Fire Protection (CALFIRE) reported over $2.6 billion in damages due to fire over the last decade (2000-2008), with an average of approximately $300 million/year (CDFFF, 2009a). In addition to the immediate threats posed by active wildfires, post-fire watershed conditions and their hydrologic consequences can pose serious hazards to life, property, and public health long after the fires have been put out. Flooding, debris flows, and water quality degradations are but a few of the lingering effects of wildfire faced by downstream communities (Fairbrother and Turnley 2005; NOAA-USGS 2005).

1.2 Hydrologic impacts of wildfire

Wildfires increase contaminant mobility by altering both the hydrologic and land-surface processes in burned watershed. Watersheds undergo both physical and chemical transformations during, and immediately after, a burn. These changes dramatically alter hydrologic flowpaths, erosion potential, surface soil chemistry, and consequently pollutant

delivery to and within downstream waters. Many studies have investigated the formation of a hydrophobic layer in burned watersheds, particularly in semi-arid, chaparral dominated regions ((Letey 1969; DeBano 1981; Burch 1989; DeBano 2000; Robichaud 2000; Huffman et al. 2001; Letey 2001; Shakesby 2001; Lopez 2005). Organic compounds in plants of these water limited systems vaporize during fire and, due to steep temperature gradients in the soil, re-condense to form a water repellant layer at various depths below the soil surface (DeBano 2000; Letey 2001). This along with other land surface alterations resulting from wildfire, such as acute loss of vegetation and soil organic matter, decreased soil cohesion, and ash layer deposition significantly impacts watershed processes. The combination of decreased soil permeability and the reduction of vegetated surfaces to intercept rainfall results in significant decreases in infiltration amounts and increases water flowing in surface and near surface pathways of burned watersheds (Martin and Moody 2001; Pierson et al. 2001; Moody et al. 2008; Pierson et al. 2008; Jung et al. 2009).

Early post-fire runoff is elevated and can remain high for significant periods of time, increasing the potential for flooding several years following a wildfire (Morales et al., 2000; Martin and Moody, 2001; Rulli and Rosso, 2007; Moody et al. 2008). Increased runoff ratios occur in chaparral systems for at least five years, and sometimes much longer depending on post-fire precipitation patterns and vegetative recovery (Scott and Meixner 2004; Kinoshita and Hogue 2008). Watershed properties such as slope, soil texture, burn severity, and pre-fire vegetation along with post-fire precipitation patterns directly influence the extent of post-fire flooding and debris flows and the degree to which communities (and ecosystems) must prepare for related problems (NOAA-USGS 2005).

1.3 Water quality impacts of wildfire

Post-fire effects on downstream water quality are often attributed to extensive soil erosion during storm events (Bitner et al. 2001, Ranali 2004, Smith et al. 2011). With reductions in soil stability due to fire, post-fire run-off often carries large sediment loads, resulting in sediment laden floods and debris flows (Reneau et al. 2007, Cannon et al. 2008, Moody and Martin 2009, Kean et al. 2011). Total suspended solid (TSS) concentrations in stormwater are often increased by orders of magnitude relative to pre-burn levels; increasing the potential mobilization and transport of particulate bound contaminants in post-fire storm runoff (Neary et al. 2005, Desilets et al. 2007, Malmon et al. 2007, Moody and Martin 2009, Rothenburg et al. 2010). Increased nutrient concentrations, especially nitrate and phosphate, are commonly observed in burned systems, including Southern California's coastal mountain ranges (the subject of this study) (Riggan et al. 1985, Ranali 2004, Meixner et al. 2006, Mast and Clow 2008). Further, the potential for mobilization and transport of trace metals, e.g. mercury, iron, aluminum, lead, and other metals, can be altered by fire (Caldwell et al. 2000; Wolfe et al. 2004; De Marco et al. 2005; Antilen et al. 2006, Rothenburg et al. 2010). Trace metals tend to be particulate bound, hence elements that are released from vegetation during a fire and re-deposited on soil surface, or retained in watershed soils are accessible for mobilization and sediment-facilitated transport during post-fire storms (Loring 1991; Thomson et al. 1997, Burke et al. 2010, Schiff and Tiefenhaler 2011).

The potential for enhanced movement of Hg into downstream waterbodies following fire is of particular concern, because fire-induced conditions may also be conducive for the formation of methyl mercury (MeHg), a potent neurotoxin with a strong tendency to bio-magnify within the food chain (Caldwell et al. 2000; Amirbahman et al. 2004; Kelly et al.

2006). Researchers in Canada's Jasper National Park noted a large, unexpected pulse of both total Hg and MeHg delivered to a reservoir system in the first post-fire storm event, as well as elevated MeHg concentrations in fish in downstream reservoir following the fire (Kelly et al. 2006). Caldwell et al. (2000) measured large amounts of Hg mobilized in creek runoff in a freshly burned mixed-conifer forest, as well as a six-fold elevation in the concentration of total Hg and a 30-fold elevation in MeHg concentrations in the sediments of the receiving reservoir near the creek input. The authors hypothesized that particulate organic matter in post-fire runoff not only transported Hg, but lead to downstream sediment conditions conducive to Hg methylation (Caldwell et al. 2000).

Preliminary work following a 2005 wildfire in Southern California's Malibu Creek watershed (unpublished) found significantly elevated Hg concentrations in the first post-fire runoff event (196 ng/L and 6.1 ng/L in the unfiltered and filtered samples, respectively) in comparison to a neighboring unimpacted stream (4.7 ng/L and 2.3 ng/L, unfiltered/ filtered) indicating extensive Hg mobilization in the burned watershed following the wildfire. The increased Hg levels corresponded to an increase in total suspended sediment (3.98 g/L) in the fire-impacted stream compared to the unburned system (0.45 g/L). A six-fold increase in Hg concentrations on the suspended sediment in the burned system was also observed indicating significantly stronger partitioning to the solid phase at the fire-impacted site.

While wildfire's impacts on mercury transport has received some attention, relatively few studies have focused on the delivery of other trace metals following fire (Caldwell et al. 2000; Kelly et al. 2006, Rothenburg et al. 2010). Those that have reported significantly higher total concentrations of several metals, including As, Al, Ba, Cd, Cr, Fe, Mn, Pb, and Zn, in post-fire runoff following New Mexico's 2000 Cerro Grande Fire and

Australia's 2003 bushfires in Alpine National Park, (Bitner et al. 2001, Gallaher et al. 2002, Leak et al. 2003, Smith et al. 2011).

1.4 Motivation for the Current Study

As Southern California's increasingly large population continues to encroach upon wildlands, transitions from natural to urbanized landscapes significantly impact formerly undisturbed watersheds at the urban-fringe due to regional deposition patterns. Many studies have demonstrated the importance of atmospheric deposition in determining the presence of pollutants within a watershed (Vitousek et al. 1997; Lee and Caporn 1998; Fenn and Poth 1999; Fenn et al. 2003; Meixner and Fenn, 2004). For example, Barco et al. (2008) investigated the impacts of regional urbanization in the Arroyo Seco watershed (this study was conducted prior to the 2009 Station Fire) where hydrologically enhanced behavior was observed for nitrate. Additionally, their findings indicated that the watershed is a sink for atmospheric nitrate, which the authors hypothesize, is a result of high rates of deposition originating from the Los Angeles metropolitan region. Other regional studies corroborate these findings (Riggan et al. 1985; Herpe and Troch 2000; Butturini et al. 2003; Meixner and Fenn 2004). Riggan et al. (1985) observed nitrate concentrations of two to three orders of magnitude greater in watersheds that adjoin urban areas in a study of front range catchments located in the San Gabriel Mountains (1985). Even pre-fire, urban-fringe basins can serve as an upstream source of various chemical constituents, where winter season storms carry significant chemical loads downstream from these "natural" depositionally-affected areas into downstream (urban) river systems. The increasing occurrence of large scale wildfires is

likely to exacerbate existing water quality problems. The current study attempts to facilitate a better understanding of contaminant transport from post-fire, urban fringe watersheds.

While there is considerable literature demonstrating the effects of fire on hydrologic processes as well as on the altered stream chemistry of post-fire systems, few studies have rigorously investigated factors controlling the variability in hydro-geochemical coupling and storm-driven contaminant flushing in post-fire systems. Additionally, much of this work has either been conducted in natural systems, using seasonal (rather than high resolution storm event) datasets, or undertaken in paired catchments (due to the lack of pre/post fire data on burned watersheds). Two recent large wildfires (the 2006 Day Fire and the 2009 Station Fire; Table 1) occurred within close proximity to the Los Angeles Basin, providing the opportunity to investigate each fire's impact on local hydrology and water quality in both an undisturbed (Day Fire) and an urban fringe watershed (Station Fire).

1.5 Research Objectives

The objectives of the current study are to better understand complex hydro-geochemical coupling and mass loading in burned, semi-arid landscapes in order to provide guidance for post-fire watershed management practices and to facilitate the development of mitigation and warning strategies for related impacts. The work is focused around three primary questions.

1) What are the impacts of wildfire on soil Hg storage and subsequent transport of sediment bound Hg within burned watersheds?

2) How are other common contaminant concentrations and loads altered in post-fire storm runoff and what are the hydrologic factors that control these alterations?

3) How can existing modeling tools be utilized to predict post-fire variability in contaminant loads from burned systems in a cost-effective and parsimonious manner?

1.6 Organization of the Thesis

To address the first question, an extensive dataset of Hg concentrations within the sediments, storm runoff, and soils in a burned, semi-arid watershed (Day Fire), as well as a regional soil Hg concentrations in burned and unburned soils of three fire-impacted watersheds (including one urban fringe watershed), have been collected and analyzed. Results from this work are published in the Journal of Water, Air and Soil Pollution (Burke et al. 2010), and are presented in Chapter 2.

Results from the Day Fire research provided motivation for directing the research focus toward burned, urban fringe environments and to expand the scope of work to include a more extensive trace metal analysis in post-fire storm runoff. Comprehensive pre and post-fire storm event chemistry datasets in a burned urban fringe watershed (Station Fire) have been collected and analyzed to address the second question, and will be presented in Chapter 3. Results from this work have been submitted for publication in the Journal of American Water Resources Association.

Observations from the literature review, Day Fire work, and Station Fire results suggest that the transport of many constituents of concern are proportional to sediment transport. The final, and ultimate, goal of the current study is to utilize existing modeling tools to predict contaminant loading post-fire systems in a cost-effective and simple manner, as stated the third question. Methods for identifying the relationships between contaminant

and sediment concentrations, a description of the models employed, initial estimates of contaminant loads delivered to the Los Angeles River during the first post Station Fire storm season, and steps to develop a predictive tool are presented in Chapter 4.

Finally, the major findings of this work are summarized and future directions for follow-up research are discussed in Chapter 5.

Chapter 2. Wildfire's Impacts on Soil Mercury

Mercury stores in vegetation and soils are known to be released to the atmosphere during wildfires, increasing atmospheric stores and altering terrestrial budgets (Harden et al. 1999; Friedli et al. 2001, 2003a, 2003b; Sigler et al. 2003; Mailman and Bodaly 2005; Engle et al. 2006; Biswas et al. 2007; Dicosty et al. 2007). Increased erosion and transport of sediments is well documented in burned watersheds, both immediately post-fire and as the watershed recovers, however, understanding post-fire mobilization of soil Hg within burned watersheds remains elusive. The first goal of the current study is to better understand the impact of wildfire on soil-bound Hg during the immediate post-fire period as well as during recovery, to assess the potential for sediment-driven transport to and within surface waters in burned watersheds, and to quantify Hg loading to downstream waters in post-fire storm run-off.

2.1 Study Areas

Piru Creek watershed (Day Fire)

The Day Fire, which started on September 4, 2006 and was contained by October 13, 2006, burned for over a month and consumed 162,702 acres (Table 2). The burned region is approximately 70 miles north of the city Los Angeles, primarily located in Ventura County and almost entirely within National Forest lands (Los Padres and Los Angeles) in the Transverse Mountain Range (Figure 1). Approximately fifty percent of the 512 km^2 Piru Creek watershed was burned during the Day Fire, with Piru Creek serving as the northern fire boundary. Upper Piru Creek watershed (hereafter noted as Piru Creek watershed) feeds into Pyramid Reservoir, a storage system for imported water from the California State Water

Project, which provides drinking water for the Los Angeles metropolitan region. The watershed is essentially undisturbed with much of it located within Los Padres National Forest's Chumash and Sespe Wilderness areas. Though in close proximity to the Los Angeles Basin, prevailing coastal winds tend to carry urban pollutants west rather than north towards Piru Creek Watershed. Mean annual precipitation in the region is approximately 480mm/yr. Chaparral is the dominant vegetation, but the watershed's high relief (elevations ranging from 792m to 2690m) and Mediterranean climate allow for a wide range of vegetation to exist (Scott et al. 1968). The geology is characterized by pre-Cretaceous igneous and metamorphic basement rock, overlain by thick sedimentary sequences of Eocene marine sandstones and conglomerates with interbedded shales (Scott et al. 1968). Soils are generally shallow and of coarse texture (Scott et al. 1968). The soil texture at sampling locations was determined to be sandy loam. The Day Fire dataset presented here includes seasonal soil depth profiles (from 0-15cm at 2.5cm increments) at 6 burned and 3 unburned sites, stream water grab samples, and high resolution storm samples from selected storm events spanning 1.5 years following the fire.

Malibu Creek Watershed (Topanga Fire)

The Topanga Fire started on September 28, 2005 and was active until October 13, 2005. The fire burned 98km^2 in the Santa Monica Mountains along the border of Los Angeles and Ventura Counties (Table 2). The fire was located primarily in the headwaters of the 282 km^2 Malibu Creek watershed (Fig. 1), which is located approximately 35 miles west of Los Angeles and extends from the Santa Monica Mountains and adjacent Simi Hills to the Pacific Coast. Malibu Creek drains into Malibu Lagoon and ultimately into Santa Monica

Bay. 20% of the watershed is developed, with a mixture of residential (13%), commercial/industrial (4%) and agricultural (3%) land use patterns (Ambrose and Orme 2000). Vegetation in the remainder of the watershed is primarily chaparral and scrub oak. Elevations range from 450 to 600m, and the average annual precipitation in approximately 450mm/yr. The upper reaches of Malibu Creek consist of marine sandstones, shales, intrusive tertiary basalts and andesites, and semi-consolidated materials (Ambrose and Orme 2000). Soils are predominantly coarse and granular in structure, but can vary greatly depending on the parent material (USDA Natural Resource Conservation Service 2007). The dominant texture of soils from the sampling locations was determined to be in the sand-sized fraction. The Topanga Fire dataset includes two soil sites sampled immediately post-fire and prior to the first storm event at depths of 2.5 and 10 cm.

The Arroyo Seco Watershed (Pines Fire)

The Pines Fire occurred in the headwaters of the Upper Arroyo Seco watershed (hereafter noted as Arroyo Seco), located on the eastern edge of Los Angeles County in the San Gabriel Mountains (Figure. 1). The fire started September 19, 2006, and was contained by September 23, 2006, reaching only approximately 1 km^2 in size (Table 2). The Arroyo Seco River runs within a deeply carved canyon that begins near the top of the San Gabriel Mountains in Los Angeles National Forest. After exiting the upper basin, the stream is channelized and eventually converges with the Los Angeles River near downtown Los Angeles. The Arroyo Seco watershed consists of approximately 42km^2 of steep, mountainous terrain with elevations ranging from 426 to1820m above sea level. Due to its elevation, the Arroyo Seco experiences relatively high precipitation (840mm/yr) compared to

the Los Angeles basin (375mm/yr) (NWS 2009). Vegetation in the watershed is primarily chaparral (75%), with coniferous forests (23%) in limited regions of the uppermost part of the watershed. Though the Arroyo Seco watershed is essentially undeveloped, the basin is located on the leeward side of the Los Angeles basin and in highly impacted by atmospheric deposition of contaminants originating from the metropolitan region. Soils are poorly developed and are underlain by mainly igneous rock including tonalite, granite, gneiss, echo granite, granodiorite, and to a lesser extent, siliceous metasedimentary rocks, and alluvial deposits (Department of Conservation of California 1998). Shallow, coarse soils are found throughout the watershed, composed mostly of silty sand and gravelly silty sand (Department of Conservation of California, 1998). The Arroyo Seco dataset includes soil depth profiles (from 0-15cm at 2.5cm increments) collected from 4 burned and 1 unburned sites sampled immediately post-fire and prior to the first storm

Table 2. General site descriptions and sampling information for the three study areas.

	Malibu Creek (Topanga Fire)	**Arroyo Seco (Pines Fire)**	**Piru Creek (Day Fire)**
Fire Dates	9/28/05 - 10/13/05	9/19/06 - 9/23/06	9/4/06 - 10/13/06
Area Burned	98 km^2	1 km^2	660 km^2
Annnual Precipitation	450 mm	840 mm	480 mm
Primary Vegetation	chaparral	chaparral	chaparral
Dominant Soil Texture	sand	sandy loam	sandy loam
Bedrock	Miocene Marine Deposits	Miocene Non-Marine Deposits	Permian-Triassic Granite
# of Burned Sites	4	4	6
# of Unburned Sites	0	1	2

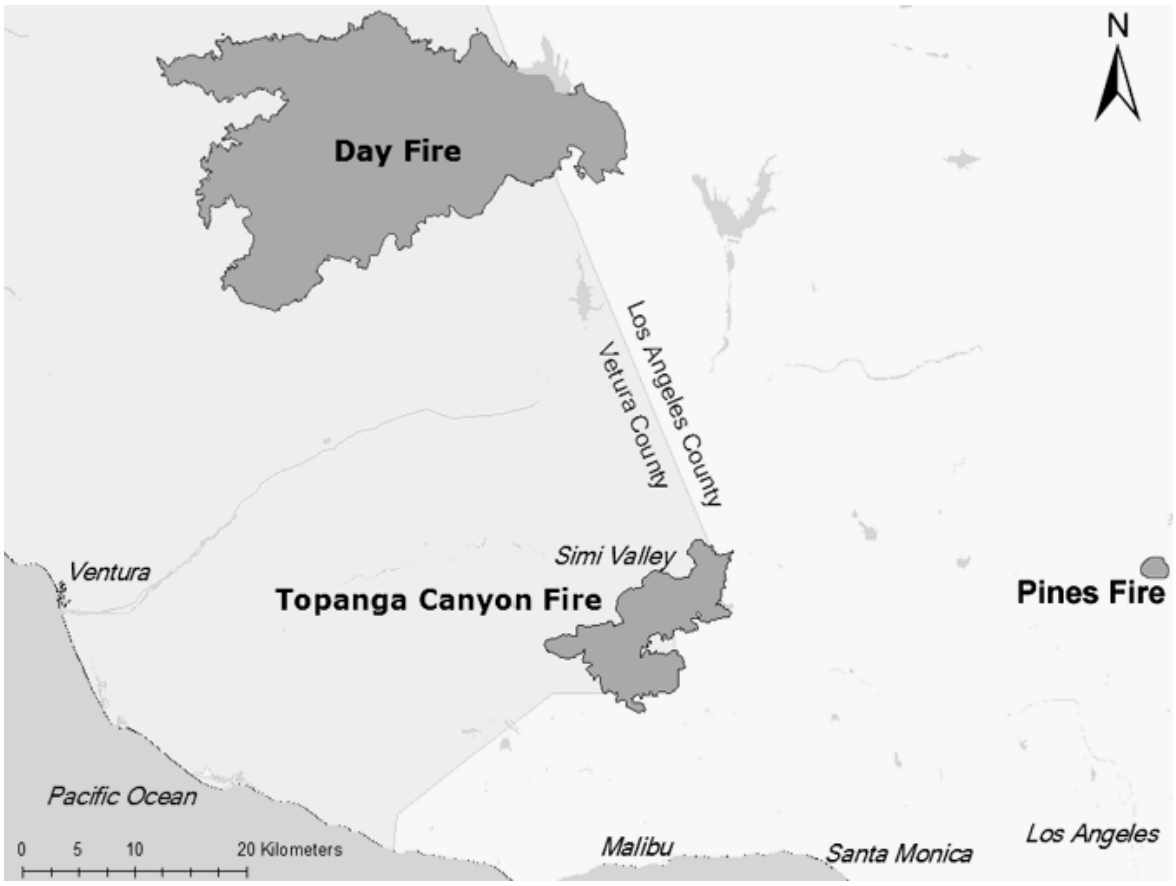

Figure 1. Locations of the Topanga (Malibu), Pines (Arroyo Seco) and Day Fire (Piru Creek) study areas.

2.2 Methods

2.2.1 Sample Collection

Mercury concentrations were determined in soils collected from three Southern California watersheds with similar vegetation and soil characteristics immediately following the wildfires 2005 Topanga Fire (Malibu Creek watershed) and 2006 Pines Fire (Arroyo Seco watershed), and the 2006 Day Fire (Piru Creek watershed) (Table 2; Figure 1). Burn severities at each of the study areas were estimated using Moderate Resolution Imaging Spectroradiometer (MODIS) differenced Normalized Burn Ratio (dNBR) and verified with field observations, to provide guidance for the selection of sampling locations. Water Drop

Penetration Tests (WDPT) and infiltration studies were conducted in each watershed immediately post-fire to assess soil hydrophobicity (DeBano 1981).

In a more extensive exploration of Piru Creek watershed (Day Fire), including both temporal sampling of soil profiles and grain-size analysis, soils were collected immediately following the fire (Fall 2006) and prior to the first storm, as well as seasonally throughout 2007 and the winter of 2008. Piru Creek watershed (Day Fire) investigations also included collection and analysis of post-fire storm and inter-storm samples. In situ measurements were taken of standard stream water parameters including temperature, pH, total dissolved solids (TDS), turbidity, and dissolved oxygen (DO) using a hand-held meter by Hanna Instruments, and a YSI 55 DO meter.

An ISCO auto-sampler was installed over two seasons (winter 06-07 and 07-08) for storm event sampling co-located with the long-term USGS/CADWR stream gauge site. Stringent sampling protocol (Clean Hands-Dirty Hands) was followed during field collections where all samples were collected in new, acid-washed, environmental sampling bottles with Teflon-lined lids using acid-washed plastic shovels. All bottled samples were stored in double plastic bags to avoid contamination, acid-preserved (aqueous samples), and held at 4˚C until analysis.

2.1.2 Laboratory Analysis

Soil analysis included measurement of total Hg (by dual-stage gold amalgamation/cold vapor atomic fluorescence spectrometry (CVAFS), using EPA method 7473) and Total Organic Carbon in soils (by LOI, using ASTM Method D 2974-00). Additional soils were collected at each study area for texture classification, and sieve and

hydrometer analysis was used to separate material into sand (2mm – 0.05mm) silt (0.05mm – 0.002mm) and clay fractions (>0 0.002mm) to determine soil texture using the USDA NRCS classification system (USDA Natural Resource Conservation Service, 1993). The aqueous samples were analyzed for aqueous total and filtered Hg (by CVASF, using EPA Method 1631 Revision E) and total suspended solids (TSS). All Hg analyses were conducted in Professor Jay's lab and in partnership with the Jay research group, with invaluable contributions from Marcia Ferreira (aqueous analysis), Carolina Mendez and Bridget Navarro (soil analysis), and Chu-Ching Lin (overall guidance). Total Suspended Sediment (TSS) concentrations were measured in the UCLA CEE water quality lab. TSS is measured by weighing a prepared filter (M_0), filtering (1.5µm particle retention) a known volume of sample (V), drying the filtered material for 1 hour at 105 C, then reweighing the filter + retained sediments (M_1), and calculated with the following equation:

$$TSS = \frac{M_1 - M_0}{V} \qquad \text{Eq. 1}$$

2.1.3 Data Analysis

Analysis of variance (ANOVA) was used to compare differences in Hg concentrations and TOC between groups (study areas, seasonal sampling periods, and grain sizes). The analysis was performed using the anova1 function of the Matlab computing program (Mathworks Inc., 2005), with F-tests and p-values used as a guide to determine significance at the 5% level.

2.3. Results

2.3.1 Regional Analysis

Mercury levels varied greatly between the three study areas. Significantly higher ($p < 0.05$) Hg concentrations were observed in the Arroyo Seco soils compared to the other two sites (Figure 2). Both the Malibu and Piru sites (which exhibited similar Hg levels) are located west and north of the urban/metropolitan center and regional winds carry urban pollutants inland and away from these regions. These sites exhibit Hg concentrations that are consistent with previously published values in natural, semi-arid systems, such as a Nevada desert wildfire site with measured values of 47.4 ng/g (+/- 26.8 ng Hg/g) and 49.4 ng Hg/g (+/- 11.3 ng Hg/g) of Hg in unburned and burned soils, respectively (Engle et al. 2006).

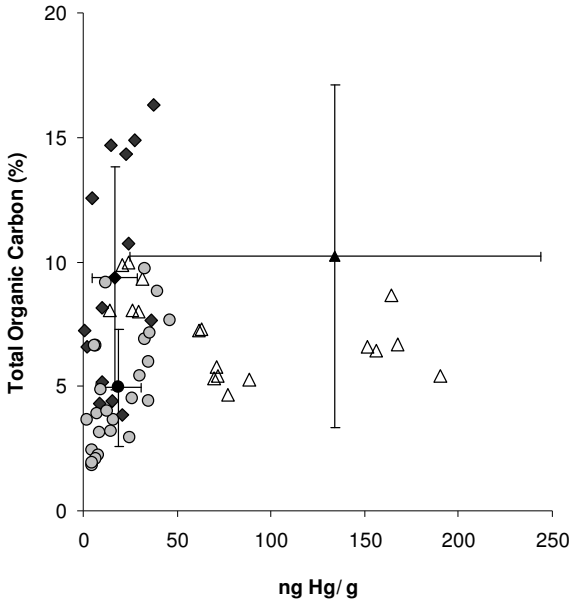

Figure 2. Scatter plot of Total Organic Carbon (%) vs. Hg (ng Hg/g) in each of the three study areas: Malibu (dark grey diamonds), Arroyo Seco (white triangles), and Piru Creek (light grey circles). The solid shapes correspond to the data symbols with the same shape and error bars show the mean values (center symbol) and standard deviation at each site

Hg Concentrations measured in the Arroyo Seco, on the other hand, are more comparable to those measured in more humic soils, such as peat bogs in northwestern Ontario where

Mailman and Bodaly (2005) measured Hg concentrations of 162 ng/g (+/- 132 ng Hg/g); or even to contaminated areas such as those reported by Palmieri et al. (2006), where soil Hg concentrations ranged from 90 to 1230 ng Hg/g at a site draining an abandoned cinnabar (HgS) mine.

In addition, TOC measurements from the sampled Arroyo Seco sites were in the same range as those observed in the Malibu sites (both were significantly higher than the Piru Creek soil TOC) ($p < 0.05$) (Fig. 2), and similar burn severities (and presumably, similar loss rates of Hg due to volatilization during the fires) were observed in all three study locations. Hence we hypothesize that the primary factor for Arroyo Seco's elevated soil Hg concentrations is its location/proximity to anthropogenic (urban) sources originating from the Los Angeles Basin.

2.3.2. Temporal Analysis

Overall, the freshly burned soils exhibited lowest concentrations of Hg at the soil surface (top 0.0 -2.5cm) in all but one of the nine sites were depth profiles were samples (Piru and Arroyo) burned to moderate severity. The only burned soil profile that did not exhibit this behavior was subject to low burn severity, highlighting the importance of burn severity on Hg mobilization during wildfires. In the three unburned soils sites the highest Hg concentrations were observed at the soil surface. This behavior was observed both in the Piru Creek watershed, located in a remote location, where the background Hg levels (2 to 87 ng Hg/g) were characteristic of a natural, semi-arid region, and in the enriched soils of the Arroyo Seco watershed, where Hg concentrations of >300 ng Hg/g were observed. The impacts of fire on organic carbon also play an important role in soil Hg dynamics. A few of

the freshly burned depth profiles exhibited the highest Hg concentrations between depths of 2.5 and 7.5cm, with the highest TOC concentrations and soil hydrophobicity also measured in this range.

Following the initial volatilization of Hg at the soil surface during wildfire, the burned soils experienced an accelerated accumulation of Hg following the fire in comparison with the unburned soils of Piru Creek watershed (Figure 3). Water year (WY) 2006 was one of the driest years on record, and surface soil Hg did not appear to be transported during the first post-fire rainy-season.

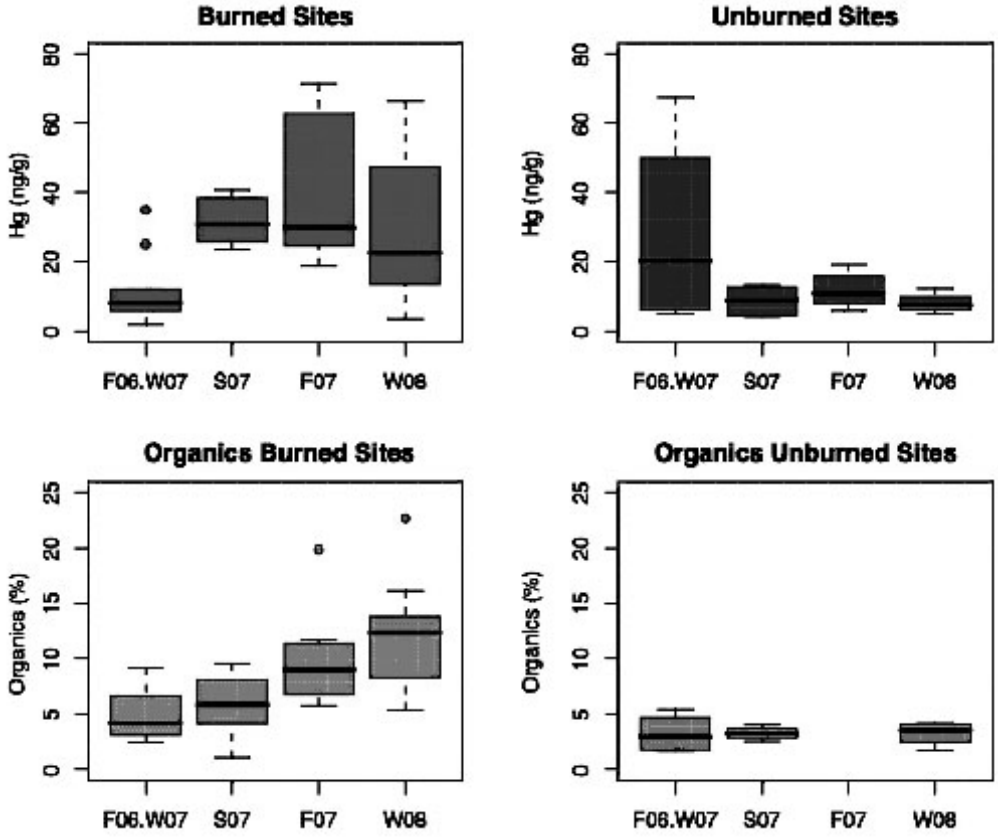

Figure 3. Boxplots representing the seasonal Hg concentrations at the soil surface (0cm and 2.5cm depth intervals) for the burned (top, left) (n = 10: F06/W07, F07, 8: S07, and12: W08) and unburned sites (top, right (n = 4: F06/W07, S07, F07, and 3: W08)) and seasonal surface TOC levels in both burned (bottom, left (n = 10: F06/W07, S07; 8: F07, 12: W08)) and unburned soils (bottom, right (n = 4: F06/W07, S07, W08; 0: F07)) within Piru Creek watershed. Top and bottom edge of each box represents the 75th and 25th percentile, respectively, the line bisecting the box represents the median, circles are outliers

Instead, a four-fold increase in mean surface soil Hg concentrations was observed one year following the Day Fire, corresponding to an increase in the mean surface TOC measurements as well as moderate (observed) vegetative recovery (Figure 3). However, the Hg/TOC concentration relationship was not straightforward, as one of the burned sites exhibited much higher soil Hg concentrations one year after the fire with only a slight increase in organic material. We hypothesize that heat-induced changes in soil organic matter resulting from the fire allowed the charred surface soils to more efficiently complex and retain atmospheric Hg.

WY 2008 produced precipitation totals closer to the normal range for Piru creek watershed, and low surface Hg concentrations were observed in the burned and unburned sites following the second post-fire rainy season,. Conversely, the organic content of the burned soils continued to increase as the watershed's vegetation began recover. We attribute the loss of Hg in at the soil surface to soil flushing and enhanced erosion (observed) during the winter storms. These results underscore that the observed accelerated accumulation of Hg in the burned soils, along with elevated potential of erosion, could result in increased delivery of organic- or particulate-bound Hg to surface waters. And, depending upon precipitation patterns, this risk may extend beyond the first post-fire rainy season and persist in the years following the fire.

2.3.3. Grain Size

For the burned soils at Piru Creek watershed (all soil samples, integrated over the entire depth profile) 41.94% (+/- 19.75%), 18.88 % (+/- 4.68%), and 39.19% (+/- 19.90%) of the soil was classified as fine, medium, and coarse grain size fractions, respectively (n = 76) (Figure 4). Significantly higher concentrations of Hg were observed in the fine and medium

grain size fractions than observed in the coarse fraction ($p < 0.05$) (Fig. 4). Overall Hg distribution in the burned soils included 37.19% (+/- 5.54%) in the fines, 35.43 % (+/- 4.68%) in the medium fraction, and 27.38% (+/- 5.51%) in the coarse grain size fraction (n= 76). Significantly lower Hg concentrations were observed in the coarse grain size fraction than in the medium and fine grained burned soils of Piru Creek ($p < 0.05$).

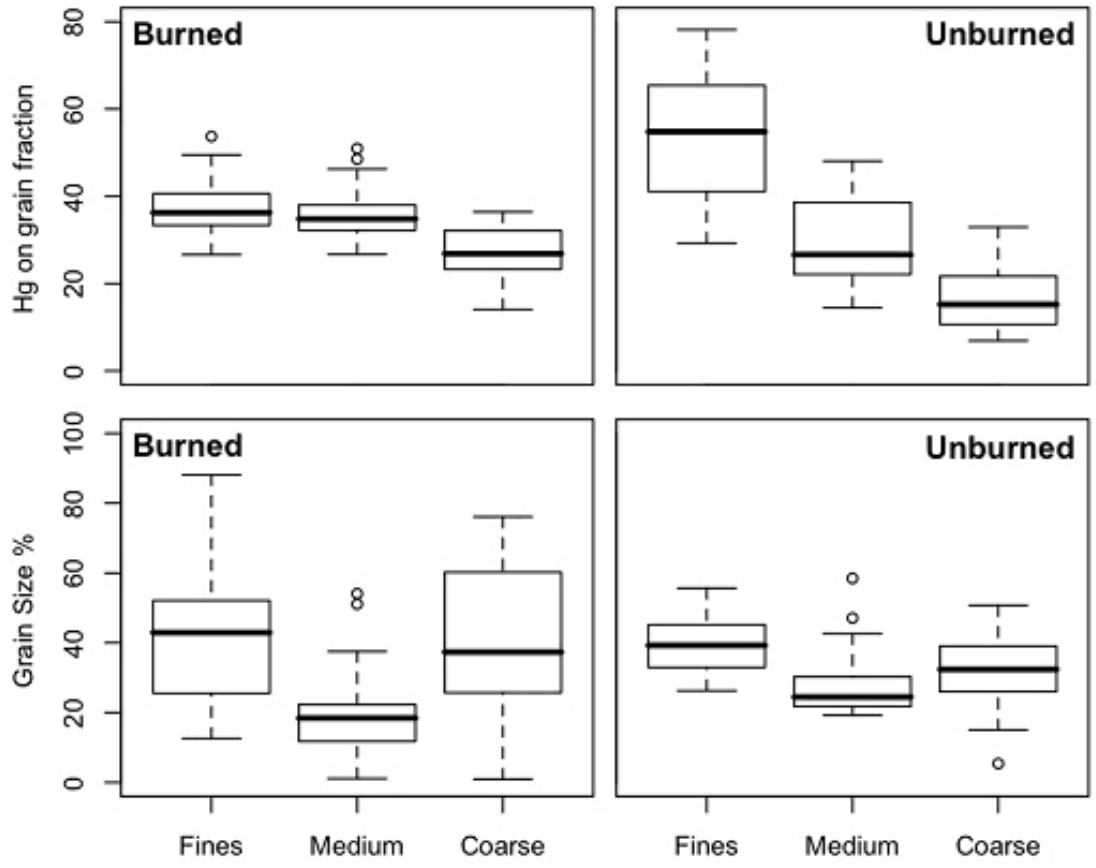

Figure 4. Boxplots representing the % of soil Hg measured in each grain-size fraction (top) and the grain-size distribution of the soil (bottom) for both burned (n = 76 for each grain size fraction) and unburned (n = 35 for each grain size fraction) soils within Piru Creek watershed. Top and bottom edge of each box represents the 75th and 25th percentile, respectively, the line bisecting the box represents the median, circles are outliers. The coarse, medium, and fines fractions are defined as 0.50-2mm, 0.25-0.50mm, and <0.25mm, respectively

The grain size distribution in the unburned soils (all soil samples, integrated over the entire depth profile) was similar to that observed in the burned soils with 40.92% (+/- 9.49%), 26.26 % (+/- 9.42%), and 32.82% (+/- 9.93%) of the soil measured as fine, medium, and coarse grain size fractions, respectively (n = 35). Hg distribution in the unburned soils included 53.70 % (+/- 13.92%), 29.47 % (+/- 9.71%), and 16.83% (+/- 7.68%) in the fine, medium, and coarse grain size fractions, respectively (n = 35). Hg appears to be preferentially bound to the fines in the unburned soils of Piru Creek, with Hg concentrations decreasing as the grain-size increased (Fig. 4). Hg concentrations were significantly different in each of the fractions ($p < 0.05$).

The grain-size distribution analysis supports that a range of grains-size fractions (not only the fine fraction) need to be considered in soil-Hg analysis (Loring 1991; Biester et al. 2002). Hg-soil partitioning with respect to grain-size was not as strong in the burned soils as in the unburned soils (where Hg preferentially bound to the finer soils). As the time since burning increases, an evolution towards the transport of more coarse sediments occurs in post-fire storm runoff (Desilets et al. 2007). Our results indicate that this coarser material may also be more likely to contain higher concentrations of soil-bound Hg.

2.3.4. Post-fire Storm Events

The first winter (WY 2007) following the Day Fire was one of the driest on record, with precipitation totals (130mm) less than one third of normal. The only significant storm (Figure 5) measured total Hg concentrations just slightly higher than the inter-storm samples (which measured > 1 ng Hg /L, and > 4 ng/L in the filtered and unfiltered samples, respectively over the entire period of record), while no change was observed in the dissolved

Hg concentrations. However, these total Hg concentrations were linearly correlated to TSS measurements ($r^2 = 0.91$) and followed the storm hydrograph (Figure 6).

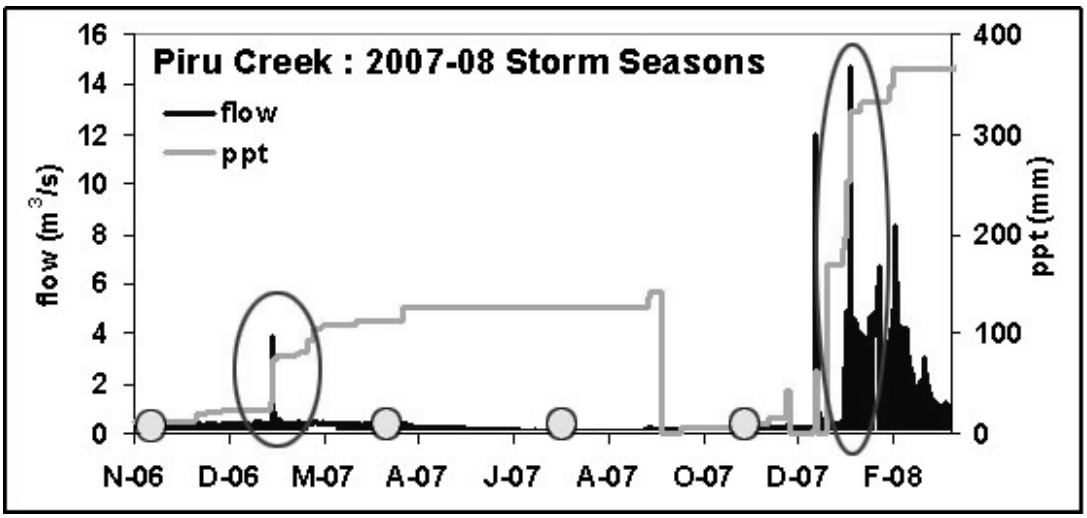

Figure 5. Selected storms sampled over the study period (circled), as well as measured interterm aqueous samples (grey circles). Streamflow shown on the left y-axis (m^3/s) and precipitation shown on the right y-axis (mm)

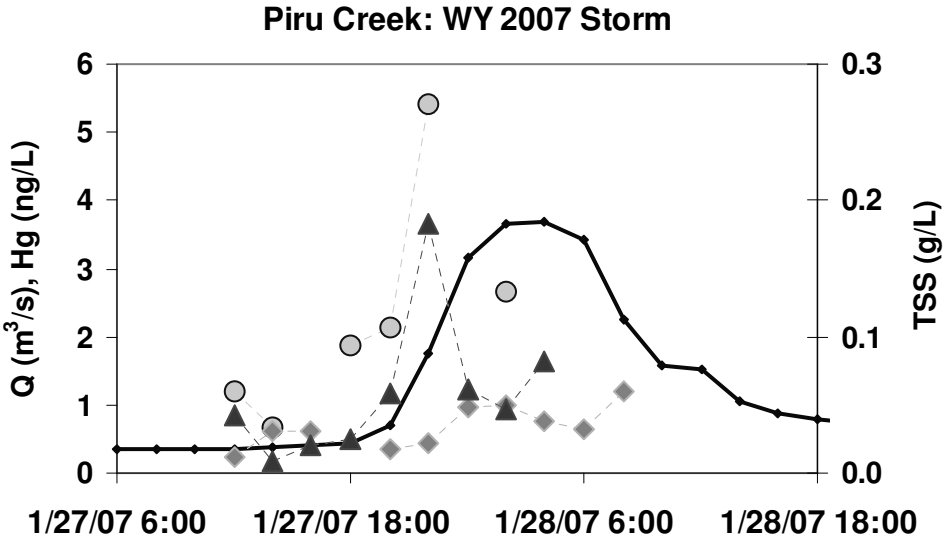

Figure 6. Storm hydrograph for the largest storm that occurred in the first rainy season following the Day Fire (WY 07), represented by the solid black line (m3/s, left y-axis), along with Hg concentrations (ng/L, left y-axis) in filtered (grey diamonds) and unfiltered (light grey circles) samples and suspended sediment concentrations (dark grey triangles, g/l, right y-axis).

The following winter (WY 2008) brought higher precipitation totals (370mm) and more intense storms. Elevated, turbid streamflow was observed in Piru Creek during many of the 2007-08 storms, and Hg was measured in the storm runoff of the largest event of the season (and period of study) (Figure 7). Little change was observed in the dissolved Hg concentrations of the storm samples; however, a two-order magnitude increase was measured in both the total Hg and TSS concentrations during the largest storms of water year 2008 (and corresponding to the loss in surface soil Hg observed on the W08 sampling date) (Figure 7). The total Hg and TSS concentrations were not as well correlated linearly in the 2007-08 storms ($r^2 = 0.50$) and the relationship was better described with a logarithmic function ($r^2 = 0.89$). These results illustrate that the sediment flux controls the Hg delivery to terrestrial waters in this burned, semi-arid watershed, and that a better understanding of sediment delivery can aid in Hg load estimations in post-fire systems.

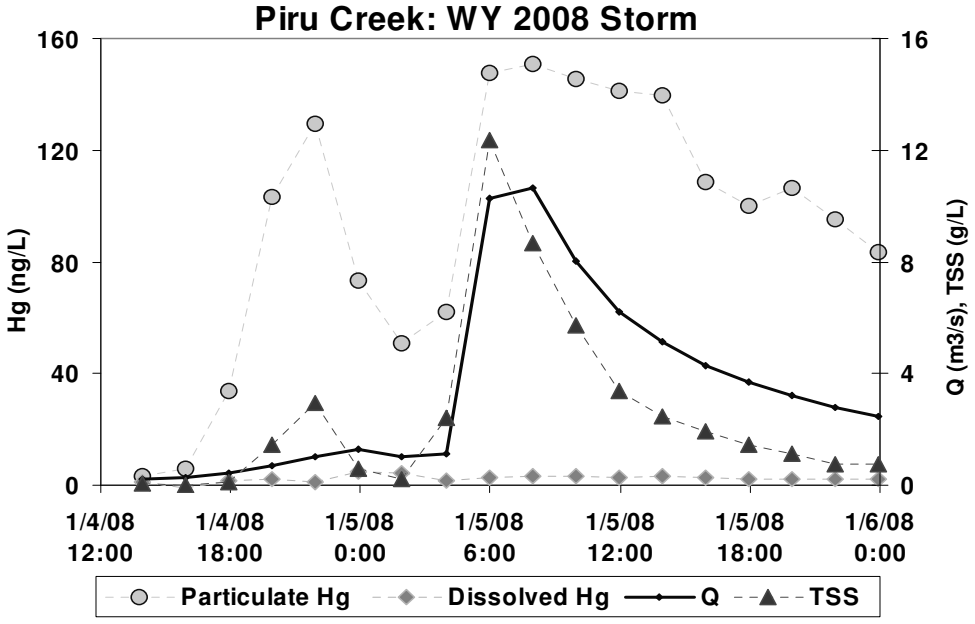

Figure 7. Storm hydrograph for the largest storm that occurred in the second rainy season following the Day Fire (WY 08), represented by the solid black line (m^3/s, right y-axis), along with Hg concentrations (ng/L, left

y-axis) in filtered (grey diamonds) and unfiltered (light grey circles) samples and suspended sediment concentrations (dark grey triangles, g/L, right y-axis).

2.4. Summary

The results from this chapter provided insight into the potential for post-fire mobilization of soil Hg within burned watersheds. The regional analysis demonstrated the importance of considering local deposition patterns, as the samples exhibiting the highest Hg concentrations of the study where obtained from an urban fringe watershed. The seasonal analysis demonstrated how wildfire can impact the storage and accumulation of Hg over time, especially when winter rains are not sufficient to flush the system. While the grain size analysis showed that all particle fractions must be considered when assessing transport potential following fire. Finally, Hg concentrations measured in storm runoff over two rainy seasons following the Day Fire demonstrated that particle-facilitated Hg transport occurred during post-fire storm events sufficient to mobilize sediment. Besides providing insight into post-fire Hg behavior in soils and water, results from this chapter served to focus the efforts of Chapter 3.

Chapter 3. Station Fire

Watersheds in the front range of the San Gabriel Mountains supply large amounts of runoff into downstream urban water ways during winter storms, which are then directed to infiltration ponds or zones for aquifer recharge, or into flood control channels that route water through dense urban areas to coastal bays. Previous work in Southern California's front-range has revealed significant nutrient and other chemical loads in the storm runoff of local urban-fringe watersheds (Fenn and Poth 1999; Meixner et al. 2001; Fenn et al. 2003; Barco et al. 2008). Post-fire storm events in urban-fringe basins have the potential to contribute significant chemical loads to downstream waterbodies, which are often already impaired and subject to management actions pursuant to TMDLs and NPDES permits (US EPA 2007). However, the potential for wildfire to exacerbate existing water quality problems in highly polluted urban fringe watersheds has not been as well studied. The Station provided an opportunity to investigate the effects of fire on stormwater loadings of metals in this type of system. The objective of is phase of the study was to better understand the impacts of wildfire on mass loading in highly-impacted, urban-fringe landscapes in order to provide guidance for post-fire watershed management practices.

3.1 Study Area

Southern California's Station fire burned for six weeks between August and October 2009, consuming 660 km^2 of primarily Angeles National Forest in the San Gabriel Mountain Range. The burned region is immediately adjacent to dense urban areas on the east (leeward) side of the Los Angeles basin. Much of the region affected by the Station Fire had not burned in over 60 years, prior to the Clean Air Act and the subsequent phase-out of lead

additives in gasoline, leaving a potentially large store of anthropogenic contaminants in vegetation and soil (Barco et al., 2008). This phase of the study focuses on a small urban-fringe basin, the Upper Arroyo Seco watershed, that was entirely burned during the Station fire.

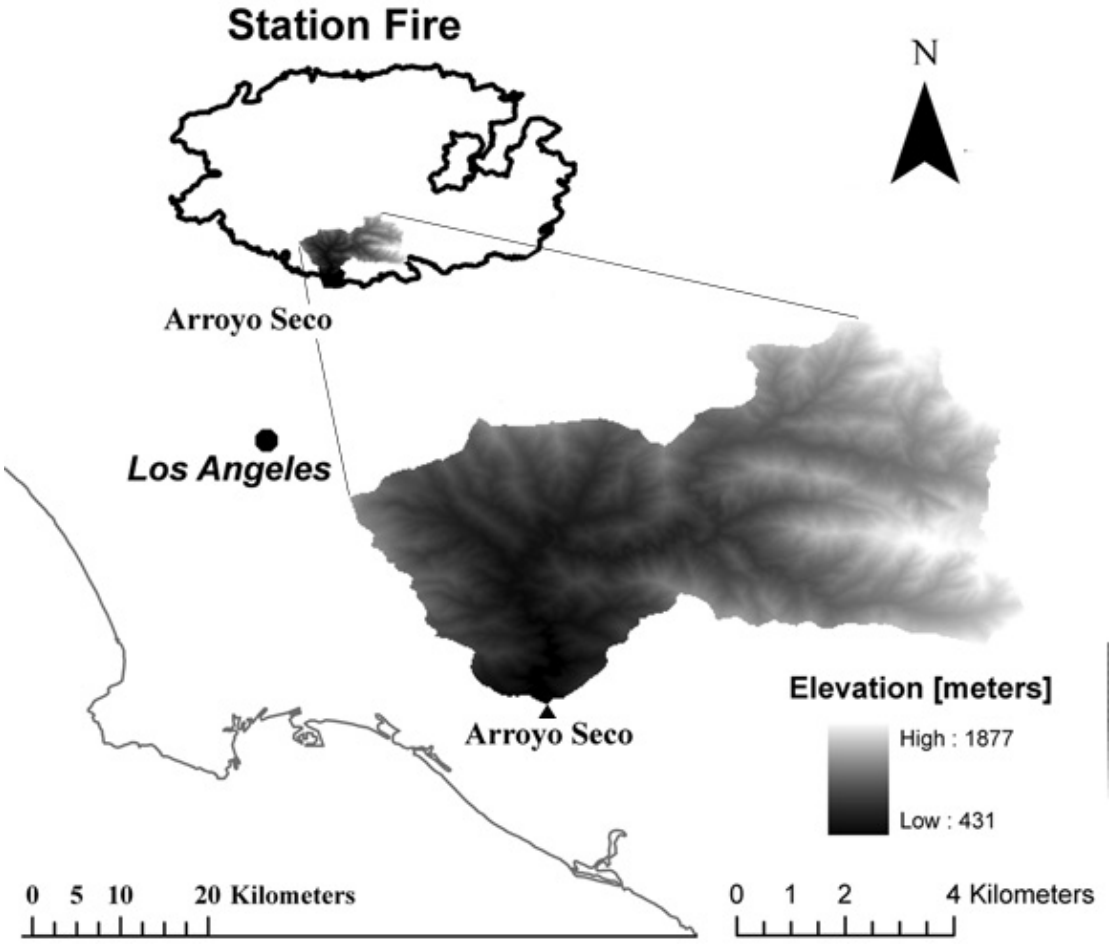

Figure 8. Location of the Arroyo Seco watershed in relation to the Los Angeles Basin and the Station Fire boundary. The inset shows the relief of the watershed as well as the location of the USGS stream gage (triangle) used in this study.

The Arroyo Seco River runs within a deeply carved canyon that begins near the top of the San Gabriel Mountains in the Angeles National Forest (Figure 8). After exiting the upper basin, the Arroyo Seco is channelized and eventually converges with the Los Angeles River

near downtown Los Angeles. Several reaches downstream of the Arroyo Seco River's confluence with the Los Angeles River are listed as impaired for Cd, Pb, Cu, Zn, and Al pursuant to Section 303(d) of the Federal Clean Water Act (US EPA 2007). The Upper Arroyo Seco watershed, hereafter noted as the Arroyo Seco watershed, consists of approximately 41.44 km^2 of steep, mountainous terrain with elevations ranging from 431 to1877 m above sea level. The watershed slope and length are estimated to be 5.7% and 17.2 km, respectively. Due to orographic effects, average annual precipitation (840mm/yr) is relatively high compared to that of the Los Angeles basin (375mm/yr) (LADPW 2010). Long term (WY 1911-2010) annual stream discharge is 0.28 m^3/s and the annual runoff coefficient is 0.22 (WY 1975-2010) (USGS 2011). Shallow, coarse soils are found throughout the watershed, composed mostly of silty sand and gravelly silty sand, and are underlain by mainly igneous rock (Department of Conservation of California 1998, NRCS, accessed 2008). Pre-fire land cover was primarily chaparral (73%), with coniferous forests (23%) in the uppermost part of the watershed. The Arroyo Seco was burned in its entirety during the Station Fire, at primarily moderate (64%) severity (USDA 2009). The remaining 8%, 17%, and 11% of the watershed was burned to very low, low, and high severities, respectively (USDA 2009).

3.2 Methods

3.2.1 Sample collection and analysis

Water quality sampling was conducted prior to and immediately following the Station Fire, over the rainy seasons (October through March) of both WY09 and WY10. Grab samples were taken during four storm events in each season (eight storms total) at primarily

two hour intervals and included at least one sample for each portion of the hydrograph (rise, peak, recession) (Figure 9).

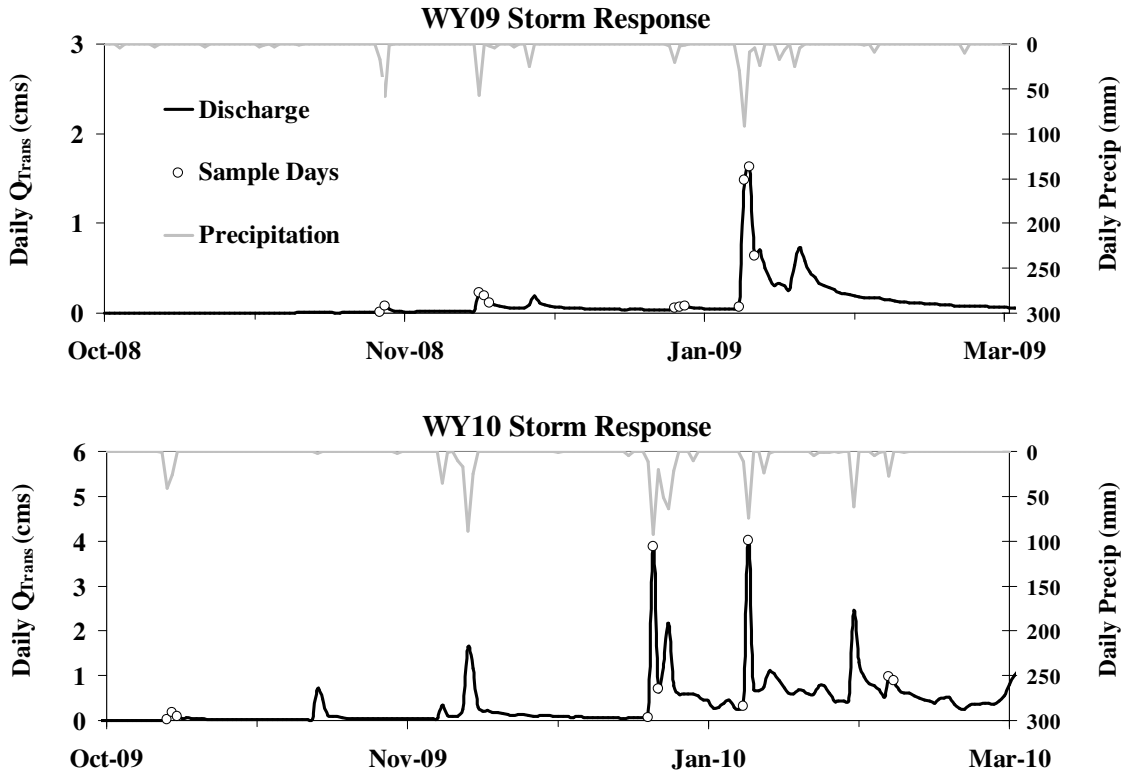

Figure 9. Daily discharge (bottom, black line) on the left axis and daily precipitation (top, grey line) during the storm seasons of WY09 (top) and WY10 (bottom) along with the sample days (open circle) of each season.

With each stream sample, measurements were also taken for dissolved oxygen (DO) using a handheld YSI 55 DO meter, and for temperature, pH, conductivity, and total dissolved solids (TDS) using a handheld pH meter by Hanna Instruments. All samples were stored on ice in the field until transported back to the lab, where they were processed and refrigerated at 4^{o}C (all samples processed and stored within 24 hours). The sampling regimes differed slightly between the pre and post-fire seasons due to safety restrictions and a shift in research objectives following the Station Fire. Efforts were made to sample every

storm with precipitation totals greater than 25.4 total mm. This was accomplished in WY09. As shown in Figure 8, two early season (December) storms and one late season (March) storms of WY10 were not sampled. However, the sample set includes the first and largest storms and spans the entire rainy season of each water year. Additional differences in the sampling between the pre- and post-fire season are discussed below.

WY09 (pre-fire) sampling was conducted at the watershed outlet collocated with USGS stream gage #11098000 over four storm events. A total of 131 samples were collected during the WY09 season; 101 250ml samples were collected for TSS analysis in HDPE bottles (triple rinsed in situ) primarily at hourly intervals. TSS was measured in all samples at UCLA using EPA Method 106.2. An additional 30 120ml samples were collected for trace metal analysis using acid washed Ichem bottles (triple rinsed in situ) at two-hour intervals during the four storms. The trace metal samples were left unfiltered, acid preserved (0.5% HCl), and stored at 4^{o}C until the occurrence of the Station Fire when they were sent to Caltest Analytical Laboratory and measured for total recoverable concentrations of: aluminum (Al), arsenic (As), cadmium (Cd), calcium (Ca), copper (Cu), iron (Fe), lead (Pb), magnesium (Mg), manganese (Mn), nickel (Ni), potassium (K), selenium (Se), sodium (Na), and zinc (Zn) by inductively coupled plasma/mass spectrometry (ICP/MS), following EPA Methods 200.8 Collision Mode.

WY10 (post-fire) sampling was conducted ~3 km downstream of USGS stream gage: Station #11098000 at the Millard Canyon Bridge due to safety constraints. A total of 108 samples were collected for TSS and trace metal (54 each) analysis during the post-fire WY10 storm season, at two hour intervals over four storm events (Fig. 8). All samples were collected in 250ml HDPE bottles prepared and provided by CRG Marine Laboratories. TSS

samples were measured at UCLA following EPA Method 106.2. Trace metal samples were left unfiltered and transported to CRG Marine Laboratories within 48 hours, where they were analyzed for total recoverable concentrations of: Al, As, Cd, Ca, Cu, Fe, Pb, Mg, Mn, Ni, K, Se, Na, and Zn by inductively coupled plasma/mass spectrometry (ICP/MS), following EPA Methods 200.8

3.2.2 Hydrologic Data Analysis

Fifteen minute discharge data were obtained from USGS Streamgage: Station #11098000 in the Arroyo Seco for the entire study period. Sampling at the downstream location during WY 2010 increased the drainage area from 41.44 km^2 to 47.10 km^2, and USGS discharge measurements were scaled by watershed area to account for increased flow at the downstream sampling location (Galster et al. 2006). Because of the flashy nature of this steep, semi-arid watershed, discharge is plotted in the transformed space (similar to log) (Hogue et al., 2000). The space transformation is as follows:

$$Q_{Trans} = \frac{(Q+1)^{\lambda}}{\lambda} \qquad eq.1$$

with $\lambda = 0.3$, where Q = discharge, and Q_{Trans} = transformed discharge.

One mm incremental and annual precipitation data were obtained from two High Sierra Electronics Model 2400 tipping bucket rain gauges located in close proximity to the Arroyo Seco operated and maintained by the Los Angeles County Department of Public Works (LADPW 2010). Theissen polygons were defined using the two LA county gages Clear Creek and Flintridge-Sacred Heart to calculate mean areal precipitation (MAP) over the watershed.

Runoff coefficients were calculated for both water years as well as for the individual storms sampled during each season. Annual runoff coefficients were calculated as the ratio of the total annual discharge per unit area to the annual MAP. For storm event runoff coefficients, the total storm discharge per unit area was divided by the total precipitation for each event. Storm discharge was assumed to begin with the onset of precipitation and continue until either another storm began or the point during the recession when flow remained at less than five times the pre-storm value for a two hour increment. Flood frequency analysis was calculated using USGS streamflow records from gage #11098000 of peak streamflow values from WY 1914-2008 and the Matlab Weibull function.

Chemical loads were estimated for each constituent for each sampled storm using measured chemical concentrations and 15 minute discharge data (scaled by area when appropriate). Loads were calculated for each storm using the following equation:

$$F = \sum C(t_i) \times Q(t_i) \qquad \textit{eq. 2}$$

Where F = output stream load from the watershed, $C(t_i)$ = constituent stream concentration at time interval i and $Q(t_i)$ = instantaneous stream discharge at i. Concentration and discharge measurements between each sample time were estimated by linear interpolation. Mass loads were divided by watershed area to facilitate comparisons of loads between storm seasons and to other systems as mass flux. Event Mean Concentrations (EMCs) were calculated as the ratio of the chemical load to total storm discharge, to provide a flow weighted mean of constituent concentrations during each event by dividing the mass load by storm volume.

In order to determine whether chemical concentrations in the samples exceeded water quality standards, measured chemical concentrations were compared to the acute Criteria Maximum Concentration (CMC) for Priority Toxic Pollutants set in the California Toxics

Rule for inland surface water (US EPA 2007). Acute CMCs are defined as highest concentrations to which aquatic life can be exposed for a short period of time (1-hour average) without deleterious effects (US Code § 131.36: Section 304(a)).

The US-EPA encourages developing site specific translators to convert from dissolved to total recoverable criterion but suggests that the conversion factors provided in the rule may be used as to represent a reasonable worst-case scenario (US EPA 1996) Using the relationships and coefficients provided in the rule, the CMC for the priority toxic pollutants measured in this study expressed in total recoverable concentration are as follows: As (360 µg/l), Cd (4.5 µg/l), Cu (14 µg/l), Pb (82 µg/l), Hg (2.1 µg/l), Ni (470 µg/l), Se (20 µg/l), and Zn (120 µg/l) (US EPA 2007).

Load duration curves were created for Cd, Cu, Pb, and Zn. A flow duration curve was created using 100 years of daily discharge data and multiplied by the calculated total recoverable CMC to estimate a maximum daily load. The EMC was applied to a 24-hour period to determine the daily load and plotted against the flow duration interval of the corresponding daily storm flow for each sampled storm.

3.3 Results and Discussion

3.3.1 Storm Discharge & Sediment

Although the Arroyo Seco Watershed experienced very different precipitation regimes during the two years of this study, the wildfire's impacts are evident when looking at individual storm events. The total annual precipitation of 460 mm for the uncharacteristically dry WY09 was only half that measured in WY10 (920 mm), when the total annual precipitation was closer to the long term (35 yr) average of 804 mm (+/- 524

mm). Both the WY09 and WY10 annual runoff ratios of 0.12 and 0.32, respectively, were within the range of variability of the watershed's long term (35 yr) runoff coefficient of 0.22 (+/- 0.14), indicating that the wildfire had a greater impact on storm response than the overall water balance. Comparing the individual storms of each season shows that the watershed's response to storms with comparable precipitation totals and intensities was highly impacted by the Station Fire (Table 3). With the exception of the first post-fire storm, a low intensity rain event, all of the runoff ratios of WY10's sampled storms ratios exceeded those of WY09 by at least a factor of two (Table 3). While other factors such as antecedent conditions (soil moisture) likely contributed to storm response in the Arroyo Seco, the largest, late season storms of each season clearly illustrate fire induced flooding. Post-fire peak flows, observed during WY10's January 17th (120 m^3s^{-1}) and February 5th storms (130 m^3s^{-1}) storms were 15 and 17 times that of WY09's largest, February 5th storm (7.65 m^3s^{-1}) and were produced with only 80% and 65% of the precipitation, respectively (Table 3). Further, flood frequency analysis conducted for pre-fire conditions in the Arroyo yielded return periods of 35 and 44.6 years for the peak flows of WY10's Jan 17th and Feb 5th storms, respectively, while the NOAA precipitation atlas identified both storms as > 2 yr events (Bonnin et al. 2006).

The increase in storm runoff following the fire was accompanied by a corresponding increase in sediment delivery. The median TSS concentration of all of the WY09 storm samples was 23.3 mg/l (ranging from 1.6 to 880 mg/l), while the median TSS concentration of the WY10 storm samples increased over 10-fold to 259.0 mg/l (ranging from 2.5 mg/l to 80,500 mg/l) (Figure 10).

Table 3. Storm characteristics for each studied storm, including runoff ratio and precipitation discharge parameters (average, peak and total).

	Runoff Ratio	Precipitation average (mm/15min)	Precipitation peak (mm/15min)	Precipitation total (mm)	Discharge average (cms)	Discharge peak (cms)	Discharge total m3
WY09							
Nov 25, 2008	0.004	1.41	3.92	75.92	0.06	0.28	12.79
Dec 15, 2008	0.018	1.18	2.96	56.87	0.21	0.48	47.75
Jan 22, 2009	0.023	0.69	2.87	25.54	0.06	0.08	26.74
Feb 5, 2009	0.094	1.44	5.85	130.94	1.81	7.65	568.24
WY10							
Oct 13, 2009	0.010	1.06	2.96	68.12	0.13	0.40	30.30
Jan 17, 2010	0.250	1.79	6.96	102.98	5.25	120.63	1187.02
Feb 5, 2010	0.371	0.99	7.59	84.82	5.39	130.82	1450.77
Mar 6, 2010	0.287	1.11	2.90	28.44	1.26	5.27	375.48

While these post-fire TSS concentrations are extremely high, they are not unheard of in semi-arid, flashy systems affected by wildfire. Researchers in the Jemez Mountains of New Mexico measured maximum TSS concentrations of 500,000 mg/l in post-fire storm runoff (Malmon et al. 2007). Additionally, the sediment load of the largest pre-fire storm (Feb 5, 2009) of 6.27 tons (t) was doubled in the first post-fire storm (Oct 13, 2009), and WY10's two largest storms (Jan 17, 2010 and Feb 5, 2010) each carried sediment loads of approximately 50,000 t. LADPW's reports of over 715,000 m^3 of sediment deposited into Devil's Gate Reservoir, a flood control structure located on the Arroyo Seco ~6 km downstream of USGS Streamgage #11098000, support these estimates (LADPW 2011). This is ten times the total volume deposited in the reservoir since its last cleanout in 1994 (LADPW 2011). The Arroyo Seco had experienced at least two major floods during this time period (El Niño years 1998 and 2005 yielded peak flows of 124.03 and 100.24 m^3s^{-1}, respectively), indicating that the sediment delivery to Devil's Gate Reservoir was a result of wildfire induced conditions, rather than flooding alone (LADPW 2011, USGS 2011).

3.3.2 Chemical Concentrations

Storm water chemistry in the Arroyo Seco varied greatly between different chemical constituent groups (trace metals and cations) reflecting differences in storm transport both prior to and following the Station Fire. Tukey's schematic box plots are used to present data distributions for all sampled constituents, and show the median, 25th and 75th percentile of metal concentrations observed over all sampled storms of each WY09 and WY10 rainy seasons (Figure 10). Both the magnitude and variability of the trace metal concentrations in Arroyo Seco's storm runoff increased following the Station Fire (Figure 10). The increase in the median concentration of all samples from WY09 to WY10 was over two orders of magnitude in Pb and Cd; over one order of magnitude in Al and Mn, and Zn; and nine, six, and four-fold in Cu and Ni, and Fe, respectively. A comparatively slight increase (< two-fold) was observed in the median As concentrations of the post-fire samples, while little change was noted in the Se concentrations. Other local studies have noted that As and Se are geologically sourced and tend to be enriched in local streams even under non-burn conditions (Yoon and Stein 2008). The trace metal enhancement is consistent with observations in the storm runoff of other semi-arid, burned systems, which authors have attributed to increased sediment delivery and release from vegetative storage (Gallaher et al. 2002, Leak et al. 2003, Smith et al. 2011). The greatest increases were seen in trace metals identified as priority toxic pollutants in the CTR, including Pb, C, Zn, and Cu. Although the Arroyo Seco is essentially undeveloped, concentrations of these constituents were higher than those observed the Los Angeles River during storm events and are in the range of those measured in channels draining highways, industrial areas, and mining operations (Thomson 1997, Blake et al. 2003, Tiefenthaler et al. 2008, Joshia and Balasubramanian 2010).

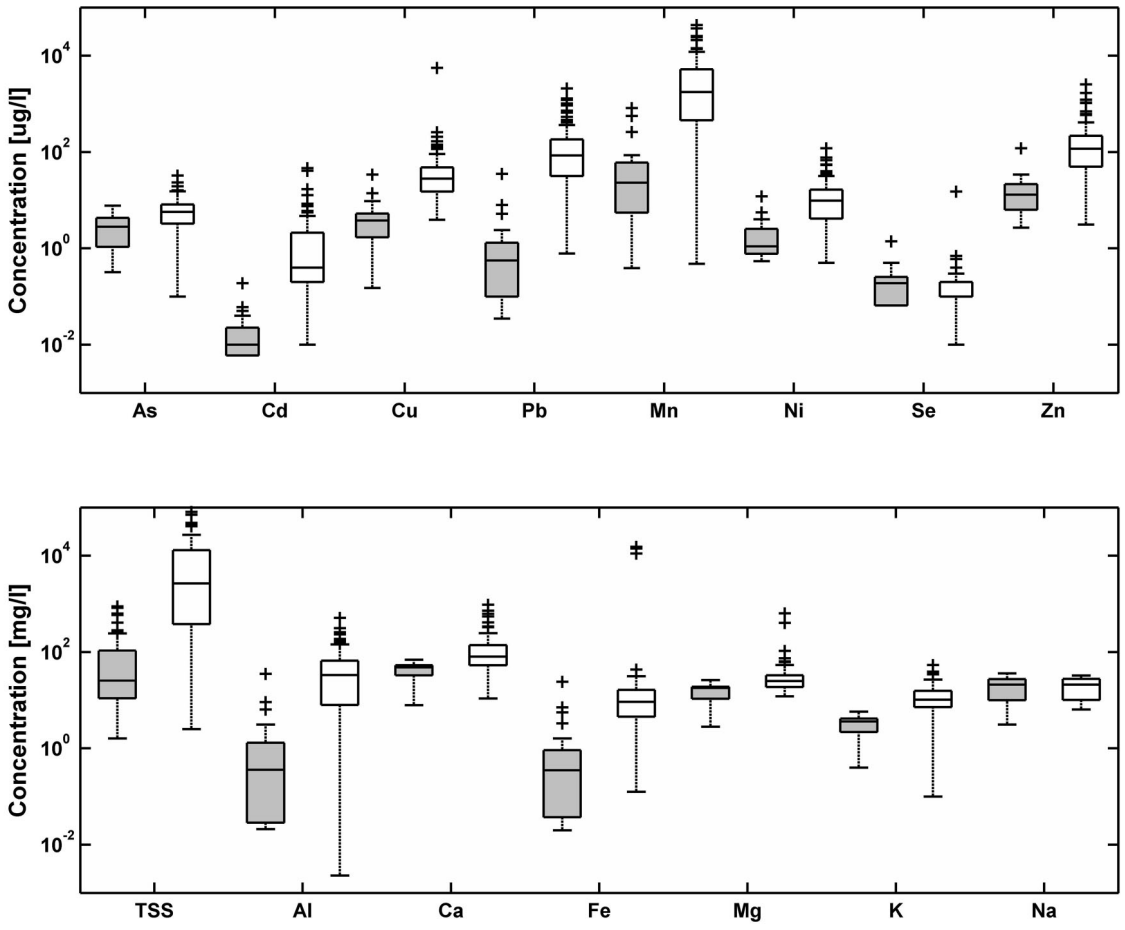

Figure 10. Tukey boxplots of the overall constituent concentrations for both the pre-fire year, WY09 (grey fill), and post-fire year, WY10 (no fill). The top and bottom edge of each box represents the 75th and 25th percentile, respectively, and the line bisecting the box represents the median.

Based on the limited studies of trace metals following wildfire, this behavior is not unique to our system, however the Pb concentrations measured in the Arroyo Seco were higher than those measured in other post-fire studies (Gallaher et al. 2002, Leak et al. 2003, Smith et al. 2011). We hypothesize that this is due to the study area's proximity to the Los Angeles basin as well as the potential for accumulation of anthropogenic Pb in the San Gabriel Range over the 60 years prior to the Station Fire.

Cation concentrations were also enriched in the post-fire samples though not nearly to the extent of most trace metals; however, unlike the trace metals, this was not accompanied

by increased variability (Figure 10). The median post-fire Mg, Ca, and K concentrations measured two, three, and four times pre-fire values, respectively. Other studies have noted elevated concentrations of these elements in post-fire storm runoff and attribute this to leaching of ash and partially burned litter on the forest floor as well as surface soil erosion (Debano 1979, Bitner et al. 2001, Ranali 2004). Prior to the Station Fire, all of these metals appear to have been primarily contributed by geologic weathering and transported in baseflow, as they tended to be diluted at high flows. The observed increase in the WY10 cation concentrations suggests both increased availability and alterations in the dominant transport mechanism of these constituents. Na was only the cation whose concentrations showed virtually no change from pre to post fire seasons (Figure 10). This is not surprising as Na was not likely to have been released from vegetation during the fire; other studies have noted that rainwater and bedrock geology are the major contributors of Na to local stream systems (Barco et al. 2008, Jung et al. 2009).

3.3.3 Intra-Storm Behavior

The Station Fire greatly impacted both the magnitude and timing of trace metal concentrations in Arroyo Seco's storm runoff (Figure 11). Prior to the fire, flushing was observed in most constituents throughout the entire rainy season, regardless of storm size. A typical first flush pattern was observed in WY09's Nov 25th (first) storm, where the highest concentrations of Pb, Zn, as well as TSS (not shown), occurred during the rising limb of the hydrograph, immediately following peak precipitation (Figure 11). Cd concentrations peaked even earlier, immediately following the first pulse in precipitation, while Cu exhibited its highest concentration on the hydrograph's falling limb. In WY09's Feb 5th (largest) storm,

the maximum trace metal (and TSS) concentrations occurred during the first rise in flow in every case, well before peak discharge. Following the fire, similar behavior was observed during WY10's first storm, which occurred on Oct 13th and was a low intensity rain event.

However, a shift in behavior was observed in WY10's Jan 17th storm and for the remainder of the post-fire season. Here, the highest trace metal concentrations coincided with peak discharge in every case (Figure 11). Cd, Cu, Pb, and Zn exceeded estimated CMCs during every sampled storm with the exception of Cd in final storm of WY10. The pre-fire storm data demonstrate that a relatively large storm was required to mobilize contaminants from Arroyo Seco prior to the Station Fire. While the post-fire data show that even small, low intensity events could significantly elevate trace metal concentrations; and, in larger storms at peak discharge, these metal concentrations could exceed water quality criterion by as much as 20-fold.

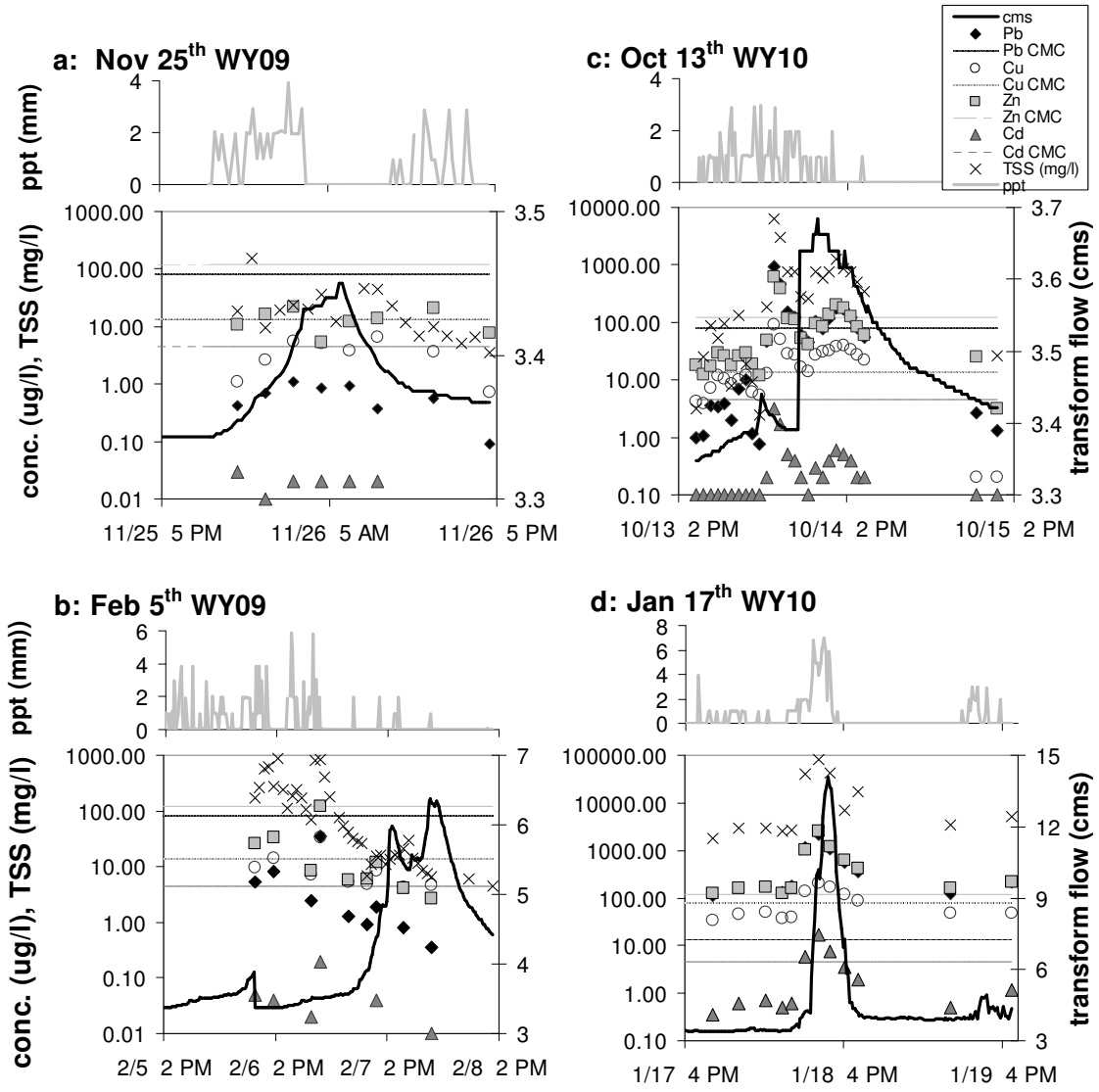

Figure 11. Precipitation (light grey line, top subplot), transformed discharge (black line, bottom subplot, right axis), TSS (grey cross), trace metal concentrations and water quality criterion (bottom subplot, left axis) for two storms sampled during WY09 (left) and WY10 (right). Trace metals shown include Pb (black diamond), Cu (open circle), Zn (light grey box), and Cd (dark grey triangle). Criterion are shown for Pb (black dashed line), Cu (black dotted line), Zn (light dashed line box), and Cd (dark grey dashed line) calculated using the variables provided in the CTR.

The pre-fire cation data supports work previously conducted in the Arroyo Seco, showing these to be primarily diluted during high flows; however, the post-fire data show a shift in behavior for many of these constituents (Barco et al. 2008, Wessel 2009) (Figure 12). Most cation and concentrations remained essentially constant throughout WY09 early season

storms, exemplified in the Nov 25th (first WY09 storm) pollutograph; although Ca, K, and Mg concentrations dropped slightly, while Na concentrations showed a slight increase as stormflow receded (Figure 12). During the Feb 5th (largest) storm during WY09, precipitation was sufficient to concentrate Ca, K, and Mg, and dilute Na (Figure 12). However, this storm also produced the lowest cation concentrations of the entire WY09 storm season with the exception of K. Following the fire, in WY10's Oct 13th (first) storm, the flushing behavior seen in the trace metals was also observed most cations, while Na concentrations peaked with discharge (Figure 12). In the WY10 Jan 17th storm, cation concentrations increased up to five fold and maximum post-fire concentrations occurred just prior to peak flow during this storm suggesting a shift transport mechanisms (Figure 12). In the case of Na, the initial flushing behavior was not observed again as it was diluted at peak flow in the Jan 17th storm and for the remainder of WY10. In fact, after the flushing of the first post-fire storm, the dilution behavior observed prior to the Station Fire was accentuated as overland flow became the dominant component in the large post-fire storms.

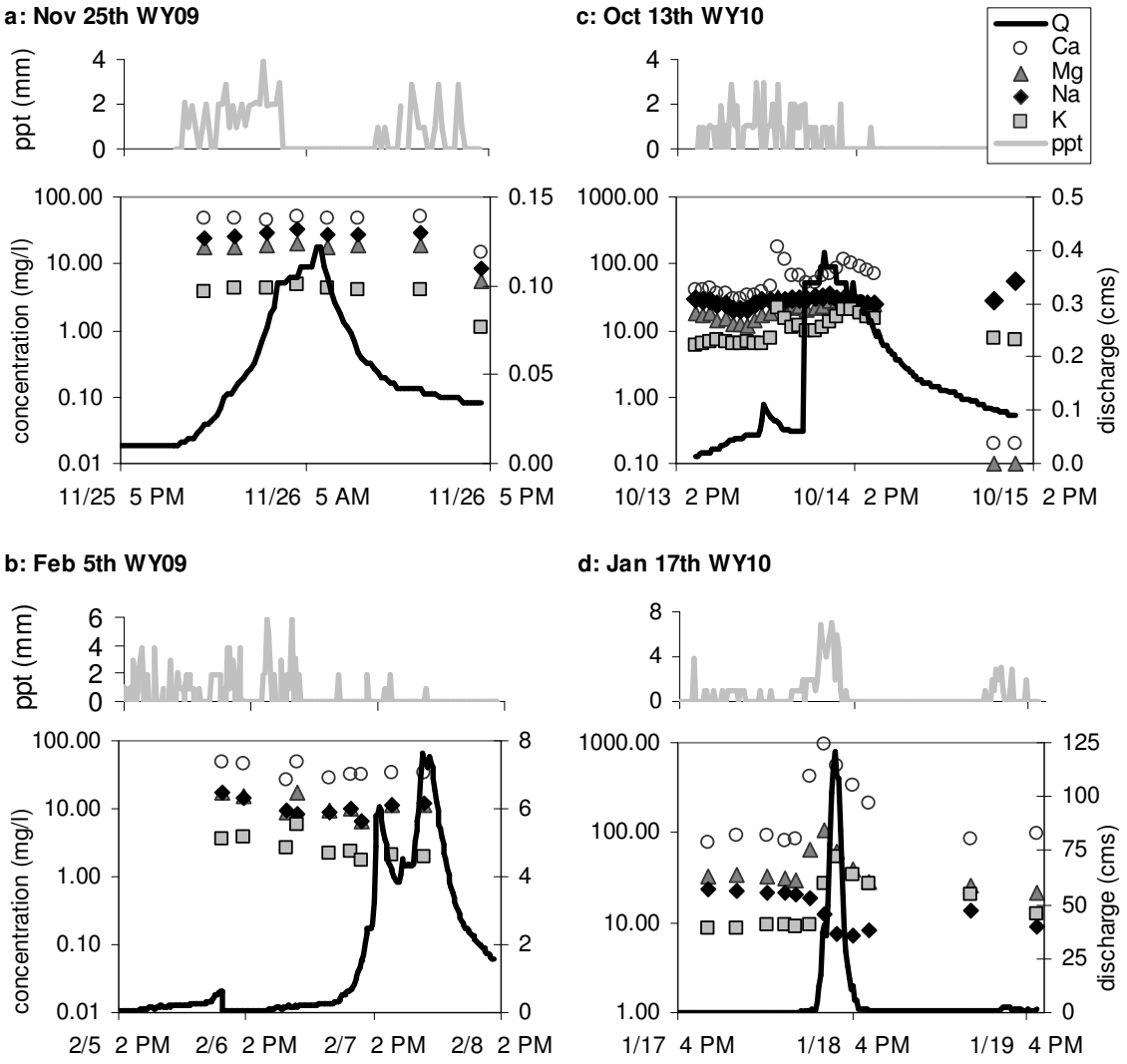

Figure 12. Precipitation (light grey line, top subplot), transformed discharge (black line, bottom subplot, right axis), and the weathering metal concentrations (bottom subplot, left axis) for 2 of the 4 storms sampled during WY09 (left) and WY10 (right). The metals shown include Ca (open circle), K (light grey box), Mg (dark grey triangle), and Na (black diamond).

3.3.4 Seasonal Distributions

EMC distributions demonstrate the Station Fire's combined impacts on storm discharge and the timing of chemical delivery affected seasonal patterns in the Arroyo Seco. Prior to the fire, most constituents (As, Cd, Fe, Mn, Ni, Na, Se, Zn), showed the highest EMC early in the WY09 rainy season (Nov 25th & Dec 8th storms) (Figure 13). This resembles other local urban-fringe systems where early season storms flushed out

constituents accumulated on the watershed's surface over the dry season (Yoon and Stein 2008). Discharge had a greater impact than seasonal flushing on Cu and Pb, which exhibited the highest EMCs in the WY09 Feb 5th (largest) storm, and on Ca, K, and Mg's whose highest EMCs occurred during WY09 Jan 9th (smallest) storm (Figure 13). It is also noteworthy that the EMCs of all constituents measured throughout WY09 remained relatively constant and rarely varied by more than a factor of two (Figure 13). Conversely, many of the post-fire trace metal and cation EMCs varied by over one order of magnitude, and, seasonal distributions closely resembled the distribution of the WY10 storm discharge, indicating that individual storm discharge had a stronger influence than early season flushing for most of the constituents (Figure 13). As seen in the pollutographs, maximum trace metal and cation concentrations corresponded to peak discharge, rather than preceding it (as in WY09). This, combined with the increased post-fire peak flows, greatly affected both the magnitude and distribution of the trace metal and cation WY10 EMCs. For most trace metals and cations, the increased post-fire concentrations were accentuated when weighted by flow. Increases of at least one and up to three orders of magnitude from the pre-fire year were observed in the trace metals, with the exception of Se which followed the flushing pattern observed in WY09 (Figure 13). Unlike Ca, K, and Mg, the pre-fire seasonal distribution of Na did not appear to be greatly impacted by the Station Fire, where the highest EMCs of both WY09 and WY10 occurred in fist storm of the season. Additionally, Na was the only measured constituent to show a decrease in EMC following the fire (Figure 13).

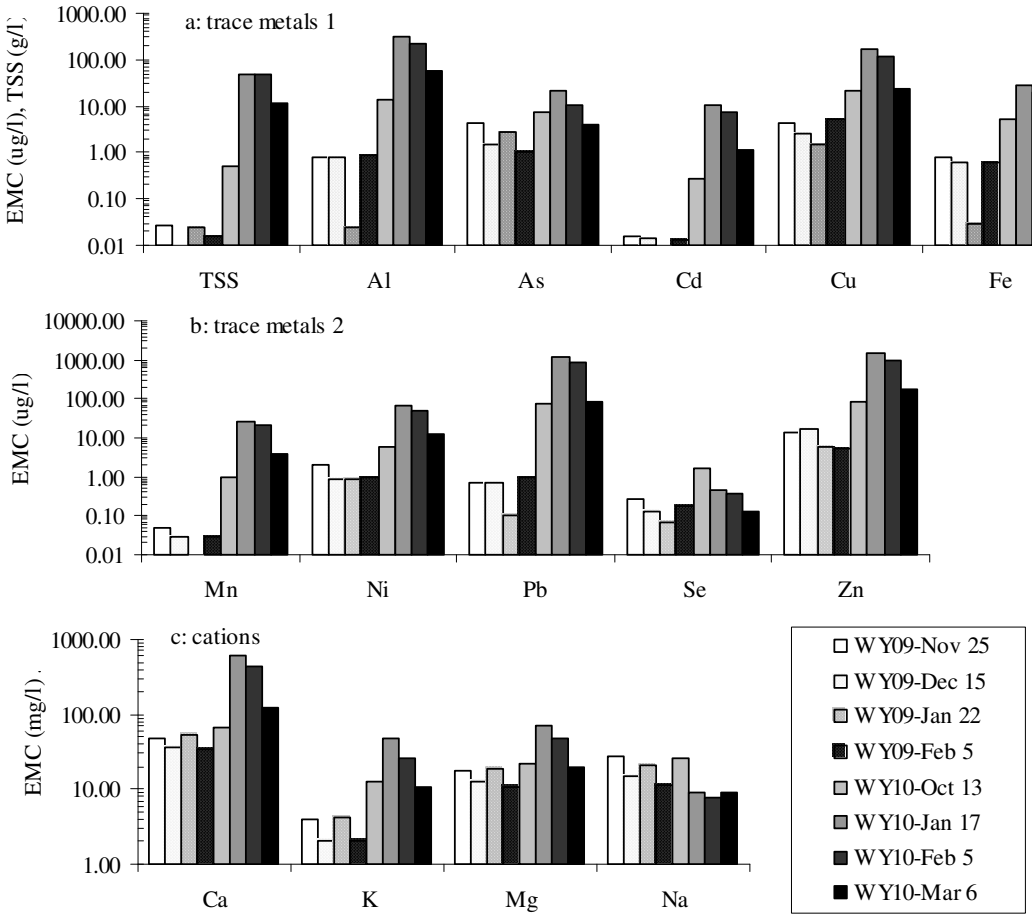

Figure 13. EMC values for trace metals (top), cations (bottom left) and anions (bottom right) for each storm of WY09 (dotted bars) and WY10 (filled bars). The trace metal EMC is in ug/l, while the anions and cations are in mg/l.

In both WY09 and WY10, the seasonal load distribution of the most of the measured constituents reflected the distribution of total storm discharge throughout each season; however differences in the magnitude of the mass flux between the WY09 and WY10 storms demonstrate the wildfire's impact on sediment and chemical loads (Table 4). Increased sediment delivery in the post-fire storms is accompanied by significantly enhanced trace metal flux (Table 4).

Table 4. Maximum concentration, Event Mean Concentration (EMC), and mass flux for each storm and averaged over each season for TSS, Cu, Pb, and Zn.

	WY09			WY10		
	max conc.	EMC	mass flux	max conc.	EMC	mass flux
TSS	(mg/l)	(mg/l)	(kg/km^2)	(mg/l)	(mg/l)	(kg/km^2)
Storm 1	156.88	25.78	2.47	6,375.76	517.40	298.55
Storm 2	NA	NA	NA	80,586.25	47,482.82	1,174,613.09
Storm 3	51.60	25.44	5.60	71,773.00	46,239.45	1,230,231.71
Storm 4	881.69	16.28	151.53	47,919.23	11,555.27	40,186.50
Season Avg	363.39	22.50	53.20	51,663.56	26,448.73	611,332.46
Cu	(ug/l)	(ug/l)	(g/km^2)	(ug/l)	(ug/l)	(g/km^2)
Storm 1	6.60	4.35	0.42	90.80	20.78	11.99
Storm 2	4.00	2.64	2.57	206.60	168.65	4171.97
Storm 3	2.30	1.44	0.32	256.20	113.96	3031.89
Storm 4	34.00	5.22	48.54	36.50	22.60	78.60
Season Avg	11.73	3.41	12.96	147.53	81.50	1,823.61
Pb	(ug/l)	(ug/l)	(g/km^2)	(ug/l)	(ug/l)	(g/km^2)
Storm 1	1.10	0.69	0.07	954.59	78.81	45.47
Storm 2	1.70	0.70	0.69	2,078.00	1,231.02	30452.64
Storm 3	0.11	0.10	0.02	1,286.00	830.71	22101.55
Storm 4	35.00	0.93	8.64	276.50	81.32	282.81
Season Avg	9.48	0.61	2.35	1,148.77	555.46	13,220.62
Zn	(ug/l)	(ug/l)	(g/km^2)	(ug/l)	(ug/l)	(g/km^2)
Storm 1	34.00	13.77	1.32	606.20	82.84	47.80
Storm 2	26.00	17.33	16.90	2,544.00	1,477.21	36542.81
Storm 3	15.00	5.97	1.31	1,670.00	956.29	25442.71
Storm 4	120.00	5.07	47.18	601.90	177.72	618.07
Season Avg	48.75	10.53	16.68	1,355.53	673.51	15,662.85

One (As, Cu), two (Al, Fe, Ni, Zn) and three (Cd, Mn, Pb) order of magnitude increases were observed in the trace metal fluxes of the largest pre (Feb 5th) and post-fire (Jan 17th) storms (Table 4). During the WY10 Jan 17th storm, fluxes of the US-EPA criteria pollutants Cd, Cu, Pb, and Zn were calculated to be 0.25, 4.17, 30.45, and 36.54 kg/km^2, respectively, and in the range of those observed in watersheds draining highly contaminated mining areas (Zak et al. 2009). Ca, K, and Mg fluxes were also all over one order of magnitude greater in the WY10 Jan 17th storm than in the WY09 largest storm. Because total discharge only increased by

two-fold, we hypothesize this increase also indicates a shift to particle facilitated transport resulting from the release of these cations from vegetative and soil storage during the fire.

3.3.5 Hydro-chemical loading and transport mechanisms

Load duration curves created for the metals that exceeded CMC estimates (Cd, Cu, Pb, and Zn) show that it was unlikely that water quality thresholds would be exceeded for any constituent other than Cu in typical storms of this watershed prior to the Station fire (Figure 14). However, conditions created by the Station Fire allowed for concentrations of these constituents to exceed water quality thresholds even during relatively small storms (Figure 14). The Arroyo Seco River discharges into the Los Angeles River which is listed as impaired for Cd, Pb, Cu, Zn, and Al pursuant to Section 303(d) of the Federal Clean Water Act. Barco et al. (2008) has shown the importance of considering urban-fringe watersheds, such as the Arroyo Seco, as an upstream source of chemical contaminants to downstream waters. This is particularly true following wildfire when pollutants previously stored in a watershed's vegetation and soil may be more readily transported to downstream waters.

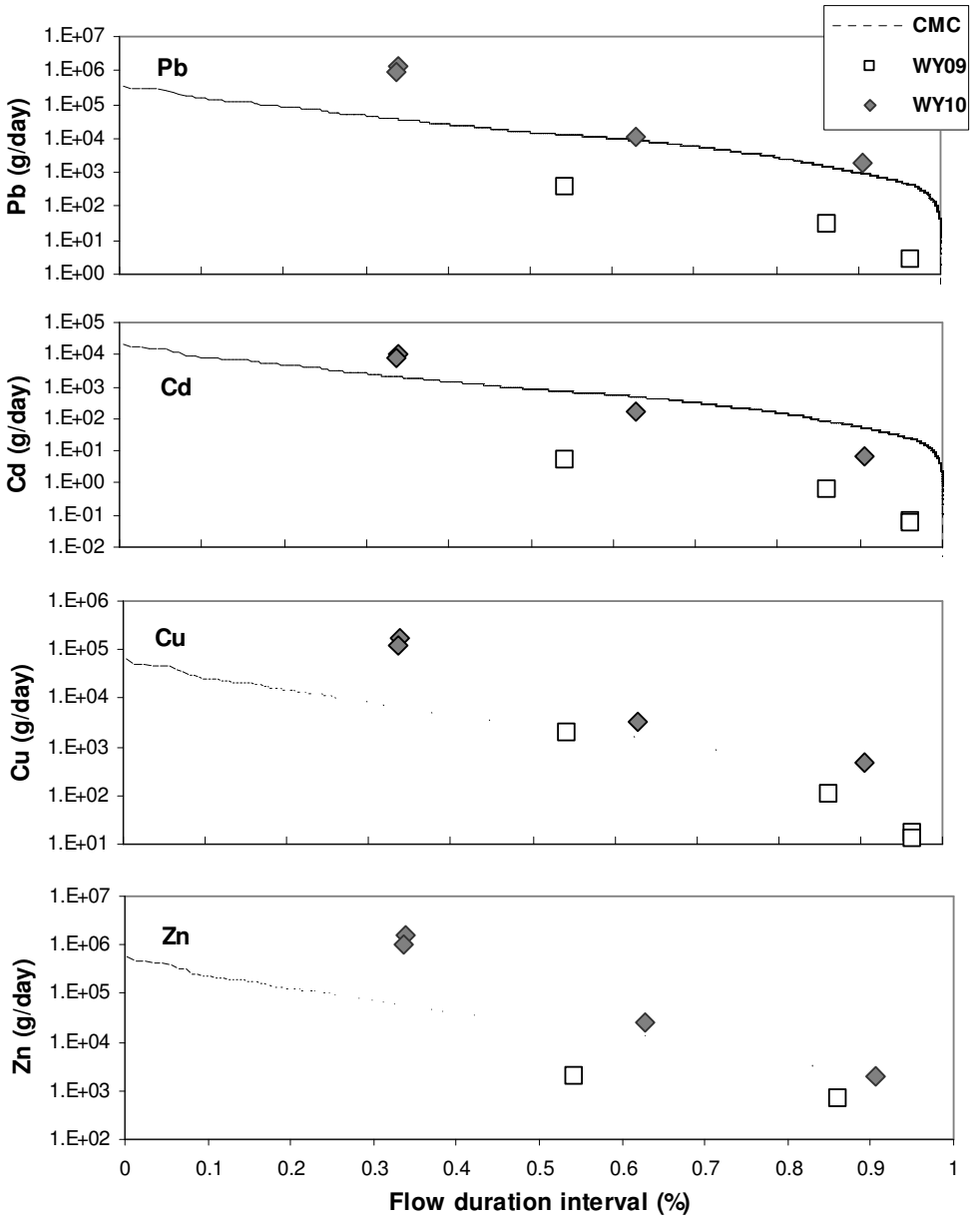

Figure 14. Load duration curves for Pb, Cd, Cu, and Zn. The EMC of each storm from WY09 (hollow square) and WY10 (solid diamond) were plotted against their flow duration interval found by matching the daily flow from each storm to its corresponding rank.

Correlations between constituent concentrations and instantaneous discharge, TSS, TDS help to elucidate fire-induced changes in hydro-chemical dynamics in the Arroyo Seco. The trace metals, exemplified by Pb, shifted from a negative to positive correlation to

discharge following the fire, while showing strong positive correlations TSS, and negative correlations to TDS in both the pre and post-fire samples (Figure 15). The post-fire trace metal samples show a vertical shift in the clustering of trace metal concentrations with respect to both discharge and TDS, while a more direct relationship is observed between increasing trace metal and TSS concentrations (Figure 15).

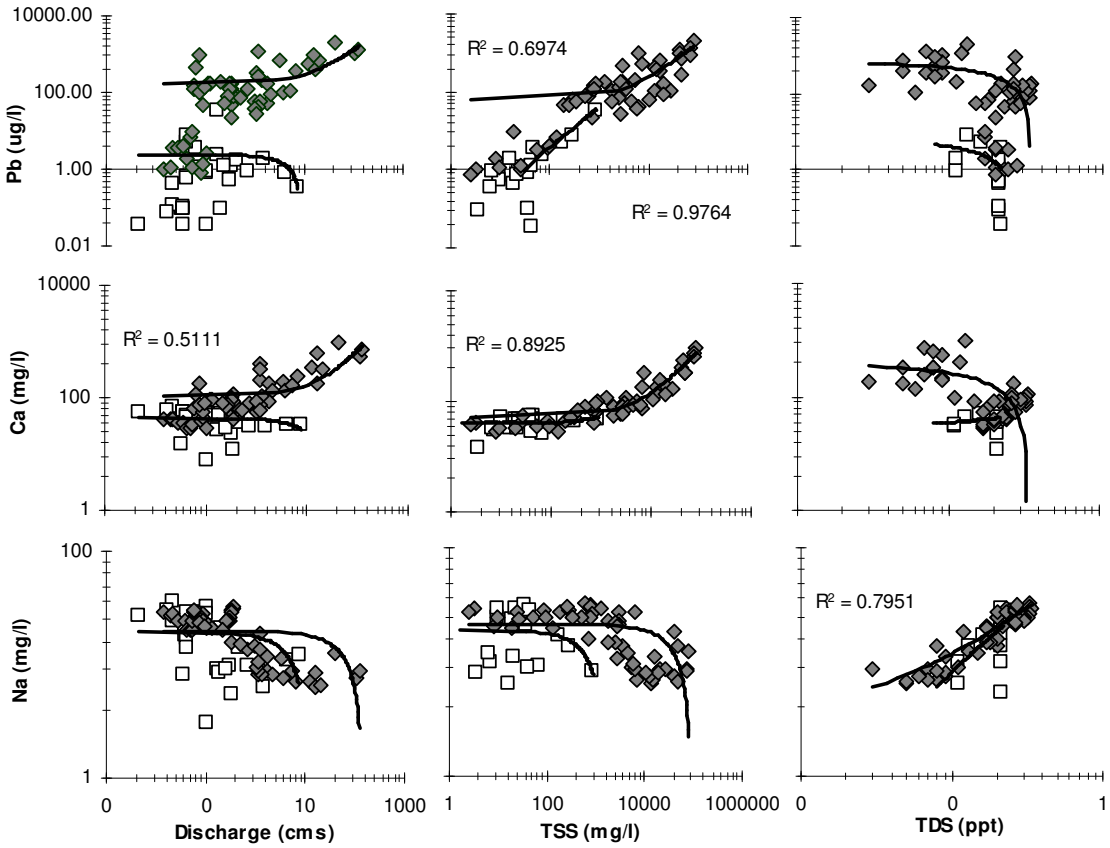

Figure 15. Constituent concentrations from each sample taken over WY09 (hollow square) and WY10 (solid diamond) plotted against instantaneous discharge (left), TSS (center), and TDS (right). R^2 values greater than 0.5 are shown for the WY09 (lower left) and WY10 (upper, right) samples.

Others have noted strong positive correlations to TSS and utilized these relationships to approximate metal transport as a function of sediment delivery (Thomson et al. 1997; Joshia and Balasubramanian 2010). Most of the cation concentrations (exemplified by Ca) remained relatively constant with respect to discharge, TSS and TDS during WY09 but

exhibited positive correlations to discharge, strong positive correlations to TSS, and a negative relation to TDS following the Station Fire (Fig. 15). In the case of Na concentrations, negative correlations to discharge and TSS and positive correlation to TDS that were observed prior to the fire, were enhanced in the post-fire samples (Fig. 15).

3.4 Summary

The Station Fire resulted in significantly higher peak flows, higher stream power, and higher sediment and chemical concentrations in the Arroyo Seco. While only the largest pre-fire storm was able to mobilize contaminants in the basin, even small post-fire storms were sufficient to yield concentrations that exceeded water quality criterion. The greatest changes were observed in trace metals, where concentrations of most constituents increased significantly following the Station Fire. Urban pollutants, such as Cd and Pb exhibited concentrations in the range of those observed in channels draining highways, industrial areas, and mining operations. Timing of chemical delivery shifted from the initial rise in flow to peak discharge in post-fire storms, which contributed to significant increases in storm EMCs and loads. For pre-fire conditions in the Arroyo Seco, variables such as seasonal timing, antecedent conditions appeared to be major factors in determining runoff chemistry for most measured constituents. However, following the Station Fire, peak discharge and especially sediment transport were the controlling factors in pollutant delivery, particularly for potentially toxic metals. Our results have significant implications for storm water management. Current treatments of storm runoff focus primarily on the early portion of storms to reduce mass loading of pollutants. However, new management strategies and treatment methods are needed for post-fire systems. The use of flood control structures that

retain sediment are likely the most effective (and available) means to mitigate detrimental impacts to downstream water quality. However, we advocate that in the future, the chemistry of captured sediment must be considered prior to disposal, especially in watersheds located near large urban centers.

Additionally, results from this chapter were used to guide the modeling efforts of Chapter 4, and metal-TSS-discharge relations obtained from this work were employed to provide initial estimates of seasonal post-fire contaminant loading from the Arroyo Seco watershed.

Chapter 4. Modeling Pre- and Post-fire Runoff and Loading at the Urban-Fringe

The third phase of this study focuses on applying results from the previous chapter to guide the development of a model that can simulate post-fire contaminant concentrations in storm runoff. This will facilitate our ultimate goal of providing water managers guidance on how to develop practical tools to predict post-fire loading from burned, urban-fringe systems. The previous chapter showed that chemical constituents with the greatest concentration elevation in storm runoff following wildfire were trace metals, which are often associated with particulate transport. Results from the previous chapter also provided the data to elucidate pre and post-fire TSS-discharge relations and trace metal-TSS relations for several trace metals listed as priority toxic metals in the Clean Water Act. In order to assess the Station Fire's impacts on water quality in varying temporal and spatial scales, The Hydrologic Simulation Program in FORTRAN modeling package (HSPF) was selected to model post-fire runoff from the Arroyo Seco watershed, and the aforementioned relations were used in conjunction with simulated discharge to estimate seasonal and annual chemical load delivery over the first post-fire rainy season.

4.1 Study area

The Arroyo Seco watershed is a small, urban-fringe basin located just east of in the Los Angeles, California in San Gabriel Mountain Range. The watershed is primarily within Angeles National Forest land and was entirely burned during the Station Fire in September of 2009. A detailed description of watershed characteristics and of the Station Fire can be found in sections 2.1 and 3.1, as it was included in the previous work on regional post-fire soil Hg analysis as well as the subject of pre- and post-fire loading analysis. The current

chapter provides a more qualitative description of characteristics that influence hydrological processes in the watershed and impacted model development decisions. The Arroyo Seco watershed is characterized by steep, mountainous terrain that is very responsive to precipitation. While the watershed's main channel, Arroyo Seco River has a relatively steep average slope, 5.7%, it receives water from several smaller tributary basins with slopes approaching 20% which greatly impact the watershed's rainfall-runoff response. Land cover in the watershed consists of chaparral (73%), coniferous forests (23%), grasses or barren land (4%), and small amount of developed area (primarily roads). The Arroyo Seco is dominated by chaparral, which is well adapted to Southern California's mediterranean climate of wet winters and long, hot, dry summers. Chaparral and other hardy, coastal desert vegetation found in the watershed have developed to not let water escape during sparse times, so litter from vegetation lends the soils a natural hydrophobicity which must be overcome before water can penetrate the soil. Watershed soils, though coarse, are also often very shallow; 76.7% (75.5% of chaparral cover, and 80.6% of forests) of the watershed's soils are classified in soil hydrologic groups C and D, which correspond to poorly and very poorly drained soils (SSURGO, 2012). The remaining watershed soils are classified in soil hydrologic group B, or moderately drained. This combination of factors results in a system where the primary runoff generation mechanism is infiltration excess. It also results in a "flashy" system that is very responsive to precipitation as is evident by Arroyo Seco's average time of concentration of 8.5 hours (Wessel, 2009). The addition of fire served to accentuate the flashy nature of the watershed by removing surface interception storage and surface roughness (i.e. vegetation) and increasing soil hydrophobicity. Additionally, the loss

of ground cover and root systems, and loss of soil cohesion destabilized soils, increasing the already high erosion potential (SSURGO, 2012).

4.2 Model selection and description

4.2.1 Model selection

The Hydrologic Simulation Program – FORTRAN (HSPF) was selected for modeling portion of this study for two primary reasons, widespread acceptance in the water quality management community and model versatility. The HSPF receives widespread endorsement and support as a regulatory tool at all levels of government, including national, state, and local. The model is supported by the EPA and is a core component of the Better Assessment Science Integrating point & Non-point Sources (BASINS) system, which was developed to support nationwide TMDL analysis (US EPA, 2001). It is also incorporates and integrates modeling tools developed by the USGS and is interfaced within the Army Corp of Engineer's Watershed Modeling Systems (WMS) (Skahill, 2003). The model has been used extensively to support water quality planning and management, as well as nonpoint source pollution and sediment erosion and transport analyses.

One of the most attractive features of HSPF is its flexibility. The model is designed to simulate water quantity and quality processes on a continuous basis over multiple land uses in both natural and man-made systems. Though it is technically a lumped parameter model, a watershed can be divided into up to 999 spatially homogenous land segments, allowing for a very detailed representation of watershed characteristics. HSPF can also be applied at a variety of spatial scales, with the option to divide larger watersheds into subbasins and output results at the endpoint of each subbasin's reach. This allows for model

applications to be developed for both pre and post-fire land cover conditions and the delineation of subbasins at scales small enough to capture the watershed's topography. Segmenting the model into smaller subbasins also provides modeled results at a range of spatial scales, which can then be extrapolated to topographically similar basins within the Station Fire burn perimeter. Additionally, an HSPF application can be as simple as a hydrologic model or as complicated as water quality model simulating in-stream process controlling the production and consumption of nutrients. In the current study, HSPF model applications will be developed to simulate pre- and post-fire hydrology, with the intention that the current results will be expanded and improved upon, with the addition of a sediment erosion and transport module to provide instream TSS concentrations. Ultimately, this will allow for the addition of a sediment erosion and transport module to provide instream TSS concentrations and for metal-TSS relationships to be specified within the modeling framework (Bicknell et al., 2005).

4.2.2. HSPF hydrologic model description

The hydrologic component of HSPF is based on the Stanford Watershed Model, one of the first computer models to update states, such as soil moisture, to simulate continuous hydrologic processes (Bicknell et al., 2005). In systems where the simulation of snow processes are not required (such as the Arroyo Seco watershed), precipitation and potential evaporation time series are provided as model inputs. Precipitation water is routed through and coincidentally evaporated from a series of storages that represent land surfaces, soil profiles, and groundwater reservoirs using functional relationships. The PERLND and IMPLND modules contain user specified parameters to define the storages and functional

relationships over pervious and impervious land areas (Figures 16, 17). Water can leave the storage zones through evaporation, percolation to another zone, or by exiting laterally to a downslope reach via surface runoff, interflow, or groundwater flow. This is shown in detail in the PERLND schematic (Figures 16, 17). The RCHRES module contains parameters to describe physical characteristics of a reach, which can either be a stream segment or reservoir. An FTABLE, which can be thought of as an extended rating curve, is defined for each reach to provide stage, surface area, and discharge relationships. Water is routed through the reach network to the watershed outlet using storage routing, or kinematic wave methods.

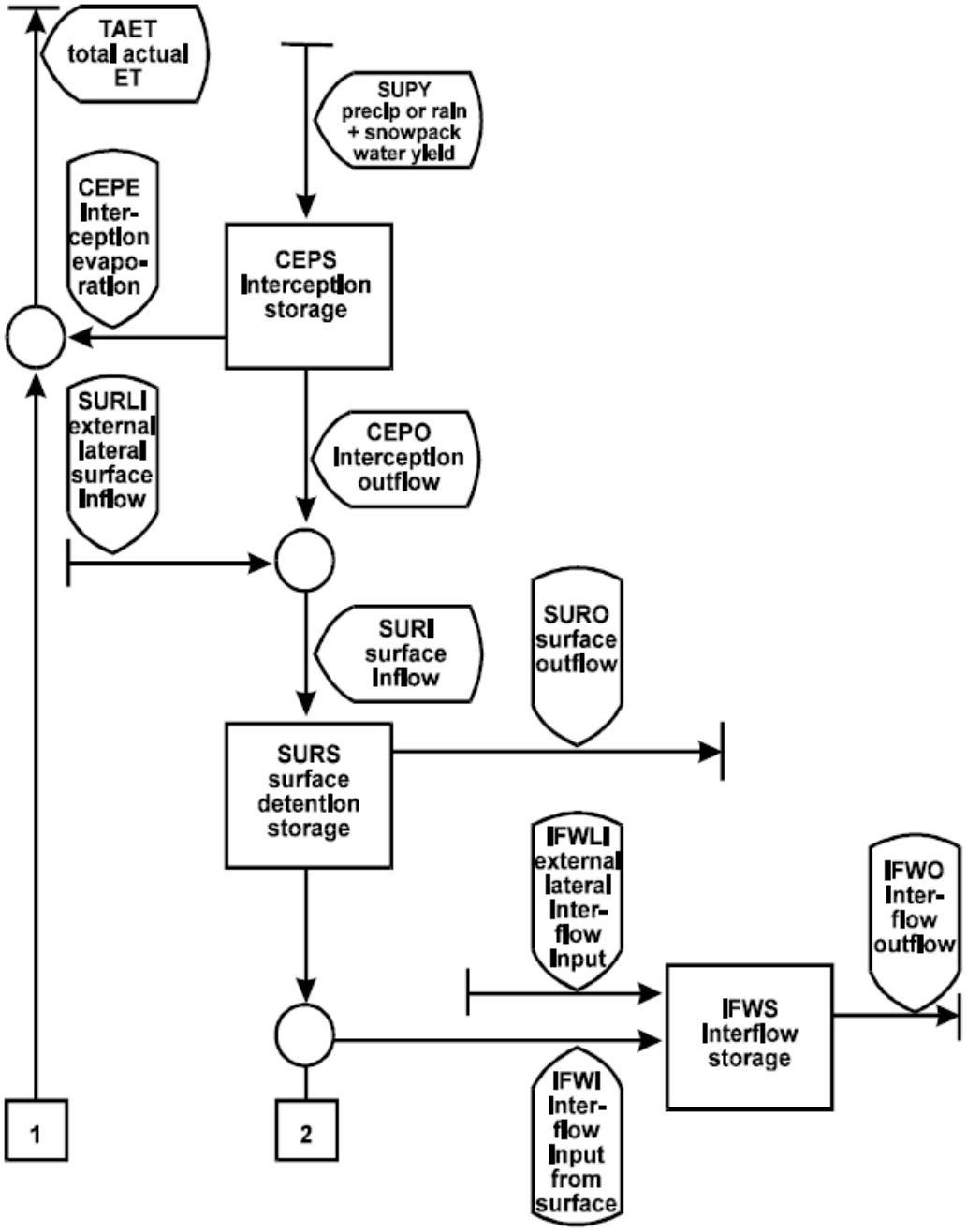

Figure 16. Schematic shoeing storages and fluxes are shown for the hydrology component of the HSPF PERLNDS module.

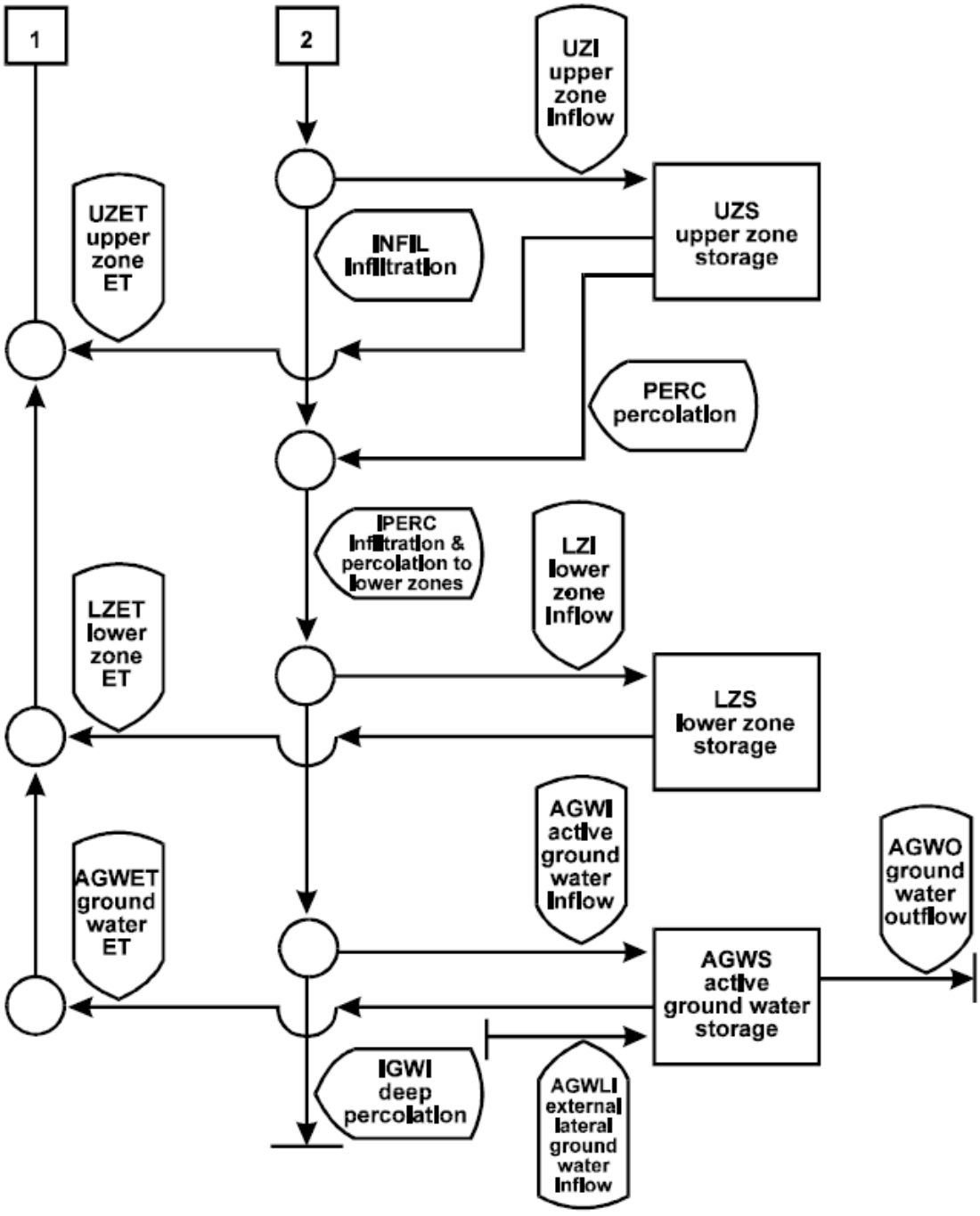

Figure 17. Schematic shoeing storages and fluxes are shown for the hydrology component of the HSPF PERLNDS module (continued).

Many of the user specified parameters in HSPF are based on watershed topography and once determined, are rarely adjusted. These will be discussed in the following section.

This section will describe the primary hydrologic parameters that define how the PERLND block stores and passes water through various zones and eventually out to a reach. The discussion will not be repeated for the IMPLND block, as is essentially a simplified version of the PERLND block. Because snow will not be simulated, the snow parameters within the PERLND block are not discussed. The primary hydrologic parameters in model calibration are interception storage (CESPC), infiltration (INFILT), the surface storage to interflow parameter (INTFW), nominal upper zone soil moisture storage (UZSN), lower zone nominal storage (LZSN), lower zone evapotranspiration (LZETP), interflow recession coefficient (IRC), groundwater recession (AGWRC), and the fraction of infiltrated water that recharges deep aquifers (DEEPFR) (Figures 16, 17). INTFW, LZETP, IRC, AGWRC, and DEEPFR are dimensionless. These parameters are defined in the remaining paragraphs of this section. The definitions of these parameters come from USEPA Technical Note 6 (US EPA, 2003).

CEPSC controls the amount of precipitation that is intercepted by plant surfaces and is eventually evaporated. Interception reduces the amount of water that reaches the ground surface, and therefore reduces potential runoff and soil moisture values. Values typically range from 0.01 to 0.40.

INFILT sets the rate that precipitation infiltrates into the soil. This parameter affects the peaks and valleys in the discharge curve by controlling the fraction of water that is available to potentially become subsurface flow. Low values result in higher peaks and shorter recession times, while higher values correspond to smaller peaks and slightly longer recession times. Values range from 0.01 in/hr to 0.25 in/hr.

INTFW is a coefficient that controls the amount of water that infiltrates into the ground from detention storage. This water becomes interflow, rather than upper zone storage

or direct overland flow. This parameter is especially important for the calibration of storm hydrographs. It can shift the timing of the hydrograph and change the magnitude of the hydrograph peak without affecting the total storm volume. Typical values range from 1.0 to 3.0, with lower values corresponding to sharper peaks.

UZSN is related to land surface characteristics, topography, and LZSN. This parameter has units of inches and represents a surface soil layer. Lower values of UZSN decrease the capacity of the upper zone of the soil profile to store water, and increase the amount of precipitation directed to overland flow. This, in turn, reduces the amount of water available for percolation deeper into the soil profile, hence the amount of water available for evapotranspiration from both upper and lower components.

LZSN determines how much soil storage is available to hold water after a storm. This parameter greatly impacts on transitions from wet to dry periods, and vice versa. Values for this parameter in semiarid regions can be estimated by taking one-quarter of the average rainfall plus four inches (USEPA, 2003). Final calibrated values are often lower than this. Typical values can range from 3.0 inches to 15.0 inches.

LZETP defines the opportunity for water from soil to be taken out of the system through evapotranspiration. High values of LZETP decrease the amount of water available for stream flow. Low values have the opposite effect. Typical values for forested areas range from 0.60 to 0.80.

IRC controls the rate at which interflow is discharged, and is a ratio of the current interflow discharge to that from one day earlier. Therefore it affects the shape of the receding limb of storm hydrographs. Water from both upper and lower zone storages is

available for interflow discharge. Values range from 0.30 to 0.85. Again, lower values are generally used for steeper hydrograph slopes.

AGWRC is a ratio of the current groundwater discharge to that from one day earlier. This parameter has the largest impact on how flows from large storm events recede or return to baseflow values, with lower values relating to faster recession rates. Typical values for the groundwater recession rate range from 0.92 to 0.99.

DEEPFR controls the percentage of the precipitation that percolates through the soil layer to recharge deep aquifers. Once this water enters the deep aquifers it becomes inactive for the remainder of the simulation.

4.3 Methods

The procedures used to develop model applications representative of both pre and post-fire conditions in the Arroyo Seco, and for applying these models to estimate post-fire pollutant loading are outlined in the following section. First, geo-spatial data were obtained and processed to delineate subbasins and determine parameters to representative of physical watershed characteristics under both baseline and burned conditions. Then, time series data were obtained and processed to provide model inputs and calibration information. Model applications were then calibrated by adjusting the primary calibration parameters listed above until acceptable agreement to observed discharge was obtained. Finally, the metal-TSS-discharge relations from the previous chapter were refined and applied to provide load estimates.

4.3.1 Geo-spatial representation

Extensive geo-spatial data were obtained and processed in ArcGIS in order to develop the HSPF model applications. The first steps in model development were to define the reach network, and determine and delineate the subbasins to be included in the model. The goals of this step were to accurately represent watershed topography in the watershed model applications. Watershed delineation was achieved by processing a twelve digit Hydrologic Unit Code (HUC-12) watershed boundary layer with a Digital Elevation Model (DEM) to delineate the upper basin of the Arroyo Seco River watershed so that the watershed outlet corresponded to the location of USGS Streamgage: Station #11098000. Next, an NHD flowlines layer was added, and tributary reaches were selected based on length, slope, and relief of the corresponding subbasin. The delineation process was repeated to define the model subbasins, which included five tributary and four main stem reaches. Reaches and subbasins were numbered so that each reach flowed into a higher numbered reach. Reach lengths and slopes as well as subbasin areas were calculated using the DEM and ArcGIS tools. This provided the data necessary to construct the RCHRES blocks and the basis for determination of many of the PERLND and IMPLND parameters. Parameters obtained in this step include: reach length (LEN, mi), change in reach elevation (DELTH, ft), and length of the overland flow surface (LSUR, ft) (Table 5). These data were also used along with cross sections collected by Professor Hogue's CEE 157L students to calculate FTABLEs for each reach.

Table 5. Explicitly represented reaches and model parameters for the RCHRES module of HSPF.

NHD Name	ReachID	NextDown	LEN	DELTH (ft)	LSUR
Colby Daisy	1	3	1.717	1715.88	161
Arroyo Top	2	3	2.677	1965.23	223
Upper Arroyo	3	4	1.771	675.86	361
Little Bear	4	6	2.006	2539.37	150
Bear Canyon	5	6	3.490	2503.29	229
Middle Arroyo	6	8	2.886	754.59	408
Long Canyon	7	8	1.449	1476.37	157
Lower Arroyo	8	9	2.188	173.88	479
Arroyo Out	9	999	1.550	242.78	449

Once model networks were determined, land cover and soil data layers were obtained from the National Land Cover Database and Soil Survey Geographic (SSURGO) Database. These were used to determine the important pervious (PERLND) and impervious (IMPLND) surfaces represented in the model. Based on the NLCD data, five distinct land cover classes were chosen to be represented in the model applications: 1) chaparral, 2) forest, 3) grass, 4) barren, and 5) developed land. The NLCD data layer simplified to represent the chosen land use classes and intersected with the model subbasins to determine the area of each land use category within each subbasin. These areas were input into the SCHEMATIC bock of the HSPF model applications to link them to the corresponding reach. Individual PERLNDs and IMPLNDs were numbered with the reach number in the tens place and the land cover number in the ones place. The SSURGO dataset was investigated using the Natural Resource Conservation Service's (NRCS) soil data viewer tool. Using this tool, data layers were created to show the hydrologic group and the erodibility index of soils within the watershed. Because the majority of watershed soils were classified as poorly to very poorly drained, and all of the watershed soils were classified as having very high erosion potential,

soil properties were not explicitly represented as unique categories in the PERLAND block. Rather, this information was taken into account when determining PERLND parameter values. Additionally, a Station Fire burn severity data layer was investigated to account for this metric when determining PERLAND parameters for the post-fire model.

4.3.2 Time series development

HSPF requires meteorological time series to effectively simulate the hydrologic processes within a watershed. Precipitation (PREC) and potential evapotranspiration (PEVT) were the minimum data requirements to drive the internal water balance. Additionally, historical stream flow data is necessary to inform parameter adjustment during and evaluate model performance during model calibration and to validate the calibrated model. A ten year simulation period, WY2000- WY2009, was established for the pre-fire baseline model. WY2010, the first water year following the Station Fire, was used for the post-fire model.

Hourly precipitation data were obtained from three High Sierra Electronics Model 2400 tipping bucket rain gauges located in close proximity to the Arroyo Seco watershed. These gauges are operated and maintained by the Los Angeles County Department of Public Works (LADPW 2010). Theissen polygons were defined using the three LA county gages Clear Creek, Camp Hi Hill, and Flintridge-Sacred Heart to calculate mean areal precipitation (MAP) over the watershed. The precipitation from the corresponding gage, or combination of gages, was assigned to each of the nine subbasins to achieve comprehensive precipitation distribution over the basin.

Hourly potential evaporation time series data were obtained from a California Irrigation Management Information System (CIMIS) station located in Glendale, CA. CIMIS calculates reference ET using a version of the Modified Penman Equation.

Fifteen minute discharge data were obtained from USGS Streamgage: Station #11098000 for comparison to simulated discharge for water years 2000-2010. These data were aggregated to by averaging over an hourly time step.

All time series data were imported into the HSPF's Watershed Data Management Utility (WDMutil) where they could be accessed by the model. The model was also programmed to write simulated discharge to the WDMutil where it could be processed and evaluated or exported for analysis using other software tools. Models were run at an hourly time step and were set to output time series at hourly, daily, and monthly intervals.

4.3.3 Model calibration and validation

Four steps were used to calibrate the hydrologic components of the watershed model. In the order of application, these steps include establishing annual and monthly water balances, adjusting low and high flow distribution, and adjusting storm hydrograph shape. The calibration parameters involved in each step were adjusted until corresponding statistics met acceptable performance criteria, and the entire process was repeated until desired criteria were met. Performance criteria were calculated using Matlab scripts provided by Seth Kenner of RESPEC Consulting and Services Inc., and employ numerous error statistics including: Pearson's correlation coefficient (r), coefficient of determination (R^2), Nash-Sutcliffe efficiency (NSE), mean error (ME), percent mean error (% ME), mean absolute error (MAE), and root mean square error (RMSE). Additionally cumulative frequency

distribution curves and annual, monthly, and storm runoff plots were created to visually compare observed and simulated discharge. The baseline model was both calibrated and validated on 4 years of continuous data, including water years 2002-2005 and water years 2006-2009, respectively.

Table 6. Initial and final calibrated PERLND parameters of the pre-fire model application and adjustments made in the calibration of the pos-fire model application are shown for the predominant land use classes in Reach 1.

	Initial		Pre-fire		Post-fire	
	Chaparral	Forest	Chaparral	Forest	Chaparral	Forest
FOREST	0.8	0.8	0.8	0.8	0	0
LZSN	6.5	6.5	**15**	**15**	**15**	**15**
INFILT	0.16	0.16	**0.25**	**0.3**	**0.07**	**0.07**
LSUR	161	161	161	161	161	161
SLSUR	0.15	0.15	0.15	0.15	0.2	0.2
KVARY	0	0	**0.12**	**0.12**	**0**	**0**
AGWRC	0.98	0.98	**0.988**	**0.988**	**0.995**	**0.995**
PETMAX	40	40	40	40	40	40
PETMIN	35	35	35	35	35	35
INFEXP	2	2	2	2	**3**	**3**
INFILD	2	2	2	2	2	2
DEEPFR	0.1	0.1	**0.2**	**0.2**	**0.2**	**0.2**
BASETP	0.02	0.02	**0.02**	**0.02**	**0.02**	**0.02**
AGWETP	0	0	**0**	**0**	**0.02**	**0.02**
CEPSC	0.1	0.15	***0.09***	***0.14***	***0.06***	***0.09***
UZSN	0.07	0.08	***0.51***	***0.70***	***0.63***	***0.73***
NSUR	0.25	0.25	**0.25**	**0.25**	**0.05**	**0.05**
INTFW	1.7	1.7	**1**	**1**	**1**	**1**
IRC	0.7	0.7	***0.44***	***0.44***	**0.3**	**0.3**
LZETP	0.5	0.6	***0.66***	***0.66***	***0.66***	***0.66***

The parameter adjustments and described effects on the simulated runoff are summarized below. Initial and calibrated model parameters are listed in Table 6 for PERLNDS 11 and 12 (i.e. the watershed's predominant land use classes, chaparral and forest, in subbasin one).

The annual water balance was established using the primary calibration parameters INFILT, LZETP, LZSN, UZSN, and DEEPFR, as well at two other evapotranspiration parameters BASETP and AGWETP. The total simulated runoff was increased or decreased by increasing or decreasing these parameters, respectively. All of these parameters were increased from their original estimated values in order to account for water losses in the Arroyo Seco. Increases in INFILT allowed more water to infiltrate to the upper and lower zones where it could then be lost to evaporation or deep groundwater storage. Higher LZETP values allowed for more evapotranspiration from the lower zone, which is the predominant soil storage component. Consequently, increases in LZSN created more opportunity for evapotranspiration from lower zone soil moisture storage and reduced total runoff volume. Likewise, higher UZSN values created more opportunity for evapotranspiration to occur in upper zone soils and reduced the total runoff volume. Higher DEEPFR allowed more infiltrated rainfall to be lost to deep groundwater aquifers. The parameters BASETP and AGWETP were also increased to represent evapotranspiration from baseflow and active groundwater, respectively. LZSN and DEEPFR were eventually set to their maximum values, and were further refined on a monthly basis as described below.

The monthly water balance was established by adjusting the AGWRC, and monthly UZSN, monthly LZETP, and monthly CESPC parameters. AGWRC is described as the previous day's baseflow that contributes to the current day's runoff. In other words, it is the ratio of base flow at the current time step divided by the baseflow at the prior time step. Higher AGWRC values shifted baseflow to a later time step, flattening the base flow recession curve. UZSN was adjusted on a monthly basis to account for properties such as natural hydrophobicity and seasonal differences in soil permeability and storage properties.

This parameter was increased during the winter months to account for increased soil moisture storage potential over the rainy season. Monthly values of LZETP were input into the model to account for seasonal vegetation growth, and were raised or lowered on a monthly basis to increase or decrease reduce runoff for the desired month, respectively. This essentially accounts for the difference between potential and actual evapotranspiration and is especially important in semi-arid watersheds, such as the Arroyo Seco, where less water is available for evaporation during the dry summer months when the potential for evapotranspiration is at its highest. Interception storage capacity was also adjusted by increasing CESPC during the spring months to account for new vegetation growth following the winter rainy season.

Low flow and high flow distributions were adjusted with INFILT, AGWRC, and KVARY. INFILT was increased to shift runoff from storm flows to baseflow and vice versa. AGWRC was increased in order to decrease baseflow recession and achieve the long recessional flows that characterize the Arroyo Seco. Decreasing KVARY shifted the baseflow drainage from shortly after wet periods to dry periods to maintain baseflow volumes during the dry summer period. The storm hydrograph shape was adjusted with IRC and INTFW. Decreases in IRC and INTFW increased peak flows without affecting the total storm volume. IRC parameter was also distributed monthly to allow for sharper hydrographs in early season storms.

The pre-fire model was adjusted to represent post-fire conditions primarily by increasing AGWRC and KVARY, and by decreasing INFILT, INFTW, and IRC. IRC was set to its lowest possible value; hence monthly values were not used. Two additional parameters that are not normally used in the calibration procedure were employed in an attempt to capture peak flow variability of the burned system. These include the infiltration

exponent, INFEXP, and NSUR, which represents surface roughness (akin to Manning's n). INFEXP is typically set to a default value of 2 but was increased to its maximum possible value of 3 to decrease infiltration. NSUR was set to the lowest possible value of 0.5.

4.3.4. Relationship refinement and load calculations

As discussed in the previous chapter, relationships between TSS and individual trace metal concentrations in pre- and post-fire storm runoff samples were developed for metals of concern in the Arroyo Seco. The applicability of logarithmic and power functions were also investigated but did not perform as consistently as the simple linear regression. Additional trace metal-TSS relations were calculated using a linear regression to include all of the metals for which impairments exist in the Los Angeles River downstream of its confluence with the Arroyo Seco. These metals include: Al, Cd, Cu, Pb, and Zn.

Because only initial model development was undertaken in this phase of the study (hydrologic modeling), the TSS outputs needed to employ these relationships and simulate post-fire loading was not available. Hence TSS-discharge relations were developed from observational data to determine TSS concentrations as a function of discharge. TSS-discharge relations in the pre-fire samples were relatively poor and were not employed, and it was determined that the sediment module must be completed before pre-fire metal concentrations could be simulated. For the post-fire samples, the TSS-discharge relations were combined with the developed trace metal-TSS relations to simulate daily, monthly, and seasonal metal loading from the Arroyo Seco watershed using both observed and simulated discharge. Trace metal-discharge relations were also determined and used to calculate loading to determine whether or not a more direct calculation would perform better than the

extrapolation. Daily results were compared to previously calculated storm event mean concentrations (EMCs), and seasonal results were compared to an average of all samples collected over the WY 2010 storm season. An exact match was not expected, since the WY 2010 concentrations were all obtained during periods of high flow. Rather these comparisons were made to ensure that the relationships provided reasonable estimates.

4.4 Results

4.4.1 Calibrated baseline hydrology model

The developed pre-fire baseline hydrology model does an acceptable job of simulating discharge in the Arroyo Seco watershed. Excellent r, R^2, and NSE values were achieved indicating that the model did especially well capturing high flows during the calibration period. The remaining error statistics, though acceptable, show that there is still room for model improvement in the simulation of total runoff volumes. The model still performs well when applied to the validation period but statistics are slightly poorer. R^2, and NSE values drop from 0.96 to 0.81 and 0.80, respectively, and the percent mean error increase by approximately 20% (Table 7).

Table 7. Model fit statistics for the pre-fire baseline model application over both the calibration and validation periods.

	Calibration Period WY 2002 - WY2005		Validation Period WY 2006 - WY2009	
Model-fit statistic	Daily	Monthly	Daily	Monthly
Number of years, months, or days	1461	48	1461	48
Correlation Coefficient (r)	0.98	0.99	0.90	0.91
Coefficient of determination (R^2)	0.96	0.98	0.81	0.82
Nash-Sutcliffe efficiency (NSE)	0.96	0.98	0.80	0.75
Mean error (cfs)	1.62	1.56	1.85	1.86
Percent Mean Error (%)	11.15	10.60	39.77	39.77
Mean absolute error (cfs)	5.04	2.97	3.45	2.85
Root mean square error (cfs)	19.25	6.74	9.43	4.98

Further investigation shows that the time period selected for model calibration and validation were subject to very different precipitation regimes. This is unfortunate, but it can still provide insight into model performance in the watershed under varying climate patterns.

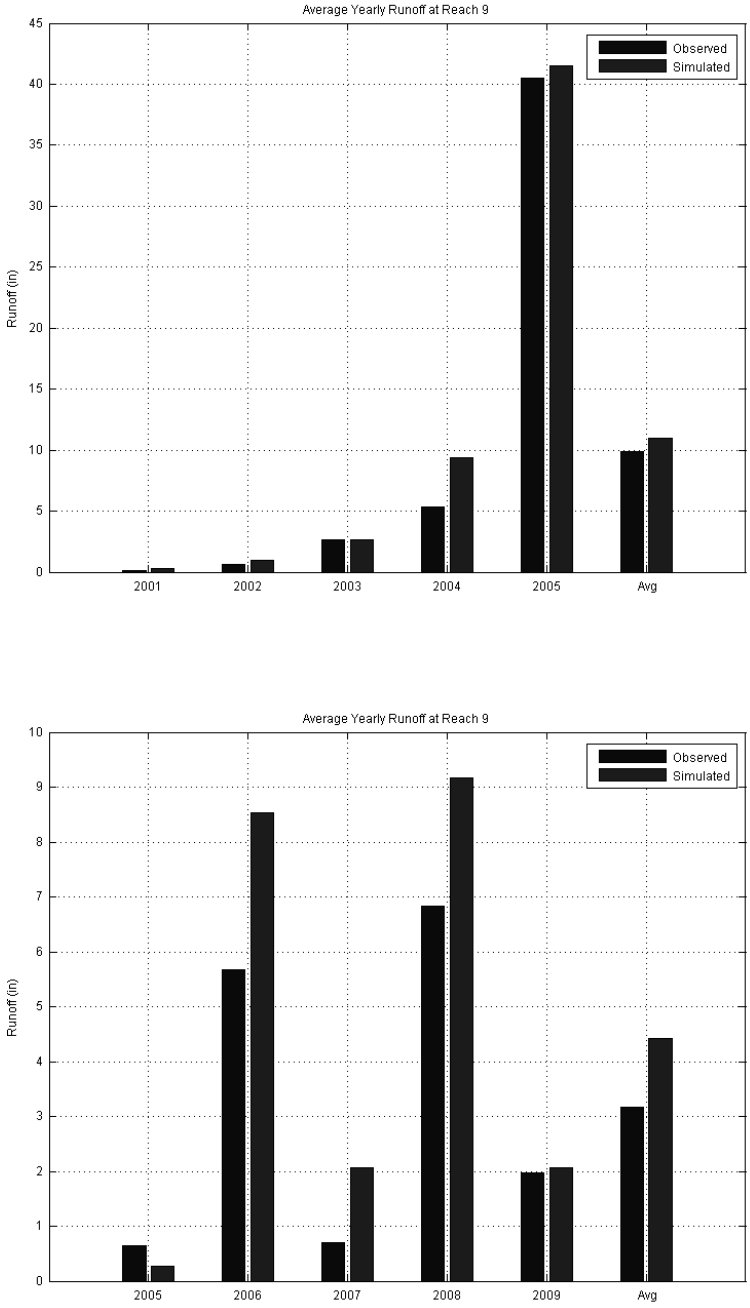

Figure 18. Annual observed (left) and simulated (right) discharge is shown for the pre-fire baseline model for the calibration (above) and validation (below) periods are shown.

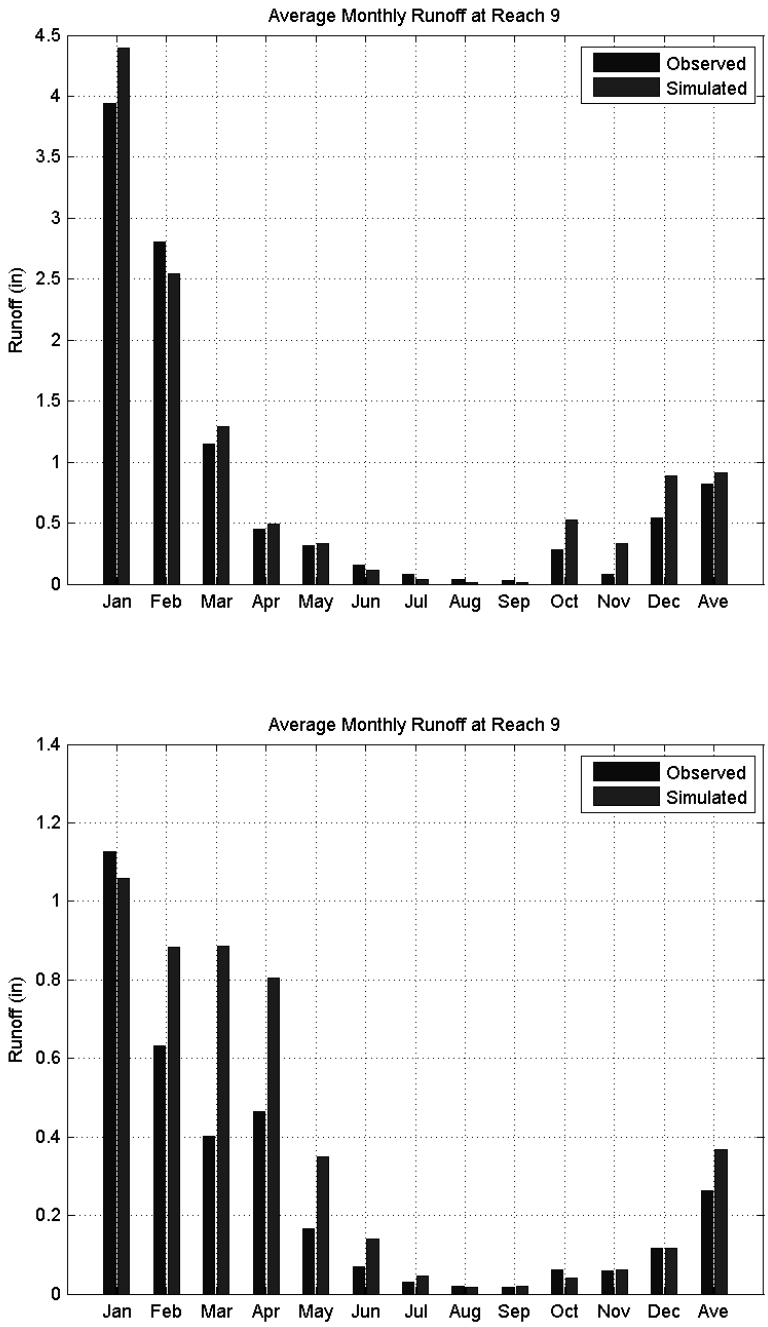

Figure 19. Monthly observed (left) and simulated (right) discharge for the pre-fire baseline model for calibration (above) and validation (below) periods.

Figure 18 shows that the model consistently over-simulates discharge. The calibrated model (top) achieves a good overall water balance during WY 2005, an El Nino year, while

the water balance representation for the rest of the time period is similar to that of the validation period. Based on the overall water balance plots, it appears as though model performance during the calibration period is controlled by one extremely wet year, and that poorer performance observed during the validation period is related to the drier conditions of this time period.

Again, the monthly water balance plots look much better for the calibration period, especially during the spring months (Figure 19). This can most likely be attributed to a good simulation of large winter storms and the long recessional flows that characterize the Arroyo Seco during wetter periods (i.e. El Nino year). However, it can also be seen that acceptable values are achieved for the summer months during the drier validation period, and the model appears to perform better in extreme conditions. These plots also show that the model could be improved by refining the monthly storage, recession, and evaporation parameters.

Further insight can be gained by comparing how the model simulates both large and small storms during each simulation period. Figure 20 shows the wettest years of both the calibration (top) and validation (bottom) simulation periods plotted, at a daily time step. First, although the model did not perform equally well in simulating the magnitude of these storms, the storm timing was simulated rather well in both cases. The model did an excellent job simulating the El Nino year storm (WY 2005). However, while the model was unable to simulate the peak of WY 2008's largest storm. Recessional flows were over simulated in both cases. The most obvious difference here in is in the magnitude of the two observed storms, where the storm peak of the WY 2005 was approximately 10 times that observed in WY2008. The HSPF model is designed to simulate storm flow through saturation excess, rather than the infiltration excess processes, that normally occur in the Arroyo Seco. In the

case of the El Nino year, surface soils were likely fully saturated allowing the model to perform as it was intended. Another likely contributing factor is the temporal scale of the precipitation input.

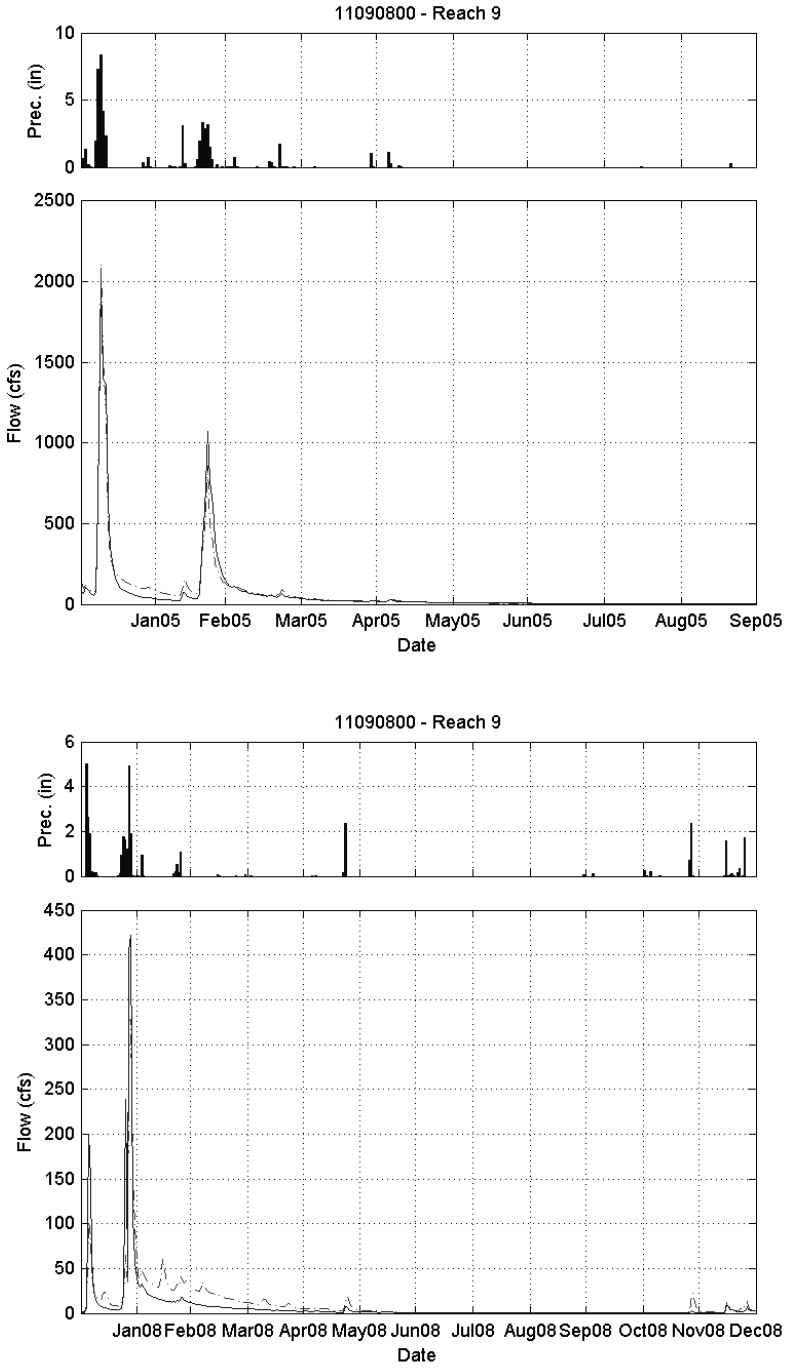

Figure 20. This figure shows daily observed (solid) and simulated (dashed) discharge hydrographs and hyetographs for the wettest years of the calibration (above) and validation (below) periods.

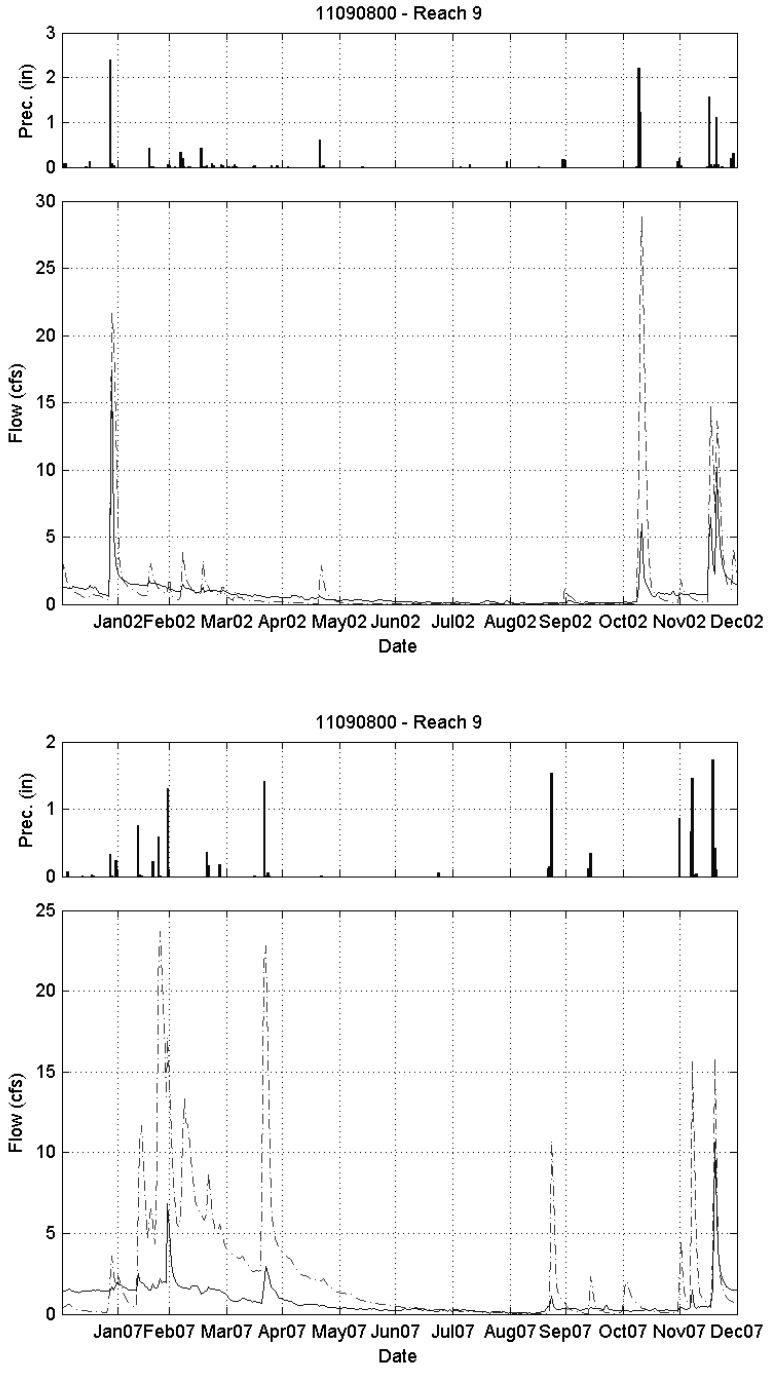

Figure 21. This figure shows daily observed (solid) and simulated (dashed) discharge hydrographs and hyetographs for the driest years of the calibration (above) and validation (below) periods.

The WY 2005 storm was a result of a prolonged rain event, or series of events, while the WY 2008 storm resulted from a shorter duration, higher intensity event. Running the model at a higher temporal resolution would likely improve its ability to simulate peaks of smaller storms as well as overall performance.

Daily observed and simulated discharge for the driest years of the calibration (top) and validation (bottom) periods are shown in figure 21. Both years show that the model over simulates very small storms. While the simulation of the magnitude of these storms is poor, the timing is captured very well. A better fit could be achieved by lowering the infiltration parameter INTFW to allow more water to infiltrate the soil and reduce hydrograph peaks. However, this would reduce the peaks for larger storms as well, which the model already has more difficulty simulating. For the purpose of this study, we advocated that it was more important to simulate peak flow than low flows, and this parameter will not be adjusted.

Overall the pre-fire baseline hydrology model provides very acceptable discharge simulations. The model captures very large storms very well and large storms reasonably well, while small storms are over simulated. While it would be preferable to be able to simulate all storm conditions, we note that it is more optimal to be able to represent large storms than small storms, as they have a greater impact on contaminant loading. Moreover, storm timing is well represented regardless of storm size. Improvements could likely be made by refining monthly parameters and running the model at finer temporal resolutions.

4.4.2 Calibrated post-fire hydrology model

The HSPF model application was adjusted to represent post-fire conditions primarily by adjusting parameters to reduce infiltration, surface roughness, and interception. This post-fire model application did not perform as well as the pre-fire baseline model. The r, R^2, and NSE values show that the post-fire model was not able to capture high flows as adequately as the pre-fire model. Monthly averages showed a better fit to performance criteria error statistics, indicating that this model may be acceptable enough to provide rough seasonal estimates (Table 8). However, only a 12 month period was used in these calculations, so the small sample size likely influenced error statistic performance (Table 8) The remaining error statistics are in the same range as the pre-fire model, indicating that the post-fire models does a similar job simulating low flows and total discharge.

Table 8. Model fit statistics for the pre-fire baseline model application over both the calibration and validation periods.

Model-fit statistic	Post-Fire Model WY2010 Daily	Monthly
Number of years, months, or days	364	12
Correlation Coefficient (r)	0.79	0.91
Coefficient of determination (R^2)	0.62	0.82
Nash-Sutcliffe efficiency (NSE)	0.43	0.63
Mean error (cfs)	1.56	1.52
Percent Mean Error (%)	11.32	10.86
Mean absolute error (cfs)	9.36	4.37
Root mean square error (cfs)	27.81	9.27

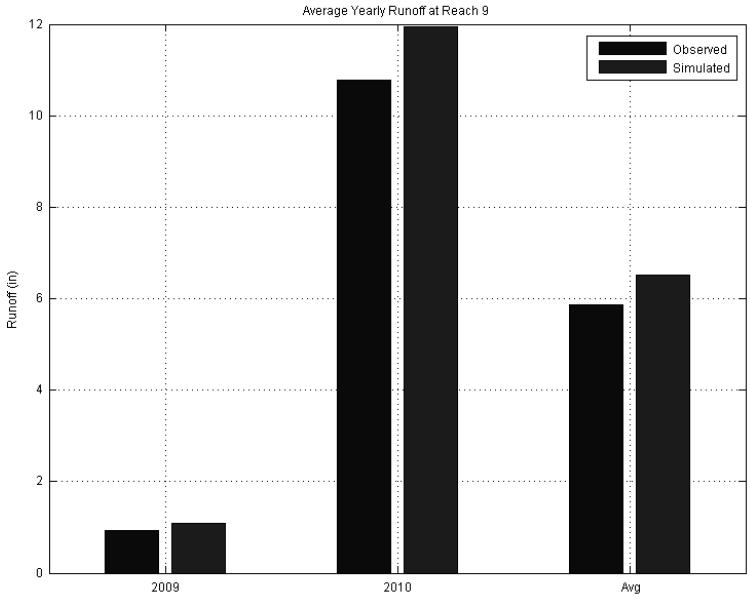

Figure 22 shows annual observed (left) and simulated (right) discharge totals for WY 2010..

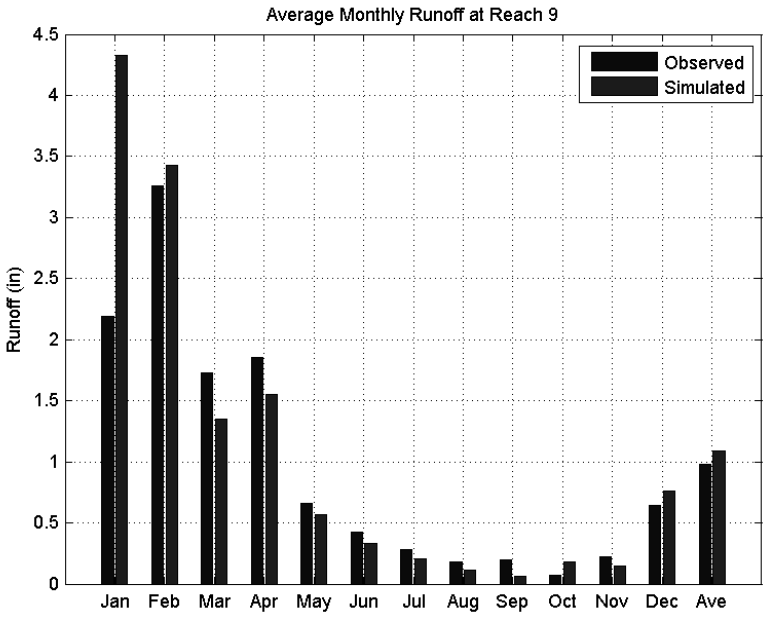

Figure 23. Monthly observed (left) and simulated (right) discharge totals for WY 2010.

The annual and monthly water balance plots support that the model does an acceptable job at a coarser temporal resolution (Figures 22, 23). These water balance plots show post-fire model performance similar to that of the pre-fire baseline model for the wet calibration period and better than what was observed for the dry validation period. However, these plots do not provide much insight into overall model performance. Post-fire impacts cause the water to travel through the system much more quickly, exiting nearly simultaneously. However, little change is seen in overall runoff volumes. Consequently, it is possible to accurately simulate annual, monthly, and even daily storm volumes without capturing the flow regimes that characterize a burned system.

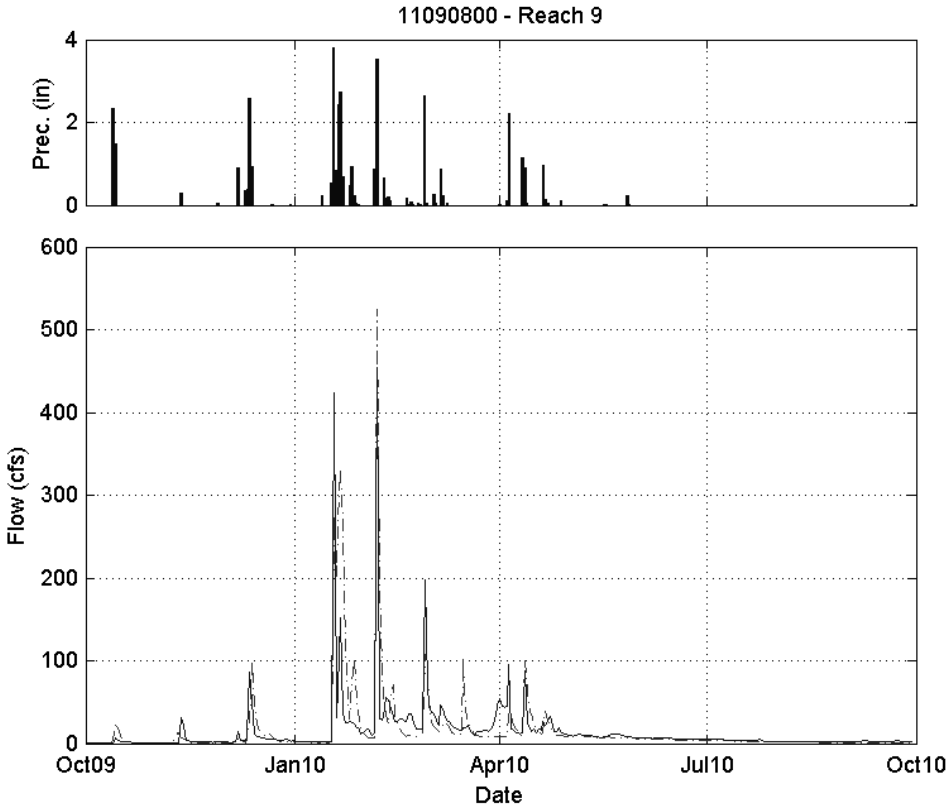

Figure 24. This figure shows daily observed (solid) and simulated (dashed) discharge hydrographs along with a hyetographs for the post-fire model application.

The daily time series plots of observed and simulated discharge provide a better estimate of how the model is able to capture post fire storm flow (Figure 24). The daily plots show the model doing an adequate job of simulating the magnitude of observed peak discharge, but the timing tends to be delayed. Again, this may not be a prohibitive factor in achieving daily loads estimates and should have minimal impact on seasonal load assessments.

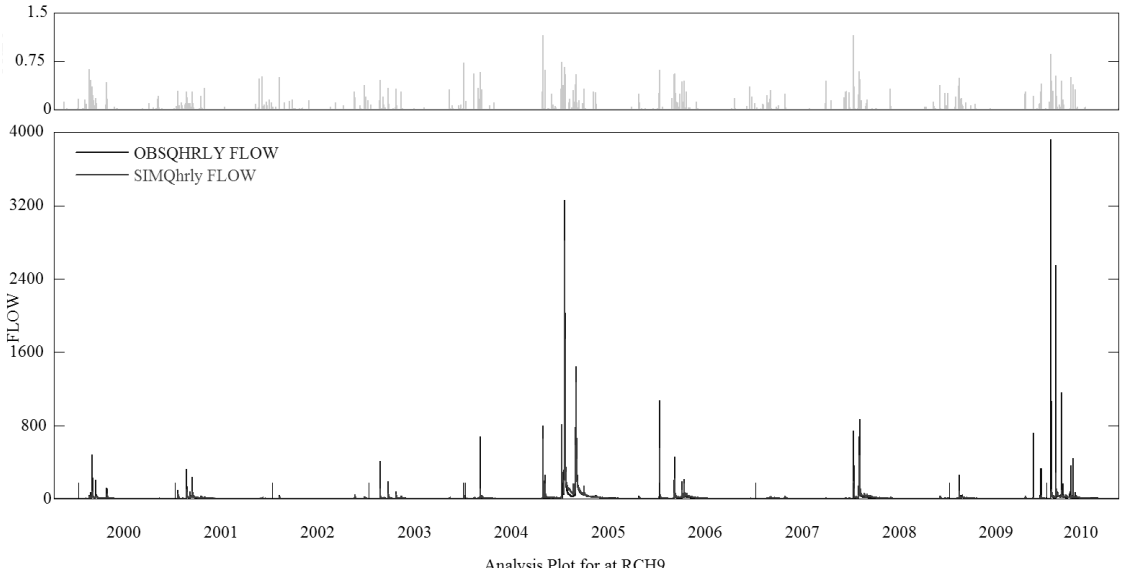

Figure 25. Hourly observed (black) and simulated (grey) discharge hydrographs along with a hyetographs for the post-fire model application.

The hourly plot of observed and simulated discharge from the post-fire model shows that the model does not capture storm peaks at a higher resolution (Figure 25). In fact, the magnitude of hourly post-fire peak flows could not be achieved even by setting the parameters at the limits of their possible ranges (i.e. minimal infiltration capacity, surface water storage, and surface roughness), which is akin to a smoothly paved system with essentially zero infiltration and surface water storage capacities. Moreover, this plot shows

that a model calibrated to post-fire conditions (i.e. minimal infiltration capacity, surface water storage, and surface roughness) is unable to simulate storm peaks at an hourly time step even for the unburned system. Observations from the previous chapter have shown that following wildfire, maximum sediment and trace metal concentrations coincide with, rather than precede, peak flow and that the magnitude of peak discharge primarily controlled post-fire pollutant loading. Consequently, it is critical that post-fire model be able to simulate post-fire peak flows, which will require the model to be run at a higher temporal resolution.

4.4.3. Calculated loads

Season average concentrations and loads as well as event mean concentrations (EMCs) were estimated in the using the calculated relations in order to obtain trace metal concentration and both observed and simulated discharge. Calculated concentrations were compared to average measured concentration of samples taken over the season and with the EMCs calculated in the previous chapter. It has been noted that hourly discharge simulations underestimate peak flows, so seasonal loads were calculated using daily discharge values in each scenario in order to facilitate comparisons. Two methods were used to calculate metal concentrations. The first involves calculating TSS using a linear relation to discharge, then by applying the TSS concentration to the established metal-TSS relations. The second uses a more direct linear metal-discharge relation to calculate concentrations. Linear relations were chosen over power and log functions, because method consistency was desired and they performed better for most constituent groups.

Table 9. Average seasonal metal concentrations calculated using metal/TSS/Discharge relations.

Seasonal Average Concentration

	Samples	ObsQ	SimQ
Al (mg/l)	69.3	24.6	24.7
Cd (ug/l)	1.7	0.1	0.1
Cu (ug/l)	45.6	23.4	23.5
Pb (ug/l)	246.5	71.2	71.7
Zn (ug/l)	281.8	67.3	67.8

Table 10. Average seasonal metal concentrations calculated using metal/Discharge relations.

Seasonal Average Concentration

	Samples	ObsQ	SimQ
Al (mg/l)	69.3	53.3	53.3
Cd (ug/l)	1.7	1.1	1.1
Cu (ug/l)	45.6	38.5	38.5
Pb (ug/l)	246.5	184.4	184.4
Zn (ug/l)	281.8	203.1	203.1

Table 11. Seasonal metal loads calculated using metal/TSS/Discharge relations.

Seasonal Loading

	Samples	ObsQ	SimQ
Q (m^3)	12292574	12292574	13680027
Al (Mg)	851	303	338
Cd (kg)	21	2	2
Cu (kg)	560	288	321
Pb (kg)	3030	876	980
Zn (kg)	3464	827	928

Table 12. Seasonal metal loads calculated using metal/Discharge relations.

Seasonal Loading

	Samples	ObsQ	SimQ
Q (m^3)	12292574	12292574	13680027
Al (Mg)	851	655	729
Cd (kg)	21	14	16
Cu (kg)	560	473	526
Pb (kg)	3030	2267	2523
Zn (kg)	3464	2497	2779

Tables 9 and 10 show average seasonal concentrations calculated using metal-TSS-discharge relations (Table 9) and metal-discharge relations (Table 10). Seasonal loading calculated using metal-TSS-discharge relations (Table 11) and metal discharge relations (Table 12) is also shown.

Table 13 shows the EMCs calculated in the previous chapter (top), using metal/ TSS/ discharge relations (middle), and using metal discharge relations (bottom).

EMC calculate with measured samples

	Al (mg/l)	Cd (ug/l)	Cu (ug/l)	Pb (ug/l)	Zn (ug/l)
Obs. Q					
Storm 1	14.1	6.7	20.8	78.8	82.8
Storm 2	304.1	10.2	168.6	1231.0	1477.2
Storm 3	212.0	7.2	114.0	830.7	956.3
Storm 4	59.4	1.1	22.6	81.3	177.7

EMC calculated with metal/ discharge relations

	Al (mg/l)	Cd (ug/l)	Cu (ug/l)	Pb (ug/l)	Zn (ug/l)
Obs. Q					
Storm 1	52.0	1.1	37.9	179.0	196.4
Storm 2	52.8	1.1	38.2	182.4	200.6
Storm 3	86.4	2.4	54.1	322.0	375.7
Storm 4	53.0	1.1	38.3	182.9	201.2
Sim. Q					
Storm 1	53.4	1.1	38.5	184.9	203.8
Storm 2	53.6	1.1	38.6	185.7	204.8
Storm 3	92.3	2.6	56.9	346.6	406.5
Storm 4	52.3	1.1	38.0	180.2	197.8

EMC calculated with TSS/ discharge, then metal/ TSS relations

	Al (mg/l)	Cd (ug/l)	Cu (ug/l)	Pb (ug/l)	Zn (ug/l)
Obs Q.					
Storm 1	24.2	0.1	23.2	69.4	65.1
Storm 2	52.7	1.4	37.8	184.3	204.5
Storm 3	54.7	1.5	38.8	192.3	214.2
Storm 4	25.0	0.1	23.6	72.8	69.1
Sim Q.					
Storm 1	25.4	0.2	23.8	74.5	71.2
Storm 2	42.7	1.0	32.7	144.1	155.8
Storm 3	60.0	1.8	41.5	213.4	239.9
Storm 4	24.4	0.1	23.3	70.4	66.3

Based on the load estimates, it appears that a more direct metal-discharge relation works better to estimate concentrations and loads over the entire season. The metal-TSS-discharge relationships grossly underestimate concentrations and loads. Both methods underestimate the measured concentrations and loads. However this is to be expected, as most samples were taken during periods of high flow. However, by employing the established metal-discharge relations, managers can still obtain a rough estimate of post-fire metal loading from the Arroyo Seco.

Table 13 shows the EMCs calculated in the previous chapter (top), using metal-TSS-discharge relations (middle), and using metal discharge relations (bottom). These data show that on an event basis, the metal-TSS-discharge relations perform better for most metals, for the smaller storms. Again, both methods underestimate EMCs for two largest storms, which is likely due to the extremely large peak flow. We note that the method can likely be refined using hourly data once a calibrated hourly post-fire model in achieved.

4.5. Discussion

An acceptable daily pre-fire HSPF model application is achieved for the Arroyo Seco by running the model at an hourly time-step, refining monthly calibration parameters. Further, based on previous work in this system, it is also expected that the model can be calibrated to simulate in stream sediment concentrations (Lopez et al., 2012). This is a critical step in obtaining pre-fire metal concentrations and loads, as the TSS-Discharge correlation is poor in the unburned system, which is attributed to the fact that peak sediment (and metal) concentrations precede peak flow. However, in the unburned system, trace metal and TSS concentration show strong correlations, so once sediment calibration is achieved in

the HSPF model application, good estimates of pre-fire metal concentrations and loads can be simulated for this, and similar systems.

The post-fire HSPF model application provides an adequate simulation of storm runoff at the daily time step but performs much better at coarser (monthly) temporal resolutions. Reasonable estimations of annual, monthly, and daily stream flow from the burned system are obtained by running the model with hourly input data. Moreover, the shift in sediment and metal transport mechanisms following the fire results in more direct observed relationships between TSS (and metal) concentrations to stream discharge. Applying these relations to the simulated discharge provides a range of in stream metal concentrations that compared favorably to seasonal and annual average concentrations and storm event EMCs calculated with observed data. Approximate post-fire concentration and load estimates can be obtained without the addition a sediment module to the model application, for all but the largest post-fire storms. This is significant because it can allow for the use of a relatively simple hydrologic model to give a "quick and dirty" estimate of post-fire contaminant loading. It is expected that more accurate estimates can be obtained at a finer temporal scale application of the post-fire HSPF model by recalibrating the model using 15 minute precipitation data and adding a sediment transport component.

Both HSPF model applications had difficulty capturing the observed hourly variability in storm runoff, especially regarding peak discharge, when run with hourly input data. This is especially true for the post-fire model and corroborates previous findings of the USFS BAER teams and NOAA-USGS debris flow task force that fifteen minute precipitation intensity is a primary driver of peak flow and sediment concentrations in burned areas (USDA 2009, Kean et al. 2011). When precipitation intensities are averaged out, the model

simply cannot capture the observed variability, especially following wildfire. Additionally, the hydrology component of the HSPF model uses a saturation excess procedure to compute runoff and may not be capable of simulating the extreme cases of infiltration excess (i.e. post-fire runoff). However, the model has been successfully applied to man-made impervious-type systems, which could provide guidance on how to better represent burned land surfaces within HSPF (Lopez et al., 2012). This can be further investigated by revising model applications to run at a 15 minute interval and through the use of the IMPLND block to represent burned surfaces.

4.6. Summary and future work

The initial HSPF pre- and post-fire hydrologic modeling applications along with the investigations into applicability metal-TSS-discharge relations provide initial estimates of post-fire metal loading at a seasonal scale, as well as information on HSPF model capabilities and limitations and how to approach model refinement to achieve more accurate simulations of both pre- and post-fire conditions in semi-arid regions. Further steps to achieve the culminating objective of this work, the development of a practical tool to predict post-fire loading from burned urban-fringe systems, have been identified. These steps include: recalibration of the both HSPF model applications using 15 minute input data; investigation of IMPLND parameters to better represent post-fire hydrologic processes; development of a sediment transport component for the pre-fire HSPF model application; adjustment of the sediment transport component for the calibrated post-fire model; incorporation of the established trace metal-TSS relationships within the framework of the HSPF model applications; and, finally, application of the developed post-fire model to assess

the cumulative loading impacts of the Station Fire to the Los Angeles River and Santa Monica Bay by scaling model outputs to other basins within the fire perimeter.

.

Chapter 5. Contributions and Future Directions

This study employed a variety of field, laboratory, and modeling methods to investigate the impacts of wildfire on regional soils with respect to mercury (Hg) storage, accumulation, and transport potential; on storm runoff chemistry in an urban fringe watershed highly impacted by regional atmospheric pollutants; and on procedures required to model hydrologic response and predict contaminant loading at the urban-fringe. This resulted in body of work that provides an increased understanding wildfire's effects on Southern California's soils and water and on what is required in order to predict these impacts. The major contributions of this research are presented in response to the questions posed in Chapter 1.

1) What are the impacts of wildfire on soil Hg storage and subsequent transport of sediment bound Hg within burned watersheds?

Temporal and spatial investigations of Hg concentrations in three Southern California watersheds revealed new information regarding Hg dynamics following wildfire. Burned soils exhibited initial Hg loss, likely due to volatilization, at the soil surface followed by accelerated accumulation of Hg at burned soil surfaces comparison with the unburned soils. It would be expected for higher Hg concentrations be found on the smallest grain size fraction, due to a higher surface area to volume ration; however, the wildfire effects diminished the influence of grain size in Hg partitioning in burned soils. Elevated Hg concentrations were found in surface soils of the urban-fringe watershed. While concentrations at the other sites remained within the range of background levels, regardless of fire size, emphasizing the importance of urban-fringe basins as a potential source of

contaminants following wildfire. Particle-facilitated Hg transport was observed during post-fire storm events large enough to mobilize sediment.

2) How are other common contaminant concentrations/loads altered in post-fire storm runoff and what are the hydrologic factors that control these alterations?

Analysis of pre and post-fire runoff from an urban fringe watershed showed shifts in both the timing and magnitude of chemical delivery. The greatest changes were observed in trace metals, where concentration increases measured up to three orders of magnitude. Urban pollutants, such as Cd and Pb exhibited concentrations in the range of those observed in channels draining highways, industrial areas, and mining operations. For pre-fire conditions in the Arroyo Seco, variables such as seasonal timing and antecedent conditions appeared to be major factors in determining runoff chemistry for most measured constituents. However, following the Station Fire, peak discharge and, especially, sediment transport were observed to be the controlling factors in pollutant delivery, particularly for potentially toxic metals. The shift in timing of chemical delivery from the initial rise in flow to peak discharge contributed to significant increases in storm EMCs and loads. These results suggest that management tools such as flood control structures and sediment detainment basins are likely the most effective means to mitigate detrimental impacts to downstream water quality. They also indicate that the chemistry of captured sediment must be considered prior to disposal, especially in watersheds located near large urban centers.

3) How can existing modeling tools be utilized to predict post-fire variability in contaminant loads from burned systems in a cost-effective and parsimonious manner?

The investigation into modeling post-fire hydro-chemical impacts allowed for rough estimates of seasonal loading to be made and provided insight into how to develop a tool to simulate post-fire sediment and metal concentrations at higher temporal resolutions. The selected modeling package (HSPF) offers widespread regulatory approval and allows for flexibility to build model applications sequentially. A pre-fire model application was developed that provides very acceptable simulations of daily discharge, and a post-fire model application was developed that provides acceptable discharge simulations on a monthly basis. Additionally, insights were gained into the limitations of conducting simulations at an hourly time-step. This is especially valuable, because not only did it allow for the identification of steps to improve model performance; it also provides water managers a way to parse out costs. For example, if it is known that high resolution precipitation data is not available to drive the model, attempts to estimate loading with this method should be confined to seasonal scale. Metal-discharge and metal-TSS-discharge relations were developed and applied to simulated discharge providing reasonable estimates of seasonal loading.

These results provide the necessary guidance to attain the culminating objective of this work, the development of a practical tool to predict post-fire loading from burned, urban-fringe systems. Follow up research will result in a future publication of methodologies to used developed this tool and its application to estimate post-fire contaminant loading to downstream waters. The following steps will be taken to achieve these goals: recalibration of the both HSPF model applications using 15 minute input data; investigation of IMPLND parameters to better represent post-fire hydrologic processes; development of a sediment transport component for the pre-fire HSPF model application; adjustment of the sediment transport component for the calibrated post-fire model; incorporation of the established

sediment/ trace metal relationships within the framework of the HSPF model applications; and, finally, application of the developed post-fire model to assess the cumulative loading impacts of the Station Fire to the Los Angeles River and Santa Monica Bay by scaling model outputs to other basins within the fire perimeter.

Further, this work raises additional science questions that are beyond the scope of the proposed follow up research. Here are two in particular that merit additional investigation. We hypothesized that the enhanced accumulation of Hg in burned soils was due to the charred surface functioning as an activated carbon to more efficiently adsorb atmospheric Hg. Further investigation of this hypothesis through laboratory experiments could provide beneficial information, especially to regions that contain wetland ecosystems and are experiencing the impacts of changing climate regimes (i.e. the September 2011 Pagami Creek Fire in the Boundary Waters Canoe Area). We also hypothesized that the extremely elevated concentration of potentially toxic metals (particularly Pb) in post-fire storm runoff from the Arroyo Seco were related to long term accumulation and storage of atmospheric contaminants originating from the Los Angeles metropolitan area. Further investigations into the source of these contaminants using isotopic signatures could parse out geologic versus anthropogenic contributions. This could help determine whether the observed concentration elevations are due to local conditions or pose similar concerns for other fire prone environments located near large urban centers.

Appendix: Supplementary Figures

Hg fluxes and loads were calculated for the Day Fire storms and are shown below.

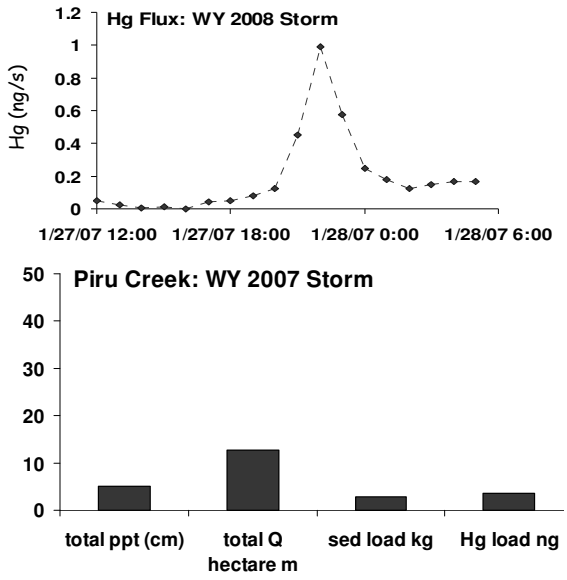

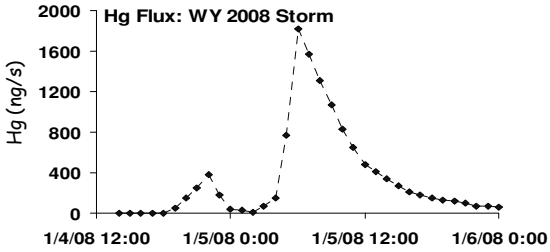

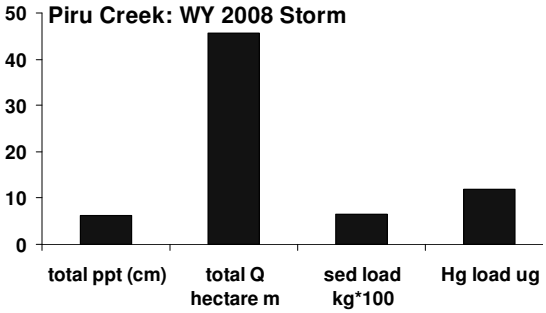

A comparison of Post-fire Storms to Flood 2, 5, 10, 25, 50, 100, and 200 year storms in the Arroyo Seco watershed is shown below.

Flood frequency analysis results for the Arroyo Seco.

Peak Q (cfs)	Peak Q (m^3/s)	Non-Exceedance	Exceedance	Return Period (yrs)
570	16	0.5	0.5	2
1607	46	0.2	0.8	5
249	7	0.1	0.9	10
3770	107	0.04	0.96	25
4792	136	0.02	0.98	50
5856	166	0.01	0.99	100
8467	240	0.002	0.998	500

Calculated return periods for post-fire storms and sampled WY 2010 storms.

Date	Peak Q (cfs)	Peak Q (m^3/s)	Non-Exceedance	Exceedance	Return Period (yrs)
10/14/09	14	0.4	0.03	0.97	1.03
11/12/09	2110	60	0.87	0.13	7.45
12/12/09	521	15	0.47	0.53	1.9
1/18/10	4260	121	0.97	0.03	35
1/20/10	306	9	0.34	0.66	1.52
1/21/10	1370	39	0.76	0.24	4.11
2/6/10	4620	131	0.98	0.02	44.6
2/27/10	1480	42	0.78	0.22	4.5
4/5/10	497	14	0.46	0.54	1.86
4/12/10	680	19	0.55	0.45	2.23

Chloride, fluoride, nitrate, and phosphate were also sampled in the Arroyo Seco. However pre-fire samples Cl, F, and NO^3 samples were filtered prior to analysis, while whole water samples were analyzed following the fire. PO^4 was not sampled in pre-fire storms. Hence they did not facilitate a rigorous comparison. Post-fire pollutographs are included here, because of concern regarding nutrient transport in the Arroyo Seco watershed and because of concerns regarding the use of phosphates in fire retardants. These figures show concentration behavior for NO3 and PO4 and dilution behavior for F and Cl. Additional data can be made available upon request.

Pollutograph (anions): October 13, 2010

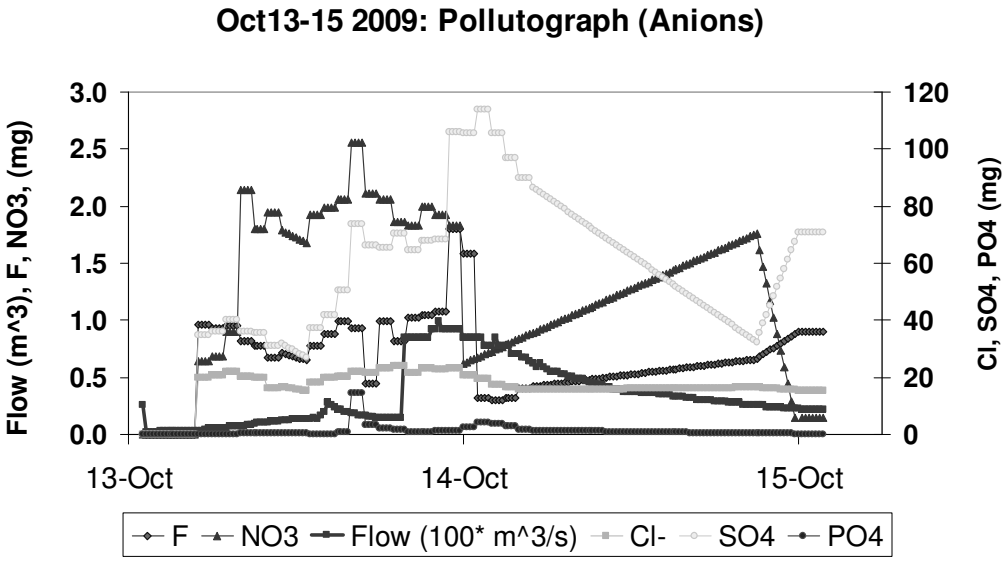

Pollutograph (anions): January 17-19, 2010

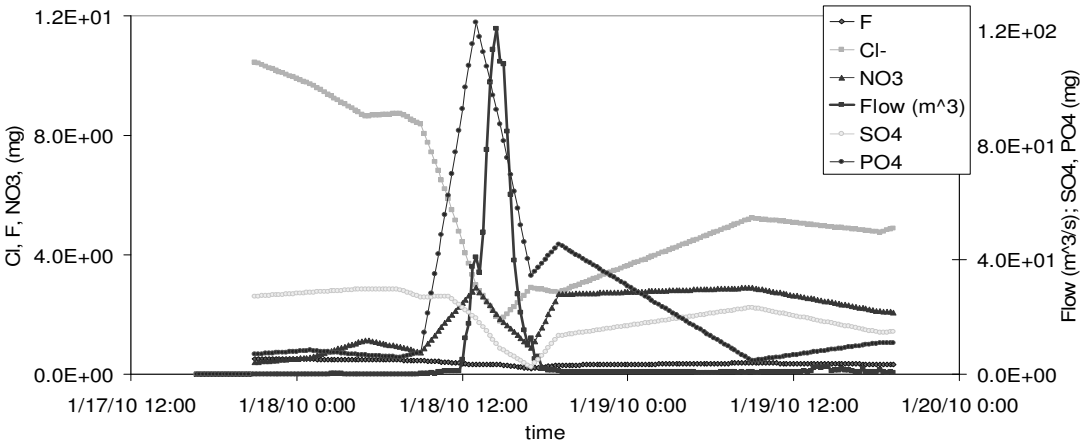

Pollutograph (anions): February 5-6, 2010

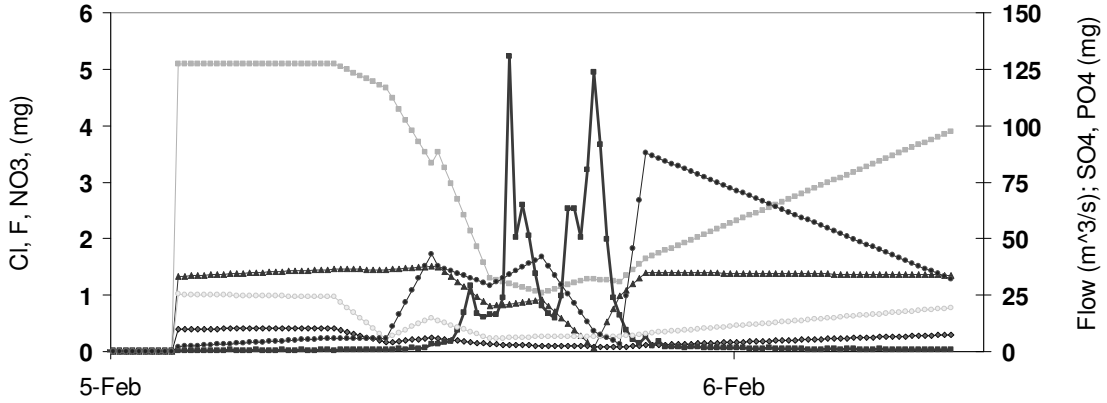

Pollutograph (anions): March 6-7, 2010

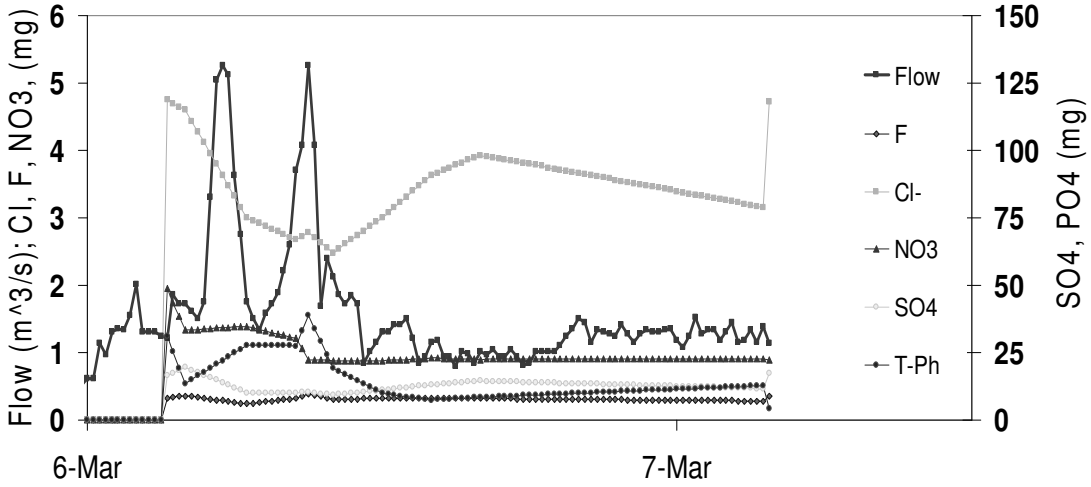

Hg was also sampled in the post-fire storms, but again it was not samples prior to the fire. Hg loads calucluated for each storm, along with a cumulative frequency distributions of Hg of Hg concentration normalized to discharge are shown due to the interesting observed behavior. Hg concentrations and loads increase over the first post-fire rainy season, regardless of discharge, supporting the findings of Chapter 2, where enhanced accumulation of Hg in burned surface soils was observed. Additional data can be made available upon request.

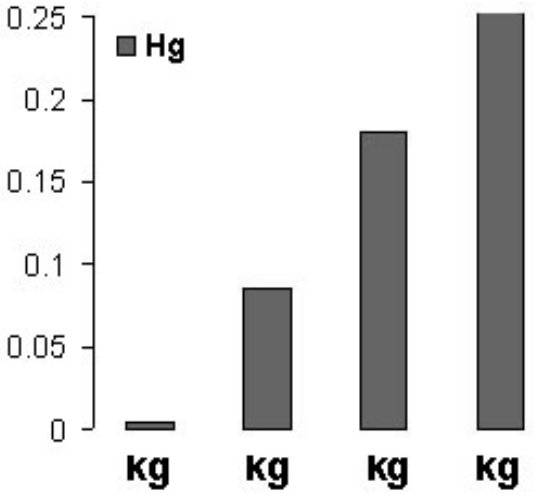

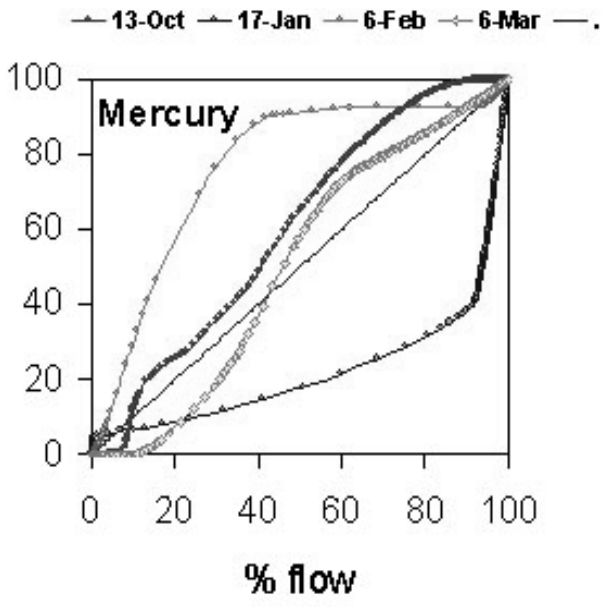

Arroyo Seco Watershed Restoration Plan Water Quality Objectives:

Table 2. Water Quality Objectives
(note: only displayed for contaminants which were detected in the Arroyo Seco)

Parameter	Source	Sample Type	Value	Units	Notes
Aldrin	Ocean Plan	30-day mean	0.000022	ug/L	No instantaneous objectives
Aluminum	Basin Plan	Instantaneous	1.0	Mg/L	MCL
Ammonia (as N)	LA River TMDL	One-hour Average	8.7	Mg/L	
Antimony	Basin Plan	Instantaneous	0.006	mg/L	MCL
Arsenic	Basin Plan	Instantaneous	0.05	Mg/L	MCL
Barium	Basin Plan	Instantaneous	1.0	Mg/L	MCL
Beryllium	Basin Plan	Instantaneous	0.004	Mg/l	MCL
Cadmium	LA River TMDL	Instantaneous	0.0031 (W)	Mg/l	MCL
Chloride	Basin Plan	Instantaneous	150	Mg/l	LA River above Figueroa
Coliform, Fecal	Basin Plan	Instantaneous	400	MPN/100mL	Triggers resampling
Coliform, Total	Basin Plan	Instantaneous	10,000	MPN/100mL	Triggers resampling
Copper	LA River TMDL	Instantaneous	0.022 (D) 0.017 (W)	Mg/L	
Cyanide	Basin Plan	Instantaneous	0.2	Mg/L	MCL
Diazinon	CA Dept Fish & Game	Instantaneous	0.00008	Mg/L	From LA County DPW NPDES reports
E.coli	Basin Plan	Instantaneous	235	MPN/100mL	Triggers resampling
Enterococcus	Basin Plan	Instantaneous	104	MPN/100mL	Triggers resampling
Lead	LAR TMDL	Instantaneous	0.011 (D) 0.062 (W)	Mg/L	
Mercury	Basin Plan	Instantaneous	0.002	Mg/L	MCL
Nickel	Basin Plan	Instantaneous	0.1	Mg/L	MCL
Nitrate (as N)	LA River TMDL	30-day Average	8	Mg/L	
Nitrate (as NO3)	Basin Plan	Instantaneous	45	Mg/L	MCL
Nitrate + Nitrate (as N)	LA River TMDL	30-day Average	8	Mg/L	
Nitrite (as N)	Basin Plan	Instantaneous	1	Mg/L	
Nitrogen (Nitrate + Nitrite)	Basin Plan	Instantaneous	8	Mg/L	LA River above Figueroa
Oil & Grease	Ocean Plan	Instantaneous	75	Mg/L	
Silver	Ocean Plan	Instantaneous	0.007	Mg/L	
Sulfate	Basin Plan	Instantaneous	300	Mg/L	LA River above Figueroa
Total Dissolved Solids	Basin Plan	Instantaneous	950	Mg/L	LA River above Figueroa
Turbidity	Ocean Plan	Instantaneous	225	Mg/L	
Zinc	LAR TMDL	Instantaneous	0.016 (W)	Mg/L	

ArcGIS maps created to guide Arroyo Seco HSPF model application development

Digital Elevation Model (DEM)

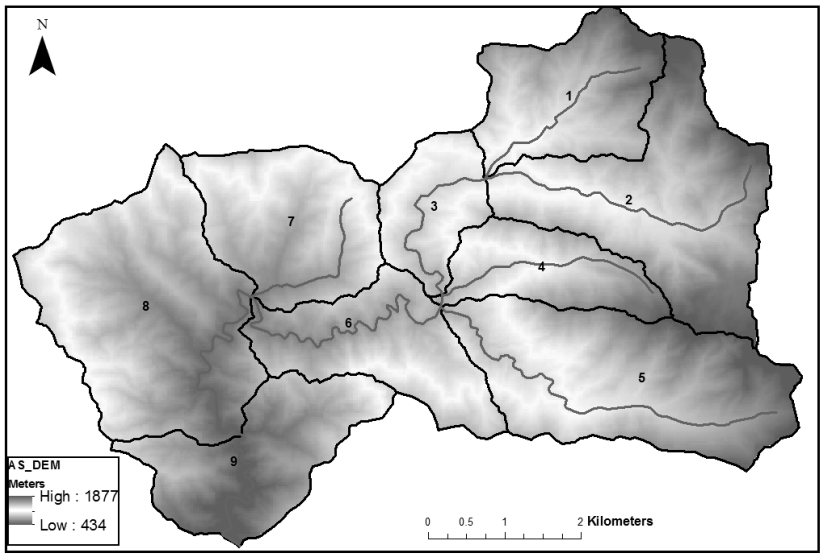

Land Cover

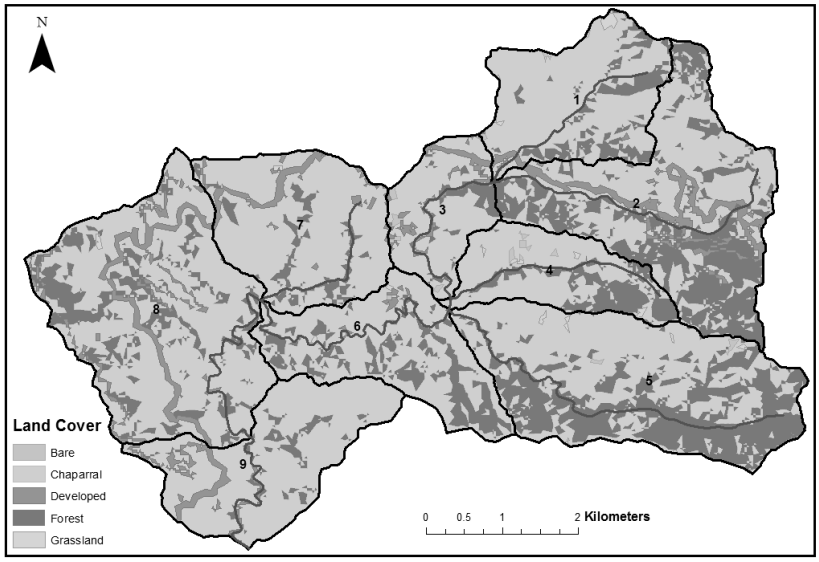

Soil Hydrologic Group

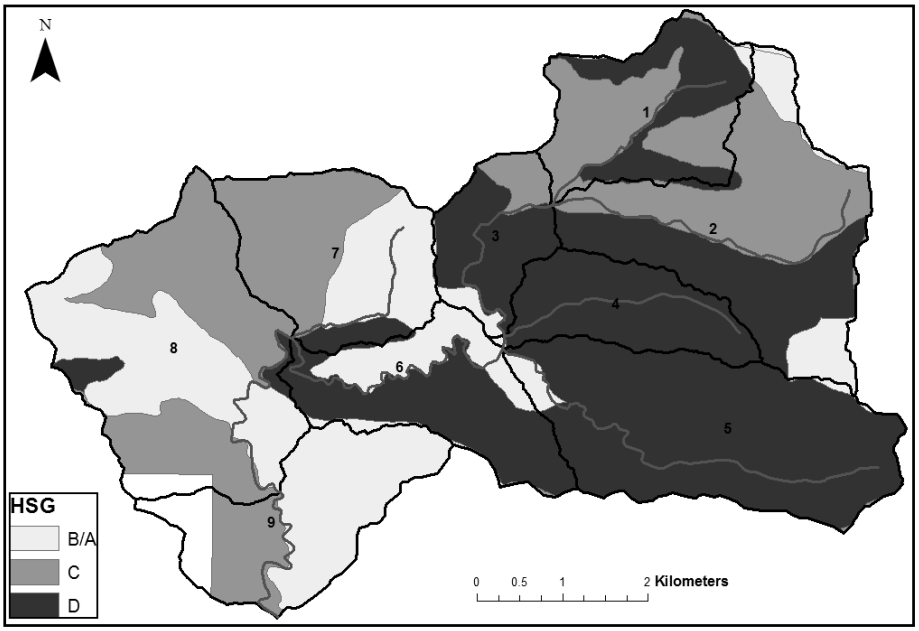

Erosion Potential

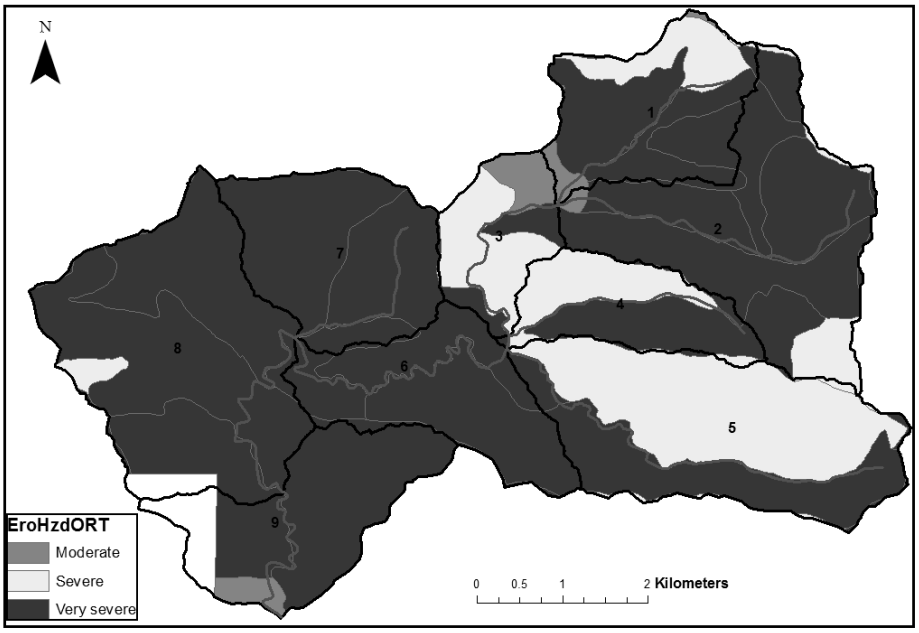

Additional Calibration and Validation Hydrographs for the pre-fire HSPF model of observed (solid) and simulated (dashed) discharge.

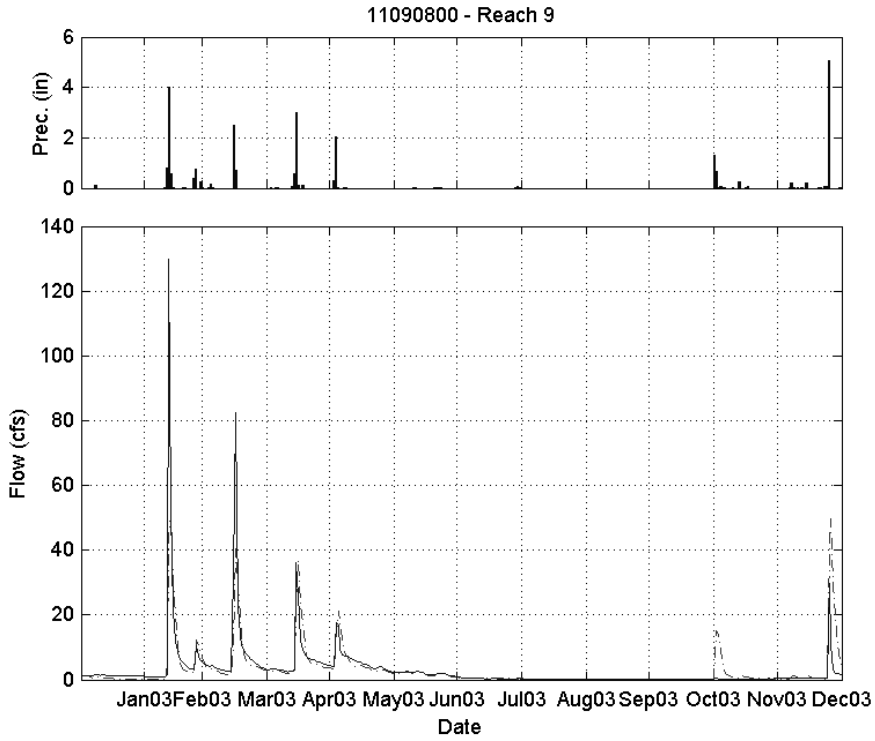

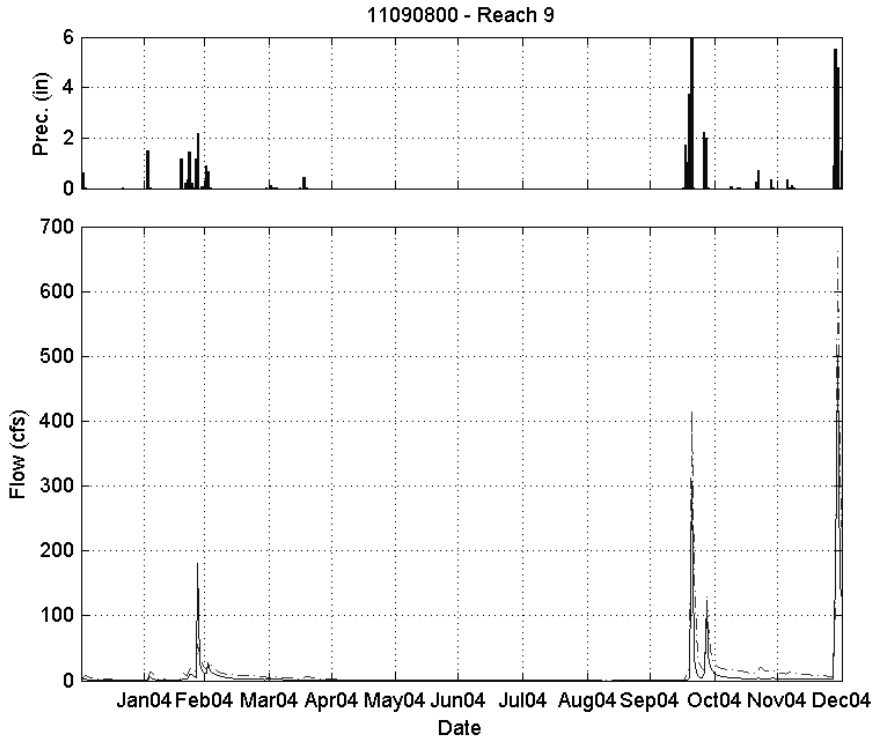

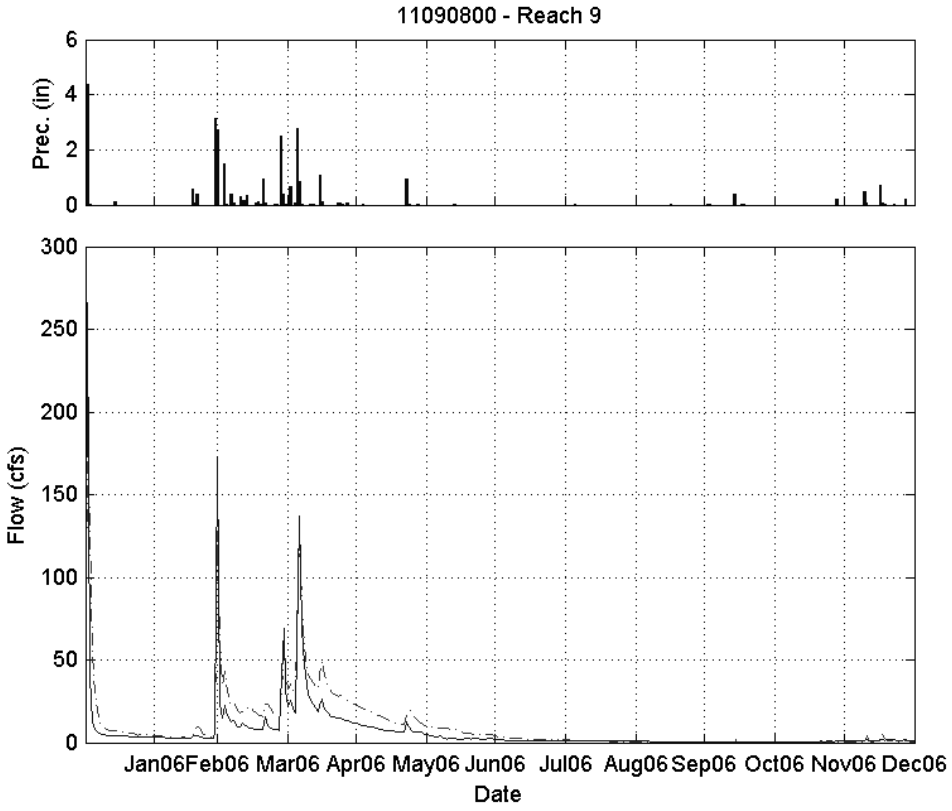
11090800 - Reach 9
Prec. (in)
Flow (cfs)
Jan06 Feb06 Mar06 Apr06 May06 Jun06 Jul06 Aug06 Sep06 Oct06 Nov06 Dec06
Date

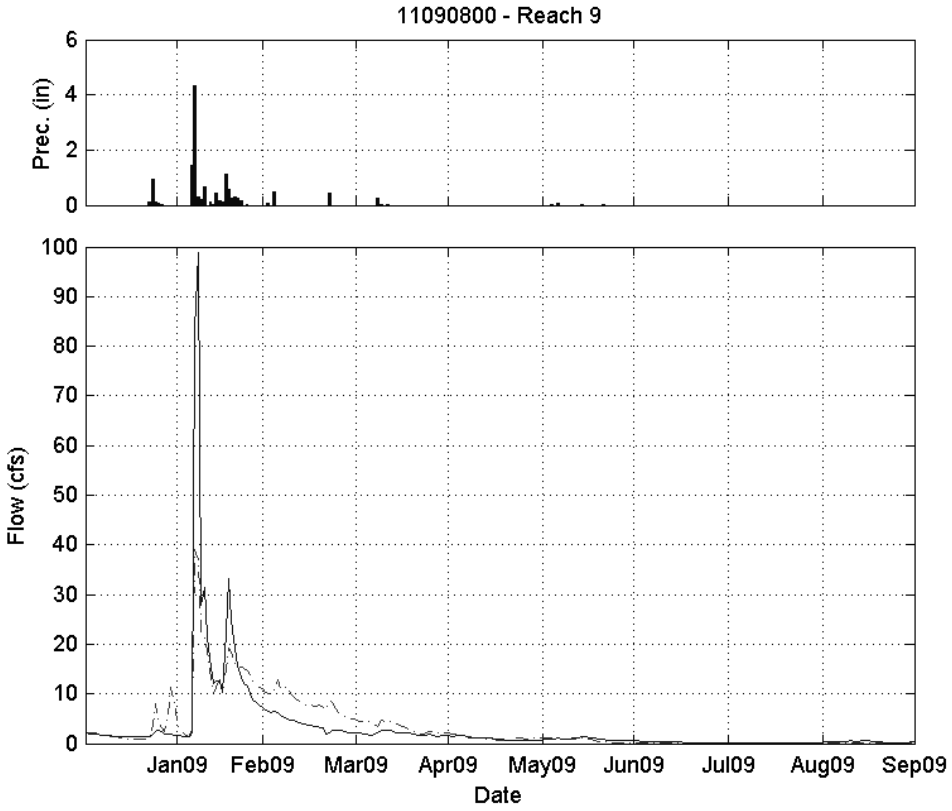
11090800 - Reach 9
Prec. (in)
Flow (cfs)
Jan09 Feb09 Mar09 Apr09 May09 Jun09 Jul09 Aug09 Sep09
Date

Cumulative frequency distribution plots of observed (solid) and simulated (dashed) discharge for Calibration, Validation, and Post-fire periods.

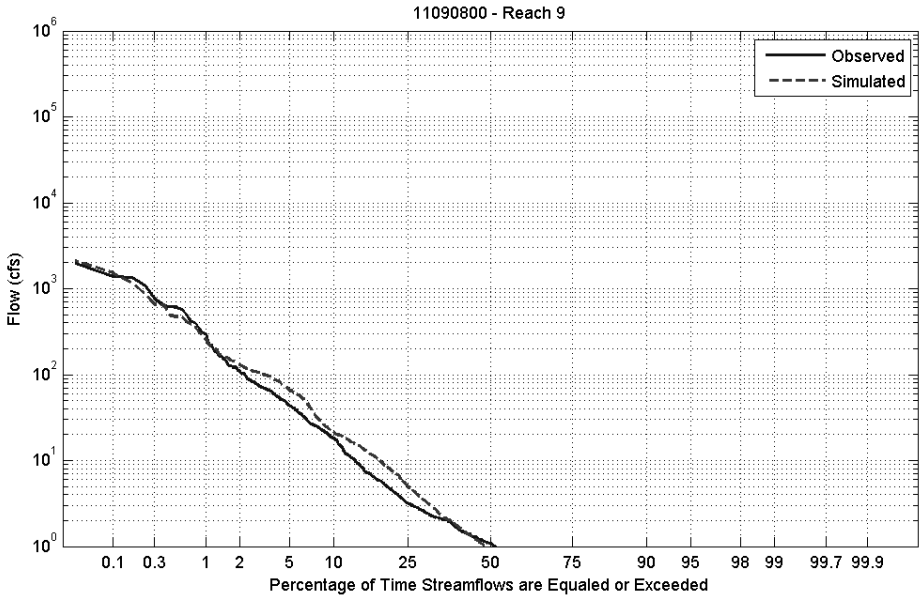

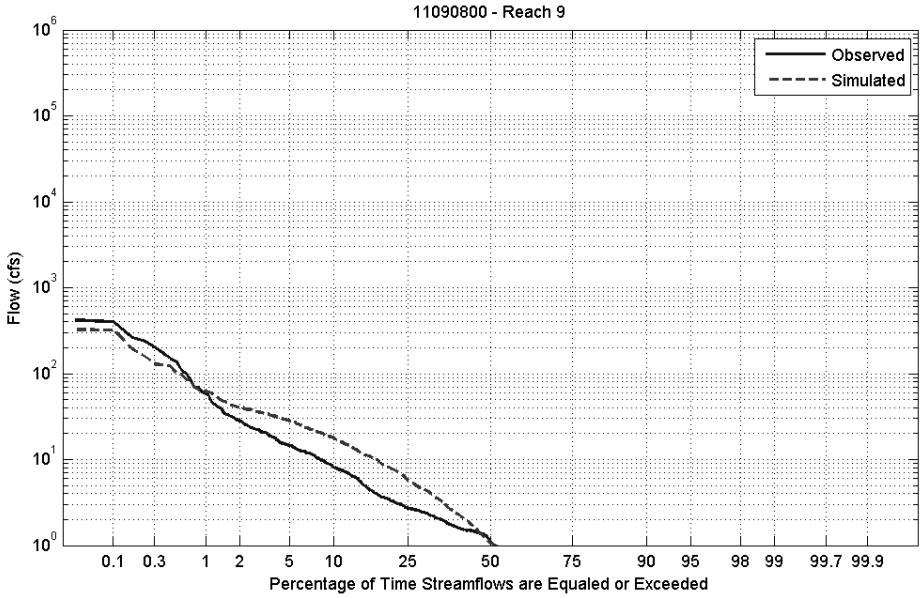

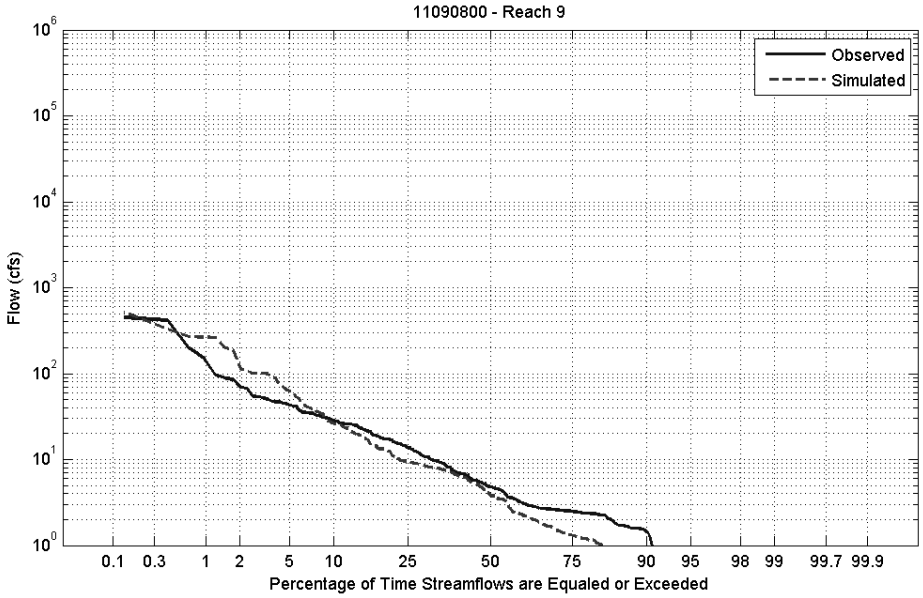
11090800 - Reach 9
Observed
Simulated
Flow (cfs)
10^6
10^5
10^4
10^3
10^2
10^1
10^0
0.1 0.3 1 2 5 10 25 50 75 90 95 98 99 99.7 99.9
Percentage of Time Streamflows are Equaled or Exceeded

References

Ambrose RF, Orme AR (2000). Lower Malibu Creek and Lagoon Resource Enhancement and Management: Final Report to the California State Coastal Conservancy. University of California, Los Angeles.

Amirbahman AR, Ruck PL, Fernandez IJ, Kahl, JS, Haines TA (2004). The effect of fire on mercury cycling in the soils of forested watersheds: Acadia National Park, Maine. U.S.A. *Water, Air and Soil Pollution*; 152: 313-331.

Antilen M, Araya N, Briceno M, Escudev M (2006). Changes on chemical fractions of heavy metals in Chilean soils amended with sewage sludge affected by a thermal impact. *Australian Journal of Soil Research;*.44: 619-625.

Barco, J., Hogue, T.S., Curto, V., Rademacher, L. 2008. Linking Hydrology and Stream Geochemistry in Urban Fringe Watersheds. J. Hydrol. 360, 31-47.

Bicknell, B.R., Imhoff, J.C., Kittle, J.L.Jr., Jobes, T.H., Donigian, A.S.Jr. 2005. Hydrological Simulation Program-Fortran User's Manual for Release 12. US EPA, Washington, DC.

Biswas, A, Blum JD, Klaue B, Keeler GJ (2007). Release of mercury from Rocky Mountain forest fires, *Global Biogeochem. Cycles*; 21, GB1002, doi:10.1029/2006GB002696.

Bitner, K., Gallaher, B., Mullen, K., 2001. Review of Wildfire Effects on Chemical Water Quality. Los Alamos National Laboratory LA-13826.

Blake, W.H., Walsh, M.J., Barnsley, G.P., Dyrynda, P., James, J.G., 2003. Heavy metal concentrations during storm events in a rehabilitated industrialized catchment. Hydrol. Process. 17, 1923-1939.

Bonnin, G.M., Martin, D., Lin, B., Parzybok, T., Yekta, M., Riley, D., 2006. Precipitation-Frequency Atlas of the United States. NOAA Atlas 14, Vol. 1, Version 4. NOAA, NWS, Silver Spring, Maryland.

Burch GJ, Moore ID, Burns J (1989). Soil hydrophobic effects on infiltration and catchment runoff. Hydrological Processes; (3): 211-222.

Burke, M.P., Ferreira, M., Mendez, C.B., Navarro, B.I., Lopez, S., Jay, J.A., Hogue, T.S., 2010. The Effect of Wildfire on Soil Mercury Concentrations in Southern California Watersheds. Water Air Soil Poll. 212, 369-385.

Butturini A., Bernal S, Nin E, Hellı´n C, Rivero L, Sabater S, Sabater F (2003). Influences of the stream groundwater hydrology on nitrate concentration in unsaturated riparian area bounded by an intermittent Mediterranean stream. Water Resources Research 39; (4): 1110.

Caldwell, C.A., Canavan, C.M., Bloom, N.S., 2000. Potential effects of forest fire and storm flow on total mercury and methylmercury in sediments of an arid-lands reservoir. Sci. Total Environ. 260, 125-133.

Cannon, S. H., Gartner, J. E., Wilson, R. C., Bowers, J. C., Laber, J. L. 2008. Storm rainfall conditions for floods and debris flows from recently burned areas in southwestern Colorado and southern California. Geomorphology. 96, 250–269.

CDFFP. California Department of Forestry and Fire Protection: (2007) Annual Report. Office of California State Fire Marshall.

CDFFP. California Department of Forestry and Fire Protection, (2009a). Factsheet: CAL FIRE Jurisdiction Fires, Acres, Dollar Damage, and Structures Destroyed. Office of California State Fire Marshall.

CDFFP. California Department of Forestry and Fire Protection, (2009b). Factsheet: 20 Largest California Wildland Fires (By *Acreage Burned). Office of California State Fire Marshall.

DeBano, L.F., Rice, R.M., Conrad, C.E., 1979. Soil heating in chaparral fires: effects on soil properties, plant nutrients, erosion, and runoff. USDA Forest Service, PSW-145.

DeBano, L.F. 1981. Water repellent soils: a state of the art, Gen. Tech. Rpt. PSW-46. USDA For. Serv., Pacific Southwest Forest and Range Exp. Sta., Berkeley, CA., 21pp.

DeBano, L.F., 2000. The role of fire and soil heating on water repellency in wildland environments: a review. J. Hydrol. 231-232, 195-206.

De Marco A, Gentile EG, Arena C, De Santo AV. 2005. Organic matter, nutrient content, and biological activity in burned and unburned soils of a Mediterranean maquis area of southern Italy. International J. of Wildland Fire; 14: 365-377.

Desilets, S.L.E., Nijssen, B., Ekwurzel, B., Ferr´e, T.P.A., (2007). Post-wildfire changes in suspended sediment rating curves: Sabino Canyon, Arizona. Hydrol. Process. 21, 1413–1348.

Department of Conservation of California. Division of Mines and Geology. Seismic hazard zone report for the Pasadena 7.5-minute quadrangle. Los Angeles County, California 1998.

Dicosty RJ, Callaham, MA, and Stanturf JA. 2006. Atmospheric deposition and re-emission of mercury estimated in a prescribed forest-fire experiment in Florida, USA. Water Air Soil Pollut.; 176: 77-91.

Engle MA, Gustin MS, Johnson DW, Murphy WW, Walker RF, Wright J, and Markee M. 2006. Mercury distribution in two Sierran forest and one desert sagebrush steppe ecosystems and the effects of fire. Sci. Total Environ.; 367: 222-233.

Fairbrother A, Turnley JG. 2005. Predicting risks of uncharacteristic wildfires: Application of the risk assessment process. Forest Ecology and Management: 211: 28-35.

Fenn, M.E., Baron, J.S., Allen, E.B., Rueth, H.M., Nydick, K.R., Geiser, L., Bowman, W.D., Sickman, J.O., Meixner, T., Johnson, D.W., Neitlich, P., 2003. Ecological effects of nitrogen deposition in the Western United States. Bioscience. 53 (4), 404–420.

Fenn, M.E., Poth, M.A., 1999. Temporal and spatial trends in stream water nitrate concentrations in the San Bernardino Mountains. S. Calif. J. Environ. Qual. 28 (3), 822-836.

Friedli HR, Radke LF, Lu JY. 2001. Mercury in smoke from biomass fires. Geophys. Res Letters; 28: 3223-3226.

Friedli HR, Radke LF, Lu JY, Banic CM, Leaitch WR, MacPherson JI. 2003a. Mercury emissions from burning of biomass from temperate North American forests: laboratory and airborne measurements. Atmos. Environ.; 37:253–67.

Friedli HL, Radke LF, Prescott R. 2003b. Mercury emissions from the August 2001 wildfires in Washington State and an agricultural waste fire in Oregon and atmospheric mercury budget estimates. Glob. Biogeochem. Cycles, 17.2: 1-8.

Gallaher, B., Koch, R., Mullen, K., 2002. Quality of Storm Water Runoff at Los Alamos National Laboratory in 2000 with Emphasis on the Impact of the Cerro Grande Fire. Los Alamos National Laboratory LA-13926.

Galster, J.C., Pazzaglia, F.J., Hargreaves, B.R., Morris, D.P., Peters, S.C., Weisman, R.N., 2006. Effects of urbanization on watershed hydrology: The scaling of discharge with drainage area. Geology. 34 (9), 713-716.

Harden JW, Neff JC, Sandberg DV, Turetsky MR, Ottmar R, Gleixner G, Fries TL, Manies KL. 2004. Chemistry of burning the forest floor during the FROSTFIRE experimental burn, interior Alaska, 1999, Global Biogeochem. Cycles; 18, GB3014, doi:10.1029/2003GB002194.

Herpe VY, Troch PA. 2000. Spatial and temporal variations in surface water nitrate concentrations in a mixed land use catchment under humid temperate climatic conditions. Hydrological Processes; 14 (14): 2439–2455.

Hogue, T.S., Sorooshian, S., Gupta, H., 2000. A multistep automatic calibration scheme for river forecasting models. Journal of Hydrometeor. 1, 524-542.

Huffman EL, MacDonald LH, Stednick JD. 2001. Strength and persistence of fire-induced soil hydrophobicity under ponderosa and lodgepole pine, Colorado Front Range. Hydrological Processes; 15: 2877-2892.

Joshia, U.M., Balasubramanian, R., 2010. Characteristics and environmental mobility of trace elements in urban runoff. Chemosphere. 80 (3), 310-318.

Jung, H.Y., Hogue, T.S., Rademacher, L.K., Meixner, T. 2009. Impact of wildfire on source water contributions in Devil Creek, CA: evidence from end-member mixing analysis. Hydrol. Process. 23(2), 183-200.

Kean, J. W., Staley, D. M., Cannon, S. H. 2011. In situ measurements of post-fire debris flows in southern California: Comparisons of the timing and magnitude of 24 debris-flow

events with rainfall and soil moisture conditions, J. Geophys. Res. 116, F04019, doi:10.1029/2011JF002005.

Keeley JE, Zedler PH. 2009. Large, high-intensity fire events in southern California shrublands: debunking the fine-grain age-patch model. Ecological Applications 19:69-94.

Kelly, E.N., Schindler, D.W., St. Louis, V.L., Donald, D.B., Vladicka, K.E., 2006. Forest fire increases mercury accumulation by fishes via food web restructuring and increased mercury inputs. PNAS. 103 (51), 19380-19385.

Kinoshita, A.M, and T.S. Hogue, 2011: Spatial and Temporal Controls on Post-fire Hydrologic Recovery in Southern California Watersheds*, Catena*, 87, 240-252.

Leak, M., Passuello, R., Tyler, B., 2003. I've seen fire. I've seen rain. I've seen muddy waters that I thought would never clear again. Waterworks. 6, 38-44.

Lee, JA, Caporn SJM. 1998. Ecological effects of atmospheric reactive nitrogen deposition on semi-natural terrestrial ecosystems. New Phytology; 139: 127–134.

Letey J. 1969. Measurement of contact angle, water drop pentration time, and critical surface tension, in Debano LF and Letey J (eds) Proc, of a Symposium on Water Repellant Soils, 6-10 May, 1968, University of California, Riverside, CA, pp. 43-7.

Letey, J., 2001. Causes and consequences of fire-induced soil water repellency. Hydrol. Process. 15, 2867-2875.

Lopez, S.R., Hogue, T.S., Morrissey, S., Rademacher, L., Nation, H., Curto, V., Monterrosa, A., Kong, H., 2005. The Relationship between soil type, water repellency, and permeability in the San Bernardino Mountains, California. in AGU Fall National Meeting. San Francisco, CA.

Lopez S.R., Hogue T.S., and Stein E.D. 2012. Regional Sensitivity to Climate Change using Archetypal Watershed Modeling and Historical Time series. International Journal of Climatology. *In Review.*

Loring DH. 1991. Normalization of heavy-metal data from estuarine and coastal sediments. Science; 48: 101-115.

Los Angeles County Department of Public Works (LADPW), Water Resources Division, 2011. Devil's Gate Dam and Reservoir post-fire sediment removal short term solution report for sediment accumulation along the face of the dam. WR5-A3570.

Los Angeles County Department of Public Works (LADPW), 2010. Water Resources Division, Near Real-Time Precipitation Map. http://dpw.lacounty.gov/wrd/Precip/.

Loring, D.H., 1991. Normalization of heavy-metal data from estuarine and coastal sediments. Science. 48, 101-115.

Mailman M and Bodaly RA. 2005. Total mercury, methyl mercury, and carbon in fresh and burned plants and soil in Northwestern Ontario. Environ. Pollut.; 138: 161-166.

Malmon, D.V., Reneau, S.L., Katzman, D., Lavine, A., Lyman, J., 2007. Suspended sediment transport in an ephemeral stream following wildfire. J. Geophys. Res. 112, F02006, doi:10.1029/2005JF000459.

Mast MA and Clow DW. 2008. Effects of 2003 wildfires on stream chemistry in Glacier National Park, Montana. Hydrol. Process.; DOI: 10.1002/hyp.7121.

Martin DA, and Moody JA. 2001. Comparison of soil infiltration rates in burned and unburned mountainous watersheds. Hydrol. Process.; 15: 2893-2903.

Meixner T., Fenn, M.E., Poth, M.A., 2001. Nitrate in polluted mountainous catchments with Mediterranean climates. Sci. World. 1, DOI 10.1100=tsw.2001.324.

Meixner T, Fenn M. 2004. Biogeochemical budgets in a Mediterranean catchment with high rates of atmospheric N deposition – importance of scale and temporal asynchrony. Biogeochem.; 70 (3): 331–356.

Meixner, T., Fenn, M., Wohlgemuth, P., Oxford, M., Riggan, P., 2006. N saturation symptoms in chaparral catchment are not reversed by prescribed fire. Environ Sci. Tech. 40, 2887-2894.

Moody, J.A., Martin, D.A., Haire, S.L., Kinner, D.A., 2008. Linking runoff response to burn severity after a wildfire. Hydrol. Process. 22, 2063–2074.

Moody, J.A., Martin, D.A., 2009. Synthesis of sediment yields after wildland fire in different rainfall regimes in the western United States. Int. J. Wildland Fire. 18, 96-115.

Morales, HA, Navar J, Dominguez PA. 2000. The effect of prescribed burning on surface runoff in a pine forest stand of Chihuahua, Mexico. Forest Ecology and Management; 137: 199-207.

Neary, D. G., Ryan, K.C., DeBano, L. F., 2005. Wildland fire in ecosystems: effects of fire on soils and water. Gen. Tech. Rep. RMRS-GTR-42-vol.4. Ogden, UT: USDA, Forest Service, Rocky Mountain Research Station. 250 p.

NOAA-USGS, (2005). NOAA USGS Debris Flow Warning System Final Report.

National Weather Service, Los Angeles/ Oxnard Forecast Office. Available online at: http://www.wrh.noaa.gov/lox/main.php?suite=hydrology&page=historical. Accessed: 7/30/09.

Palmieri H.E.L., Nalini Jr. H.A., Leonel L.V., Windmoller C.C., Santos R.C., de Brito W. 2006. Quantification and speciation of mercury in soils from the Tripuí Ecological Station, Minas Gerais, Brazil. Sci. Tot. Environ.; 368: 69-78

Pierson, F.B., Robichaud, P.R., Spaeth, K.E., 2001. Spatial and temporal effects of wildfire on the hydrology of a steep rangeland watershed. Hydrol. Process. 15, 2905–2916.

Pierson FB, Robichaud PR, Moffet CA, Spaeth KE , Hardegree SP, Clark PE, Williams CJ. 2008. Fire effects on rangeland hydrology and erosion in a steep sagebrush-dominated landscape. Hydrol. Process.; 22: 2916–2929.

Pincetl S, Rundel PW, Blasio JC, Silver D, Scott t, Keeley JE, Halsey R. 2008. It's the Land Use, Not the Fuels: Fires and Land Development in Southern California. Real Estate Rev.; 37(1): 25-42.

Ranali, A.J., 2004. A summary of the scientific literature on the effects of fire on the concentration of nutrients in surface waters. Open-File Report 2004-1296, U.S. Department of the Interior, USGS, Denver, CO.

Reneau, S.L., Katzman, D., Kuyumjian, G.A., Lavine, A., Malmon, D.V., 2007. Sediment delivery after a wildfire. Geology. 35 (2), 151-154.

Riggan, P.J., Lockwood, R.N., Lopez, E.N., 1985. Deposition and processing of airborne nitrogen pollutants in mediterraneantype ecosystems of Southern California. Environ. Sci. Tech. 19 (9), 781-789.

Robichaud, P.R., 2000. Fire effects on infiltration rates after prescribed fire in Northern Rocky Mountain forests, USA. J. Hydrol. 231-232, 220-229.

Rothenburg, S.E., Kirby, M.E., DeRose, M.B., Lin, C.C., Feng, X., Ambrose, R.F., Jay, J.A., 2010. The impact of over 100 years of wildfires on mercury levels and accumulation rates in two lakes in southern California, USA. Environ Earth Sci. 60 (5), 993-1005.

Rulli, M.C., Rosso, R., 2007. Hydrologic response of upland catchments to wildfires. Adv. Water Resour. 30, 2072–2086.

Schiff, K.C., Tiefenthaler, L.L., 2011. Seasonal flushing of pollutant concentrations and loads in urban stormwater. J. Am. Water Resour. Assn. 47 (1), 136-142.

Scott KM, Ritter JR; and Knott J M. 1968. Sedimentation in the Piru Creek Watershed, southern California. USGS. Water-Supply Pap. 1798-E,; 48 p.

Scott E, Meixner T. 2004. Long-term stream flow impact of wild fires in Mediterranean shrubland ecosystems. EOS Transactions, AGU 85: 47.

Shakesby RA, Chafer CJ, Doerr SH, Blake WH, WallbrinkP, Humphreys GS, Harrington BA. 2003. Fire Severity, Water Repellency Characteristics and Hydrogeomorphological Changes Following the Christmas 2001 Sydney Forest Fires. Australian Geographer; 34(2): 147-175.

Sigler JM, Lee X, Munger W. 2003. Emission and long-range transport of gaseous mercury from a large-scale Canadian boreal forest fire. Environ. Sci. Technol.; 37, 4343–4347.

Skahill, B. E. 2003. HSPF Modeling at the Engineer Research and Development Center. US ACE Research and Development Center, Vicksburg, MS.

Smith, H., Sheridan, G., Lane, P., Nyman, P., Haydon, S., 2011. Post-fire water quality in forest catchments: a review with implications for potable water supply. J. Hydrol. 396, 170-192.

Snider G, Daugherty PJ, Wood D. 2007. The irrationality of continued fire suppression: an avoided cost analysis of fire hazard reduction treatments versus no treatment. Jour. of Forestry; 104: 431-437.

Soil Survey Staff, Natural Resources Conservation Service, United States Department of Agriculture. Soil Survey Geographic (SSURGO) Database for California. Available online at http://soildatamart.nrcs.usda.gov. Accessed 11/11/2011.

Tiefenthaler, L.L., Stein, E.D., Schiff, K.C. 2008. Watershed and land use-based sources of trace metals in urban stormwater. Environ. Toxicol. Chem. 27 (2), 277-287.

Thomson, N.R., McBean, E.A., Snodgrass, W., Monstrenko, I.B., 1997. Highway stormwater runoff quality: development of surrogate parameter relationships. Water Air Soil Poll. 94, 307-347.

US Code § 131.36, Clean Water Act: EPA's Section 304(a) criteria for Priority Toxic Pollutants. Accessed online at: http://ecfr.gpoaccess.gov/cgi/t/text/text-idx?c=ecfr&rgn=div8&view=text&node=40:21.0.1.1.18.4.16.6&idno=40.

USDA, Forest Service, 2009. Soils Resource Assessment, Station Fire, Unpublished Report CA-ANF-3622..

USDA Natural Resource Conservation Service. 2007. Soil survey of Santa Monica Mountains National Recreation Area.

U.S. EPA. 1994. Method 200.8, Revision 5.4. Determination of Trace Elements in Water and Wastes by Inductively Coupled Plasma - Mass Spectrometry. Washington, D.C

US EPA, 1996. The Metals Translator: Guidance for calculating a total recoverable permit limit from a dissolved criterion. EPA 823-8-96-007, Washington, D.C.

US EPA. 2001. Better Assessment Science Integrating Point and Nonpoint Sources BASINS Version 3.0 User's Manual. U.S. EPA Office of Science and Technology, Washington, DC.

U.S. EPA. 2002. Method 7473, Mercury in solids and solutions by thermal decomposition, amalgamation and atomic absorption spectrophotometry. Washington, D.C.

U.S. EPA. 2002. Method 1631, Revision E: Mercury in water by oxidation, purge and trap, and cold vapor atomic fluorescence spectrometry. Washington, D.C.

US EPA. 2003. Technical Note 6. Estimating Hydrology and Hydraulic Parameters for HSPF.

US EPA, 2007. California's final 2004-06 303(d) List. Water quality limited segments being addressed by US EPA approved TMDLs, Washington, D.C.

USGS, 2011. USGS Real-Time Water Data for the Nation: USGS 11098000 Arroyo Seco nr Pasadena CA. Accessed on line at: http://nwis.waterdata.usgs.gov/nwis/uv/?-site_no=11098000&agency_cd=USGS.

Vitousek PM, Aber JD, Howarth, RW, Likens GE, Matson PA, Schindler DW, Schlesinger WH, Tilman, DG. 1997. Human alteration of the global nitrogen cycle: sources and consequences. Ecological Applications: 7: 737–750.

Wessel, C., 2009. Contaminant flushing from an urban fringe watershed: Insight into hydrologic and soil dynamics during the wet season. M.S. Thesis, University of California, Los Angeles.

Westerling AL, Hidalgo HG, Cyan DR, Swetnam TW. 2006. Warming and earlier spring increase Western U.S. wildfire activity. Science; 313: 940-943.

Westerling AL, Bryant BP. 2008. Climate change and wildfire in California. Climate Change; 87 (Suppl 1): S231-S249. DOI 10.1007/s10584-007-9363-z.

Whitlock C. 2004. Forests, fires and climate. Nature; 432: 28-29.

Wolfe MI, Mott JA, Voorhees RE, Sewell CM, Paschal D, Wood CM, McKinney PE, Redd S. 2004. Assessment of urinary metals following exposure to a large vegetative fire, New Mexico, 2000. Exposure Analysis and Environmental Epidemiology; 14: 120-128.

Yoon, V.K., Stein, E.D., 2008. Natural Catchments as Sources of Background Levels of Storm Water Metals, Nutrients, and Solids. J. Environ. Eng. 134, 961-973.

Žák, K., Rohovec, J., Navrátil, T., 2009. Fluxes of heavy metals from a highly polluted watershed during flood events: a case study of the Litavka River, Czech Republic. Water Air Soil Poll. 203 (1-4), 343-358.